NANOCAT

506621

NANOCAT

Tailored nanosized metal catalysts for improving activity and selectivity
via engineering of their structure and local environment

Instrument NWP3

Thematic Priority

D17: Publishable Final Activity Report

Period covered: from 1.2.2005 to 31.1.2008 Date of preparation: February 2008

Start date of project: 01.02.2005 Duration: 36 months

Project coordinator name: Professor Dmitry Yu. Murzin
Project coordinator organisation name: Åbo Akademi University

Revision [draft, 1]

Project co-funded by the European Commission within the Sixth Framework Programme (2002-2006)		
Dissemination Level		
PU	Public	X
PP	Restricted to other programme participants (including the Commission Services)	
RE	Restricted to a group specified by the consortium (including the Commission Services)	
CO	Confidential, only for members of the consortium (including the Commission Services)	

TABLE OF CONTENTS

1 PROJECT EXECUTION

1.1 Background

Production of better than existing pharmaceuticals, healthy food ingredients, perfumes, other fine chemicals, which are of immense importance for improving quality of life, is often limited by low selectivity in their synthesis over heterogeneous catalysts. Selectivity of these catalysts, bearing metals of nanoparticle size, could be enhanced by carefully adjusting the size and environment of metal nanoparticles. The project is aimed to study the influence of metal nanoparticle size and its environment on catalytic behaviour in some representative reactions of industrial importance and, finally, to establish the fundamental knowledge on atomic/molecular level relating the nanocatalyst synthesis and behaviour.

1.2 Objectives

The NANOCAT project aims to create fundamental knowledge from the synthesis of nanosized metal catalysts supported on inorganic and organic matrices as well as from the testing of these catalysts in industrially important reactions for producing fine and specialty chemicals. The most important aim is to create the link between the catalyst properties and its performance in hydrogenation/oxidation, and isomerisation reactions. These reactions yield too low selectivity of desired products over conventional heterogeneous catalysts, therefore restricting industrial synthesis of potential pharmaceuticals, food ingredients, fragrances, healthy components, which could be otherwise brought to the consumer market. Although some of the synthetic routes could be performed with homogeneous catalysts, the use of heterogeneous catalysts is an attractive alternative, because they are environmentally friendly, economic and easy to regenerate and to reuse compared to the homogeneous catalysts, in the latter case catalyst loss is often the major obstacle in commercialization.

Special emphasis within NANOCAT project was put on the deeper understanding of the nanometal particle environment, i.e. the different local metal particle environments were compared with the same metal particle sizes in different partial oxidations, hydrogenation, chemoselective hydrogenations as well as in isomerisation reactions. The work was divided in nine different subtasks: catalyst synthesis, testing, characterisation, kinetic and quantum chemical modelling, creating and disseminating of the new knowledge, prototype

catalyst preparation, characterisation and testing, economical evaluation of the prototype catalyst as well as the project management. The work created a broad scientific basis for understanding the metal particle size and its local environment as well as the surface reactions and the link between the catalyst properties and its activity/selectivity in selective hydrogenation, oxidation, and isomerisation reactions. The tested metals in NANOCAT project were Ru, Pt, Au and Pd and metal environment consisted of either inorganic micro-mesoporous matrices, carbon nanofibers or polymer based materials. The optimum conditions for stabilisation of nanosized metal particles were developed within NANOCAT project. The catalyst testing included the first catalyst screening followed by kinetic experiments with selected catalysts. The kinetic data and catalyst characterisation results served as input data for kinetic modelling and quantum chemical simulations. These two types of theoretical modelling were used to propose the surface reaction mechanisms.

The technical aim was to develop selective catalysts for producing fine and specialty chemicals, like fragrances, drugs and anticarcinogenic compounds with high purity as well as to investigate the possibility of preventing metal leaching. Another important topic was catalyst deactivation which was investigated by reusing the same catalyst in consecutive experiments.

1.3 Contractors involved

The main aim at the European level in NANOCAT project was to combine the complementary expertise of chemists, chemical engineers and physicists of five different universities, two research institutions and one company from different scientific backgrounds and geographical areas. The partners were the following ones:

Participant Role*	Partic. no.	Participant name	Participant short name	Country
CO	1	Åbo Akademi University Laboratory of Industrial Chemistry and Reaction Engineering Biskopsgatan 8 FI-20500 Turku/Åbo Finland Coordinator: Prof. Dmitry Yu. Murzin	AAU	Finland
CR	2	Tver State Technical University A.Nikitin str. 22 170026 Tver Russia Contact: Prof. Esther Sulman	TverTU	Russia
CR	3	Universite Pierre et Marie Curie Laboratoire de Reactivite de Surface UMR 7609 CNRS 4 Place Jussieu 75252 Paris France Contact: Prof. Michel Che	UPMC	France
CR	4	Foundation for Research and Technology - Hellas Institute of Electronic Structure and Laser P.O. Box 1527 Heraklion GR-71110 Crete, Greece Contact: Prof. Spiros H. Anastasiadis	FORTH	Greece
CR	5	University of Palermo Dipartimento di Chimica Inorganica e Analitica 'S. Cannizzaro' dell' Università viale delle Scienze Parco d'Orleans II, Pad. 17, I-90128 Palermo Italy Contact: Prof. Dario Duca	DIAC-UNIPA	Italy
CR	6	Utrecht University Sorbonnelaan 16 3508 TB Utrecht The Netherlands Contact: Dr. Johannes H. Bitter	UU	The Netherlands
CR	7	Evonik Degussa GmbH 63457 Hanau-Wolfgang Germany Contact: Dr. Dorit Wolf	Deg	Germany
CR	8	Zelinsky Institute of Organic Chemistry 47 Leninsky Prospect 119991 Moscow Russia Contact: Prof. Leonid M. Kustov	IOC	Russia

*CO = Coordinator
CR = Contractor

1.4 State-of-the-art

The societal, environmental and healthy issues were addressed in NANOCAT project by creating new selective and active catalysts and new cleaner and energy-saving chemical processes for the future demand of the European industry. The long-term competitiveness of the European chemical industry in economical and technical way could be guaranteed via development of new tailored catalysts for production of specialty and life science products in OECD countries. The drawback at the European level has been the lack in transfer of knowledge as well as the in real technological breakthrough in adjusting the European chemical industry into the structural changes. The NANOCAT project aimed at providing first the knowledge from the active metal surfaces and their local environment and second the knowledge how the defined metal surfaces are related to the catalytic activity/selectivity.

Metal nanoparticles formed in various media and stabilized by different mechanism are the objects of intense studies due to their unique properties, which are significantly influenced by a nanoparticle size, organization of the nanoparticle crystal lattice, nanoparticle surface and the chemical nature of the microenvironment surrounding the nanoparticle. There is a large potential for the development and the application of metal nanoparticles with tailored physical and chemical properties in both materials science and catalysis. Metal nanoparticles supported on inorganic and organic matrices have shown promising features, like higher catalytic acitivity and/or selectivity than conventional catalysts in many catalytic reactions. The origin for these effects is the size quantization of most electronic properties. The metal nanoparticles exhibit unique properties that differ from the bulk substances, *e.g.* different heat capacity, vapour pressure and melting point. Moreover, when decreasing the metal particle size sufficiently enough, there occurs the transition of the electronic state from metallic to a non-metallic one. Additionally metal nanoparticles exhibit large surface-to-volume ratio and increased number of edges, corners and faces leading to altered catalytic activity and selectivity. The higher amount of surface metal atoms in nanosized particles makes such catalysts attractive for industrial application.

The metal particle size effect on the reaction rate and on the selectivity is relatively well

known. Some examples of this effect are from oxidation and hydrogenation reactions[1,2,3,4], where high catalytic activities as well as high enantio- or chemoselectivities have been achieved over nanosized metal supported catalysts. Scientifically interesting phenomena over metal nanoparticles, like the observed highest catalytic activity in oxidation at the transition of the electronic state from metallic to non-metallic and the selectivity changes with increasing metal particle size in the hydrogenation of multifunctional compounds, need still more detailed fundamental understanding from the surface science viewpoint.

The effect of the matrix on the metal properties is not very well understood, especially when comparing inorganic and organic matrices having the same metal nanoparticle sizes. The local metal environment can effect both the metal particle size and shape/morphology[5,6]. This environment is changed for example varying the pretreatment of the catalyst[6]. Moreover the acidity or basicity of the support affects the stabilisation of the metal particle[5].

The advantage in using inorganic matrices is in their higher thermal stability compared to the organic matrices and thus broader application range. Specific type of inorganic matrices, *i.e.* micro- and mesoporous materials are potential supports for nanosized metal particles due to their tunable pore sizes and large specific surface areas. These materials including incorporated metal nanoparticles inside the matrix might exhibit shape selective properties in some reactions. Carbon nanofibres (CNF) have gained increasing attention in the last few years due to their high strength, chemical purity, non microporosity and chemical inertness which make them ideally suitable for use as a catalyst support.

At the same time organic environment also possesses specific advantages. High catalytic activities/selectivities have been obtained in several catalytic reactions over nanosized metals supported by organic matrices. The high activity was claimed to be originated from the easier accessibility of the metal particles compared to conventional catalysts.

---

[1] Sulman, E., Bodrova, Yu., Matveeva, M., Semagina, N., Cerveny, L., Kurtc, V., Bronstein, L., Platonova, L., Valetsky, P., Appl. Catal., A: Gen., 176 (1999) 75.
[2] Haruta, M., Cattech, 6, 3 (2002) 102.
[3] Schimpf, S., Lucas, M., Mohr, C., Rodemerck, U., Brückner, A., Radnik, J., Hofmeister, H., Claus, P., Catal. Today, 72 (2002) 63.
[4] Zuo, X., Liu, H., Guo, D., Yang, X., Tetrahedron, 44 (1999) 7787.
[5] (a) Riahi, G., Guillemot, D., Polisset-Rhfoin, M., Khodadadi, A. A., Fraissard, J., Catal. Today, 72 (2002) 115. (b) A.Yu. Stakheev, L.M. Kustov, Appl. Catal., A: General, 1999, vol. 188, p. 3-35.
[6] Yuranov, I., Moeckli, P., Suvorova, E., Buffat, P., Kiwi-Minsker, L., Renken, A., J. Mol. Catal. A: Chem., 192 (2003) 239. (a) Rodriquez, M., Mater. Res., 8 (1993) 3233. (b) Baker, R. T. K., Carbon, 27 (1989) 315. (c) de Jong, K. P., Geus, J. W., Catal. Rev.-Sci. Eng., 42 (2000) 481.

Moreover, the accessibility of the metal surface was controlled by the steric limitation of the protecting shell, which consists of the alkyl chain. A number of different types of polymer systems with nanoparticles have been investigated in catalytic reactions.

Although fine chemicals could be usually produced by using homogeneous catalysts with very high selectivities, their application is limited due to the difficulties in catalyst recovery. Homogeneous catalysts can also have poisonous metal complexes as well as strong alkalis or acids, which are environmentally harmful. Heterogeneous metal supported catalysts are industrially very attractive, because they are easy to reuse and separate. Moreover these catalysts are relatively inexpensive and stable compared to their homogeneous counterparts. The drawback of using heterogeneous catalysts in the field of fine chemicals is the relatively low selectivity to the desired product. Some example reactions, where selectivities are not at satisfactory level over heterogeneous conventional catalysts are chemoselective hydrogenation of α,β-unsaturated aldehydes, enantioselective hydrogenation of ketones and selective hydrogenation of alkynes and nitro-compounds, isomerisation of double bonds to conjugated double bonds as well as partial oxidation of sugars into valuable products or selective oxidation of benzylic alcohols into aldehydes (for instance, vanilin and piperonal). Usually promoters and additives are needed in order to achieve higher selectivities over monometallic supported catalysts. Also, fine tuning of the acid-base properties of the support with the proper analysis of the mutual influence of the acid-base and metallic sites is a powerful tool in designing the highly selective nanocatalysts. The most important technical aim in the NANOCAT project was to systematically test supported nanometal particles with a defined metal particle size in different local environments in selective oxidation, hydrogenation and isomerisation reactions for producing fine chemicals with high selectivities and transfer this new knowledge to catalyst manufacturers. In addition, the prevention of metal leaching and catalyst deactivation was investigated. This issue is of importance for the catalyst manufacturers and for the catalyst end-users, as the chemicals should be free from catalysts and the latter should be completely recovered.

One hypothesis for the NANOCAT project was that changing the size, the shape and the environment of a nanostructure changes also its functionality. The challenge was to get new fundamental knowledge from the connection between the properties of the catalytic nanomaterials and their performance in catalytic reactions. In spite of many experimental

evidences of the good catalytic performance of nanosized metal particles as catalysts there exist quite few theoretical approaches combining catalyst synthesis, characterisation, testing with Monte Carlo simulations and quantum chemistry calculations and finally with kinetic modelling. The final aim was to develop new fundamental knowledge at the molecular level and propose the surface reaction mechanisms. The main goal of the NANOCAT project was to study the influence of metal nanoparticle size and its environment on catalytic behaviour in some representative reactions of industrial importance. The problems addressed in the project are interdisciplinary ones and have several mutually related aspects concerning nanotechnology, material science, chemical kinetics and catalysis, and quantum chemistry as well as kinetic modelling.

The originality of the proposed work was in performing a comparative investigation with the catalysts having about the same metal particle size in both organic and inorganic supports in order to understand fully the impact of the metal environment on the catalytic activity and selectivity. There are no comparative investigations of such kind combining both organic and inorganic materials with different catalytic reactions. Moreover the environment is very often assumed to have certain effects, but the systematic studies are missing and they are incomplete to make any sound conclusions.

1.5 Approach

The NANOCAT project had following milestones: delivery of catalysts and database from catalyst characterisation, from catalyst screening and from kinetic tests, description of reaction mechanisms via kinetic and quantum chemical modelling, establishment of the fundamental knowledge on nanosized catalysts and dissemination of it, delivery of prototype catalysts including economical evaluation of these catalysts as well as arranging project meetings, mid-term assessment and final assessment.

1.6 Activities performed and results achieved

The work was divided into nine different subtasks (workpackages) and the interrelation of different workpackages in NANOCAT project is presented below

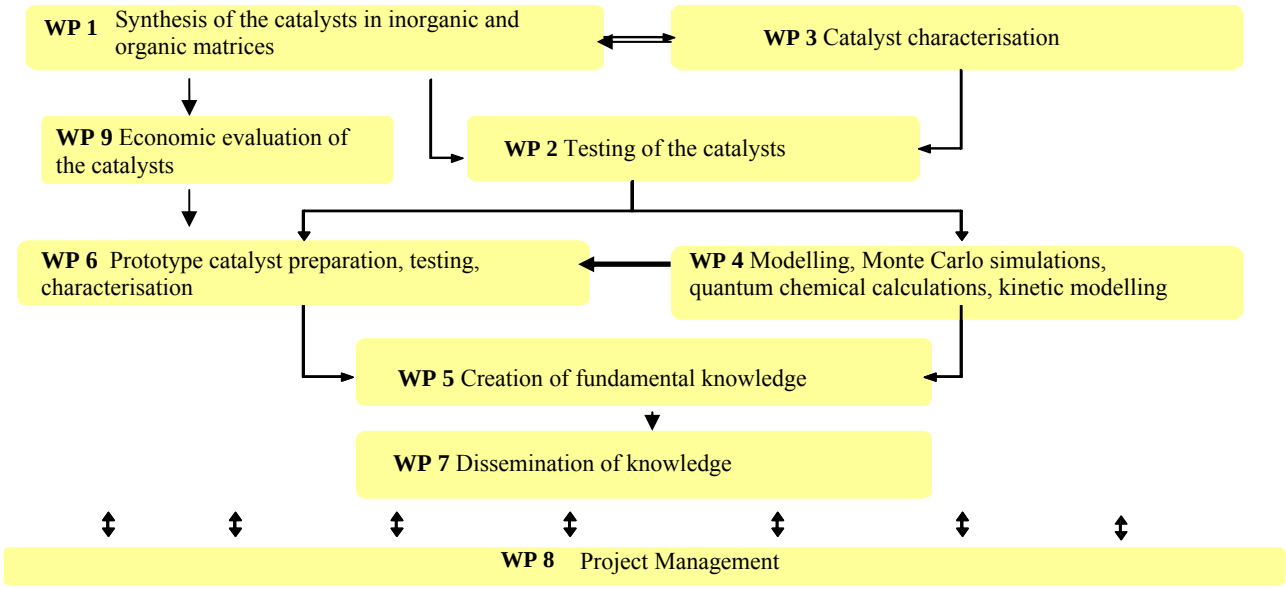

1.6.1 WP 1 – Catalyst synthesis

The objective was to prepare catalysts incorporated with nanosized metal particles (1-10 nm). Catalyst support materials, such as zeolites, mesoporous inorganic matrices, polymer matrices and carbon nanofibres, were utilized to obtain metal particles of nanosize. Palladium, platinum, gold, and ruthenium were incorporated into the organic and inorganic matrices, since these metals are commonly used in the synthesis of fine chemicals. Also bi-metallic catalysts were synthesized in order to further improve the activity and selectivity to the desired products. The objective, the milestone (M1), and the deliverables D1-D4 were all fulfilled, meaning that WP 1 has been successfully accomplished.

1.6.1.1 Micro- and mesoporous inorganic matrices

Zeolites are three-dimensional crystalline aluminosilicates containing channels and cavities of molecular dimensions. The shape and size of the pores can be varied; the pore size for zeolites ranges from 0.3 nm to approximately 1.0 nm. While the small pores can provide beneficial shape selectivity in some reactions, they can cause diffusion problems in other reactions and the pores can even be too small for some molecules to enter into. Mesoporous inorganic matrices can be used when micropores are too small for the molecule.

There are two types of acid sites, namely Brønsted (proton donor) and Lewis (electron pair acceptor). Brønsted acid sites are created on the surfaces of the zeolite when Si^{4+} is replaced by Al^{3+} (or another trivalent cation). The substitution creates a negative charge,

which can be compensated by a proton. In this way the number of Brønsted acid sites can be varied by changing the Si/Al ratio; as the Si/Al ratio decreases, the number of Brønsted acid sites (protons) increases.

Partner 1 (AAU) and partner 3 (UPMC) were involved in the synthesis of micro- and mesoporous inorganic matrices incorporated with metals of nanosize. Metal was incorporated using impregnation, ion-exchange and in-situ methods. The metal content and the concentration of acid sites were varied. Partner 1 focused on synthesis of Beta-22, MCM-22, and ZSM-5 zeolites and the mesoporous material MCM-41 and the incorporation of metal such as Pd, Pt, Au and Ru into these materials as well as into Beta-150, Beta-300, Mordenite, and Y zeolites. Partner 3 synthesized the mesoporous materials MCM-41 and SBA-15 as well as mesoporous alumina support, which were all incorporated with Pt.

The acidity of the Beta zeolite was varied by changing the SiO_2/Al_2O_3-ratio. Beta-22, having a SiO_2/Al_2O_3-ratio equal to 22, was synthesized and Beta zeolites with other ratios were supplied by Zeolyst International Company. These zeolites were incorporated with palladium using a vacuum evaporation impregnation method and palladium nitrate as precursor.

Unlike silicic and silicoaluminic materials which had been widely described in the literature, the synthesis of mesoporous aluminas, used as references exhibiting Lewis acidity only, had to be thoroughly investigated. The materials were characterized, within WP 3, at each step of their synthesis, in order to identify a sample that could be used as a support for Pt, in other terms whose structure and porosity would remain stable in aqueous solutions and upon thermal treatments. The characteristics of the samples prepared following five synthesis routes realized in water only are presented in Table 1.

Table 1 Synthesis parameters of the mesoporous aluminas and physicochemical data.

	Al precursor	Organic additives	pH of synthesis	BET surface area ($m^2.g^{-1}$)		Pore diameter (nm)	Mesoporous volume ($cm^3.g^{-1}$)
				reported	measured		
A	$Al(NO_3)_3$	Sodium dodecylsulfate	7	43-365	6	-	-
B	$AlCl_3$	$C_{16}H_{31}O_2Na$/ CTMABr	6.5	527	395	7.3	1.00
B	$AlCl_3$	$C_{16}H_{31}O_2Na$/ CTMABr	9	-	400	8.5, 15.1	1.10
B	$AlCl_3$	$C_{16}H_{31}O_2Na$/ CTMABr	11	530	308	< 4	0.22
C	$Al(NO_3)_3$	Pluronic P123	8	330	354	5.0	0.47
D	$Al(NO_3)_3$ + $NaAlO_2$	Pluronic P123	10.5	342	322	5.2	0.42
E	$Al(OiPr)_3$	Glucose	5	422	367	5.6	0.60

1.6.1.2 Polymer matrices

Among the nanoparticle syntheses that have emerged, one promising method involves nanoparticle formation within the core of amphiphilic block copolymer micelles. In this case the copolymer micelles are used as nanoscopic reaction vessels to grow inorganic metal nanocrystals resulting in hybrid nanocomposite materials. The synthesis of metal nanoparticles within the block copolymer micelles requires one block, which normally forms the micelle core and is able to coordinate with the metal compounds, while the second block in the corona provides good stability in the solvent medium.

Progress in polymer synthesis has made it possible to prepare external-stimuli responsive block copolymers known as double-hydrophilic block copolymers. These materials respond to changes in their environment such as pH, temperature and salt concentration and undergo micellization in aqueous media. Double-hydrophilic block copolymer micelles allow to adapt the nanoreactor approach of nanoparticle synthesis to aqueous systems since the functional core forming block can also interact with metal salts.

Another type of polymeric materials with unique and properties and promising applications in many fields of advanced technology, is that of chemically cross-linked polymer networks. Responsive microgels typically comprise lightly cross-linked latex particles of submicrometer dimensions that can become highly swollen in response to certain external stimuli.

Microgel-metal nanoparticle hybrid materials have been prepared using two general strategies. The first route involves metal loading of the microgels using preformed inorganic particles, while, in the second route, the nanoparticles are grown in situ within

the microgels. The former method usually suffers from low particle loading and aggregation of the nanoparticles. Moreover, the polymer matrix exerts no control over the growth and size of the nanoparticles. To avoid such problems, the synthesis of metal nanoparticles in the presence of the polymeric stabilizer has been explored.

Finally, modern hydrogels is another type of interesting polymeric materials which are water-compatible.[7] The employment of polymer networks as nanoreactors for the preparation of novel nanocomposite materials has been also proposed.[8] Unilike the double-hydrophilic block copolymer micelles, discussed above, which decompose to the unimer state upon changing the solution conditions, the network structure is stable independent of the solution pH, temperature, etc. which could be an advantage for application in a wide range of environmental conditions.

During the NANOCAT project partner 2 (TverTU) and partner 4 (FORTH) have focused on the synthesis of nanosized metal particles in polymer matrices.

Partner 4 focused on the synthesis and characterization of four different types of polymeric materials, (i) pH-responsive double-hydrophilic diblock copolymers, (ii) polymer microgel particles, (iii) random polymer networks and (iv) pH-responsive model networks, to be used as matrices for the formation of colloidal metal nanoparticles.

(i) A series of pH-responsive block copolymers have been prepared by GTP (Figure 1). Six diblock copolymers plus the two homopolymers, one of HEGMA and one of DEAEMA, were prepared, covering a range of MWs and compositions.

[7] (a) Buchholz, F.L.; Graham, A.T., Eds. *Modern Superabsorbent Polymer Technology*; Wiley, New York, **1998**.(b) Jen, A.C.; Wake, M.C.; Mikos, A.G. *Biotech. Bioeng.* **1996,** *50,* 357.

[8] (a) Gattas-Asfura, K.M.; Zheng, Y.; Micic, M.; Snedaker, M.J.; Ji, X.; Sui, G.; Orbulescu, J.; Andreopoulos, F.M.; Pham, S.M.; Wang, C.; Leblanc, R.M. *J. Phys. Chem. B* **2003,** *107,* 10464. (b) Pardo-Yissar, V.; Babai, R.; Shipway, A.N.; Bourenko, T.; Willner, I. *Adv. Mater.* **2001,** *13,* 1320.(c) Jones, C.D.; Serpe, M.J.; Schroeder, L.; Lyon, A. *J. Am. Chem. Soc.* **2003,** *125,* 5292. (d) Antonietti, M.; Gröhn, F.; Hartmann, J.; Bronstein, L. *Angew. Chem. Int. Ed. Engl.* **1997,** *36(19),* 2080.(e) Biffis, A.; Orlandi, N.; Corain, B. *Adv. Mater.* **2003,** *15(18),* 1551. (f) J. Scherble, R. Thomann, B. Ivan, R. Mulhaupt, *Journal of Polymer Science: Part B: Polymer Physics* **2001,** 39, 1429-1436.

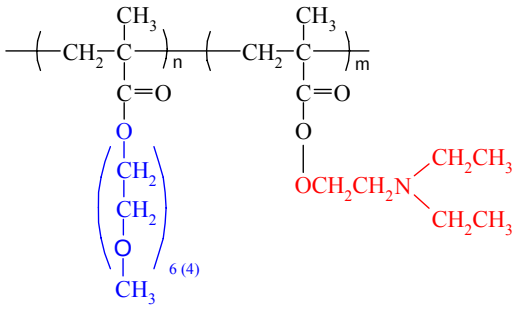

Figure 1 Chemical Structure of the PHEGMA-b-PDEAEMA diblock copolymers.

The polymerizations of this study were quantitative (yields close to 100 %), allowed good MW control and resulted in products with narrow MWDs. In all cases, the final copolymers were near-monodisperse (M_w/M_n's < 1.16) and good molecular weight control was achieved given the differences in hydrodynamic volumes between the PMMA calibration standards and the copolymers synthesized in this work.

(ii) Novel pH-responsive microgels based solely on 2-(diethylamino)ethyl methacrylate (DEA) as colloidal templates for the in situ synthesis of Pt nanoparticles at high metal loadings have been prepared. This polymer was selected because it is soluble in a remarkably wide range of organic solvents, which augurs well for its widespread use as a catalyst support. The pH-responsive PDEAEMA-based microgel particles were synthesized by emulsion polymerization of 2-(diethylamino)ethyl methacrylate with poly(propylene glycol) diacrylate cross-linker in water at pH 9 using a monomethoxy-capped poly(ethylene glycol) methacrylate (M_n = 2000) stabilizer. Ultrafiltration was used to eliminate excess stabilizer, as well as traces of monomer and initiator, in order to purify the PDEAEMA latex particles.

(iii) Random polymer gels with different functionalities were also synthesized by the free-radical copolymerization of functional monomers with a difunctional crosslinker. Six different monomers were used for the network synthesis: two basic monomers 2-(dimethylamino)ethyl methacrylate (DMAEMA) and DEAEMA carrying hydrophilic and hydrophobic tertiary amine groups respectively at neutral pH, one acidic monomer methacrylic acid (MAA), one neutral hydrophilic monomer HEGMA and two hydrophobic monomers methyl methacrylate (MMA) and benzyl methacrylate (BzMA).

(iv) Finally, we have also synthesized a series of pH-responsive model networks based on hydrophilic poly(tetra(ethylene glycol) methacrylate), PTEGMA, and ionizable, pH-sensitive poly(2-(diethylamino) ethyl methacrylate), PDEAEMA, units by GTP. Both the

network architecture and the TEGMA / DEAEMA composition were varied independently (Figure 2).

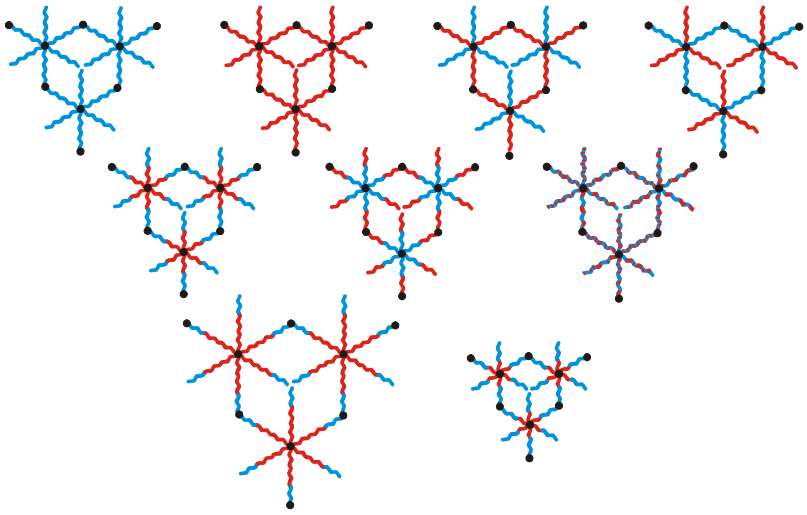

Figure 2 Schematic representation of the structures of all network architectures prepared. The TEGMA units are shown in blue while the DEAEMA units are drawn in red.

Partner 2 focused on preparation of polystyrene-poly-(4-vinylpyridine) (PS-P4VP) and poly(ethylene oxide)-block-poly-(2-vinylpyridine) PEO-P2VP polymer matrices and Ru-, Pt, Pd – containing hypercrosslinked polystyrene (HPS), PS-P4VP, PEO-P2VP, catalysts. The conditions providing formation of stable nanoparticles (Ru, Pt, Pd) of 1-2 nm in diameter in organic matrices were found.

For the report time Partner 2 developed the method to synthesize PEO-b-P2VP using ATRP. For that, two consecutive reactions were performed. First, PEG or PEGM were reacted with halogenated acid chloride to provide required functionality for ATRP:

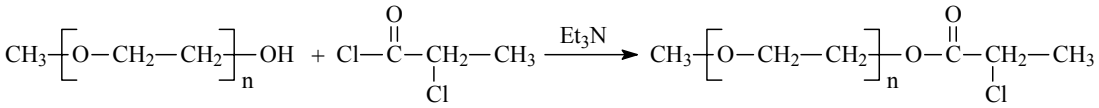

Then this compound was used in 2-vinylpiridine ATRP using Cu(I)Cl as catalyst:

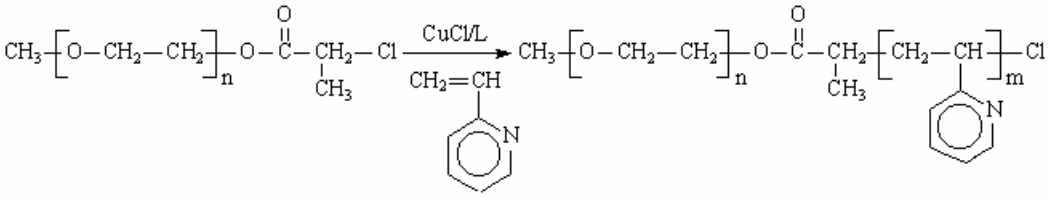

Anionic living polymerization has been used to synthesize PS-P4VP, diblock copolymers with pre-specified molecular weight and composition and with narrow molecular weight distributions. The diblock copolymers were synthesized by sequential addition of

monomer, under high – vacuum (10^{-5} – 10^{-6} Torr) in tetrahydrofuran (THF) with rigorously purified monomers and solvents.

Metal was added to PEO-b-P2VP and PS-b-P4VP through metal colloid formation (Figure 3).

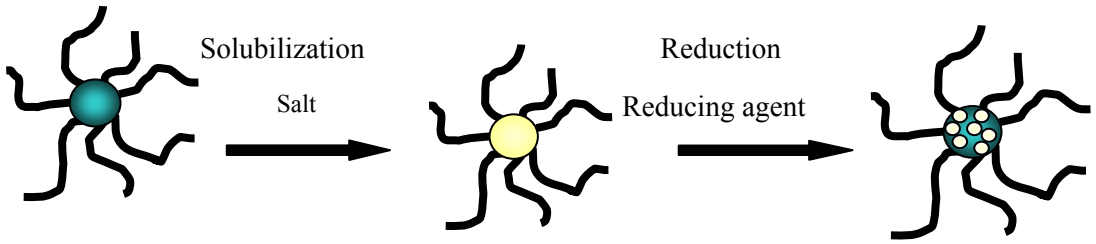

Figure 3 Metal colloid formation.

An alternative approach to the synthesis of a nanostructured catalyst is nanoparticle formation in polymer nanocavities. The impregnation of hypercrosslinked polystyrene (HPS) with tetrahydrofuran (THF) solutions containing platinic acid, palladium acid salts and ruthenium hydroxyde results in the formation of metal complexes within the nanocavities of HPS.

1.6.1.3 Carbon nanofibers

Carbon nanofibres (CNF) are grown by decomposition of carbon-containing gases on small metal particles. The material obtained is of high purity after the growth catalyst has been removed. Three common types of CNF are often described: ribbon-like (tubes), where the carbon layers are parallel to the growth axis, platelet, where the layers are perpendicular to the growth axis, and herringbone nanofibres, having layers stacked obliquely with respect to the growth axis. The CNF are pure, mechanically strong, and mesoporous, which makes them a perfect support material in liquid-phase reactions. The main aim of partner 6 (UU) was to tune the environment of noble metals on CNF and understand its influence on the activity and selectivity.

The synthesis of CNF was adapted from[9]. Homogeneous deposition precipitation (HDP) was used to deposit nickel (20 wt-%) on silica. The Ni/SiO_2 catalyst was placed in a quartz tube in a tubular oven and reduced. CNF were grown from Ni/SiO_2 by passing a synthesis gas mixture of CO, H_2 and N_2. The obtained raw material was refluxed in 1 M KOH to

[9] Toebes, M.L., et al. Journal of Catalysis, 2003. **214**(1): p. 78-87.

remove the silica (washing afterwards) and in concentrated nitric acid to remove the metal and oxidize CNF. Commercially produced nanostructured carbon of the platelet type (CNF-PL) and commercially produced CNT (CNT-MW) were obtained from FutureCarbon GmbH, Germany. These materials were also treated with 1 M KOH and concentrated nitric acid as described before in order to remove the growth catalyst.

The deposition of platinum and ruthenium was performed using homogeneous deposition precipitation (HDP) as described by Toebes et al.[9,10]. The obtained material was denoted with the prefix *Pt* or *Ru*. Part of the obtained material was treated in N_2-flow at 973K to remove the oxygen surface groups. The result is denoted using the suffix *–973*.

Platinum and ruthenium were also deposited via atomic layer deposition (ALD). In the latter method, the metal was vaporised and deposited on the support in a gas flow. The resulting catalysts differed in their metal particle size and also the amount of oxygen surface groups was adjusted to investigate its influence. For complete removal of the oxygen groups, a heat-treatment was performed at 973 K and the suffix -973 is used. Next to carbon nanofibres, platinum was also deposited on oxidized CNF-PL and CNT-MW via HDP as described before.

Pt/CNF-973 was evacuated and a tin precursor solution was impregnated on the Pt/CNF in static vacuum. The details of the impregnation can be found in Table 2. The intended molar ratio Pt/Sn is about 5:1. The impregnated Pt/CNF was kept under static vacuum, dried and reduced.

Tin was also deposited on Pt/CNF via reductive deposition precipitation (RDP) as adapted from Barbier et al. Pt/CNF was stirred in an aqueous HCl-solution or ethanol under H_2 atmosphere. Next, a HCl-solution containing $SnCl_4$ was added to the aqueous slurry or an ethanol-solution containing $Sn(C_2H_5)_4$ was added to the ethanol slurry and stirred for 30 min. After filtration, drying and reduction, the samples were treated in N_2-flow at 973 K. This material was denoted as *Pt-Sn RDP or Pt-Sn RDP-ethyl*.

[10] Toebes, M.L., et al. Journal of Catalysis, 2004. **226**(1): p. 215-225.

Table 2 Sample names, tin precursors, solvents used, tin weight percentages and Pt/Sn molar ratio's achieved after impregnation

Sample name	Tin precursor	Impregnation Solvent	Tin	Molar ratio
Pt-SnCl4	$SnCl_4$ (a)	DI water	0.38	4.8
Pt-SnCl2 (l.a.)	$SnCl_2$ (Merck)	Acidified DI water	0.37	4.9
Pt-SnCl2 (h.a.)	$SnCl_2$ (Merck)	Acidified DI water	1.61	1.1
Pt-SnC2O4	SnC_2O_4 (a)	H_2O_2 30% in water	0.34	5.3
Pt-Sn butoxide	$Sn(OC_4H_9)_4$(a)	ethanol	0.12	14.7
Pt-Sn citrate	Tin citrate			
Pt-Sn/AC (b)	-	-	0.5	6.1

(a) From Sigma-Aldrich. (b)Pt/Sn catalyst on activated carbon from Degussa.

Iron, gallium and germanium were deposited on Pt/CNF via RDP. Details of the deposition can be found in Table 3. Pt/CNF was slurried under H_2 in water or ethanol, depending on the promoter. Next, the promoter metal solution was added. Subsequently, the catalysts were filtered, dried and reduced. The oxygen surface groups were removed via a heat-treatment at 973 K. The resulting materials were denoted as *Pt-Fe(II) CNF RDP, Pt-Fe(III) CNF RDP, Pt-Ge CNF RDP or Pt-Ga CNF RDP.*

Table 3 Details of the deposition of different promoter metals on Pt/CNF

Sample name	Precursor	Solvent	Promoter	Molar ratio
Pt-Fe(II) CNF RDP	$Fe(CH_3COO)_2$	DI water	0.53	5.9
Pt-Fe(III) CNF RDP	$Fe(NO_3)_3.9\ H_2O$	DI water	1.25	5.8
Pt-Ga CNF RDP	$Ga(NO_3)_3.X\ H_2O$	DI water	0.77	5.9
Pt-Ge CNF RDP	$GeCl_4$	ethanol	0.66	5.9

1.6.2 WP 2 – Testing of the catalysts

The objective of WP 2 was to test the catalysts synthesized in workpackage 1 in several reactions. The aim was to correlate the catalytic behaviour to the catalyst properties. An additional aim was to investigate the possible metal leaching from the nano sized supported metal catalysts. The most promising materials were further used in kinetic study. The hydrogenolysis and dehydrogenation of hydroxymatairesinol, oxidation of lactose, L-sorbose, D-glucose, and piperonyl alcohol, as well as hydrogenation of crotonaldehyde and cinnamaldehyde were performed. The two milestones, a database from catalyst screening results relating catalytic activity in a variety of reactions (M2) and kinetic results from comparison between one metal of the same metal particle size (1- 2 nm) supported on inorganic/organic matrix and the correlation of the solvent nature to the

catalyst performance (M3), together with the two deliverables D5 and D6 were all fullfilled. The results from WP 2 served as input to WP 4, WP 5 and WP 6.

1.6.2.1 Hydrogenolysis and dehydrogenation of hydroxymatairesinol

Partner 1 tested palladium catalysts supported by activated carbon, zeolites, MCM-41, and carbon nanofibres (CNF) in the hydrogenolysis of hydroxymatairesinol (HMR) to matairesinol (MAT). Moreover, the promising Pd/CNF catalysts were tested in the dehydrogenation of HMR to oxomatairesinol (oxoMAT). The reaction scheme is presented in Figure 4. The reaction kinetics was investigated in detail with the most active/selective Pd/CNF catalyst. Furthermore, a deactivation study was performed and the correlation of the solvent nature with the catalyst performance was done. HMR is a lignan available in large amounts in Norway spruce knots, i.e. the part of the branch that is embedded in the stem. HMR is the only lignan that is available in large amounts in nature, but other lignans of interest can be synthesized using HMR as precursor. Lignans have anticarcinogenic and antioxidative effects and two of the lignans that have a potential to be used in pharmaceuticals, food additives or as technical oxidants are MAT and oxoMAT. The hydrogenolysis of HMR to MAT was performed in a stirred glass reactor under hydrogen flow and in an autoclave to test the influence of hydrogen pressure. The dehydrogenation of HMR to oxoMAT was done in the glass reactor under nitrogen flow.

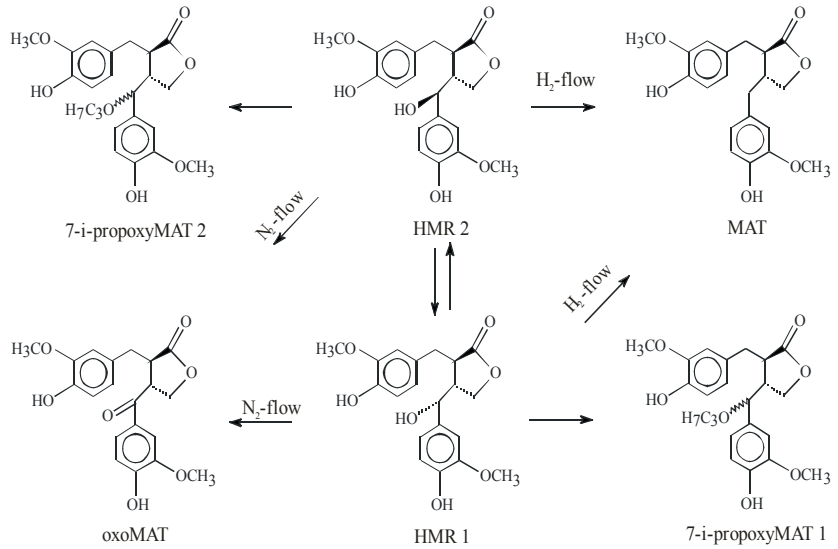

Figure 4 Reaction scheme of hydrogenolysis of hydroxymatairesinol (HMR, two diastereomers) to matairesinol (MAT) under hydrogen flow, and dehydrogenation of HMR to oxomatairesinol (oxoMAT) under nitrogen flow, and the etherification of HMR to 7-iso-propoxymatairesinol (7-i-propoxyMAT, two diastereomers) as side product.

The influence of support acidity on the activity and selectivity was investigated for the hydrogenolysis of HMR. It was concluded that for palladium catalysts supported by activated carbon and carbon nanofibres the activity increased when the concentration of acid sites on the support material increased. For the Beta zeolite, which is more acidic than carbon materials, the activity decreased when the acidity increased. For Pd/CNF catalysts, selectivity to MAT increased with acidity, for activated carbon and zeolites the selectivity was constant. The activity as well as the selectivity to oxoMAT increased with acidity when Pd/CNF catalysts were used in the dehydrogenation of HMR.

To study the solvent effects, the reaction was carried out (over a Pd/C catalyst) in ethanol, 2-propanol, *tert*-butanol, 2-pentanol, as well as in a mixture of 2-propanol and water (50:50 vol/vol). Over 70% of the hydroxymatairesinol was converted in 4 h when ethanol, 2-propanol, and 2-pentanol were used as solvents. The reaction was significantly retarded by mixing 2-propanol with water and the lowest activity was obtained in *tert*-butanol. Alcohols with shorter carbon chains were also interacting with the reactant resulting in lower selectivity; the byproducts 7-ethoxymatairesinol and 7-isopropoxymatairesinol were obtained in ethanol (the lowest selectivity) and in 2-propanol, respectively. Palladium impregnated activated carbon, and two Beta zeolites (H-Beta-300 and H-Beta-150, SiO_2/Al_2O_3 molar ratio 300 and 150) were investigated with respect to deactivation; consecutive experiments were performed with the catalysts being filtered, washed, dried, and re-reduced in between the runs. The catalysts were prone to deactivation caused by fouling; long chain alkanes and aromatic components were blocking the active sites.

In the kinetic study, the influence of mass transfer was studied by varying the stirring rate, the catalyst mass and the catalyst particle size. The influence of temperature and reactant concentration (at constant catalyst-to-reactant ratio) was studied. Moreover, the influence of hydrogen pressure was studied in an autoclave; it was noticed that the reaction rate as a function of pressure increased at lower pressures, but at higher pressure the reaction rate decreased with pressure increase.

1.6.2.2 Oxidation of lactose

Partner 1 tested palladium catalysts supported by activated carbon, zeolites, MCM-41, and carbon nanofibres (CNF) in the oxidation of lactose to lactobionic acid. Moreover, supported gold catalysts showed a very high activity in the oxidation reaction. A promising Pd/C catalyst as well as Au/Al_2O_3 were used in kinetic studies. Lactose is

available in large amounts from cheese whey, being an inexpensive material with only a small amount of it processed further to products. Lactose can be oxidised to lactobionic acid, which is a useful product since it could be used as acidulant, complexing agent, antioxidant or as feedstock for surfactant production. The oxidation of lactose was performed in a shaking reactor under oxygen flow. The reaction scheme is presented in Figure 5.

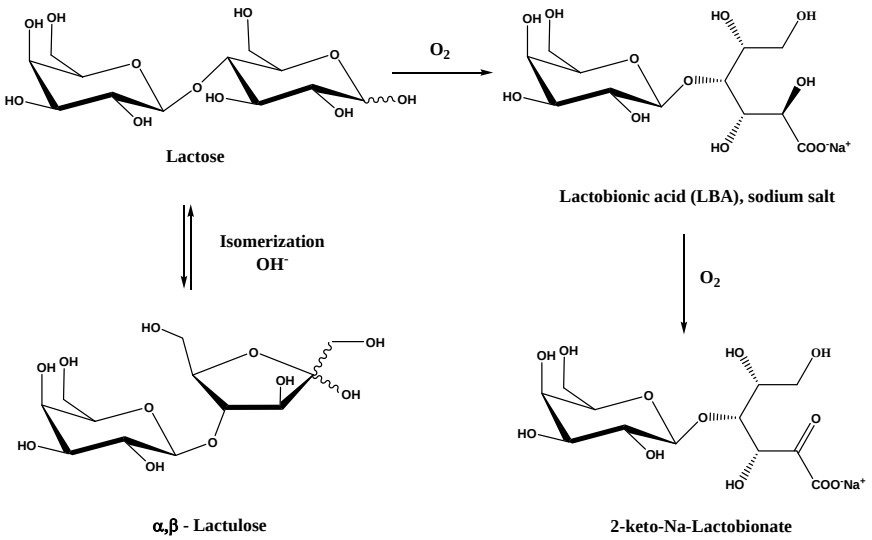

Figure 5 Oxidation of lactose to lactobionic acid (LBA) and 2-keto-Na-lactobionate.

The activity increased with the concentration of acid sites as Pd/CNF catalysts were used, whereas for Pd/H-Beta zeolite the activity decreased when the concentration of acid sites increased, e.g. showing the dependence similar to the one observed for hydrogenolysis of HMR (previous section).

The kinetics was studied by varying the oxygen feed rate, catalyst mass, temperature, pH. The highest concentration of lactobionic acid was obtained at pH 8 (pH interval 7-10) and at 70 °C (temperature interval 60-90 °C). At higher temperature or pH larger amounts of disproportionation products are formed.

1.6.2.3 Oxidation of L-sorbose and D-glucose

Partner 2 has tested catalysts on the base PS-P4VP, PEO-P2VP matrices, hypercrosslinked polystyrene impregnated with metals nanoparticles, zeolite based catalysts (NH_4-Beta-25, NH_4-Beta-75 and NH_4-Mordenite-20 based catalysts delivered from Partner 1), HEGMA PDMAEMA based catalysts (delivered from Partner 4), in L-sorbose and D-glucose oxidation. The aim of the investigation is to correlate the catalytic behaviour to the catalyst

properties and mean diameter of nanoparticles and additional aim is to investigate the possible metal leaching from the nanosized supported metal catalysts.

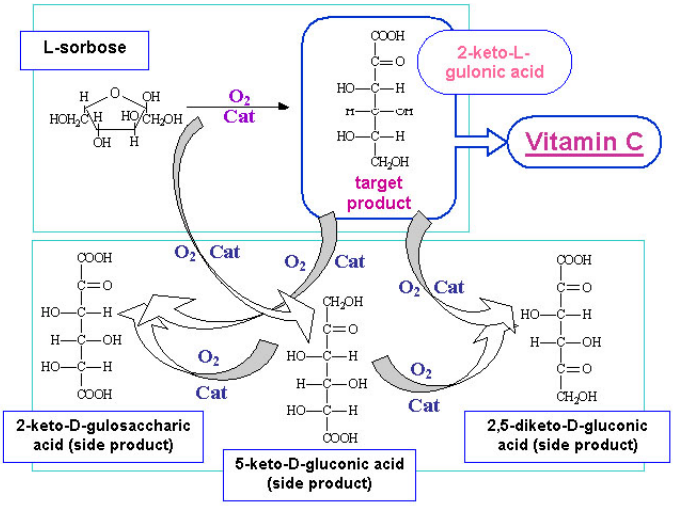

Figure 6 Reaction scheme for the oxidation of L-sorbose.

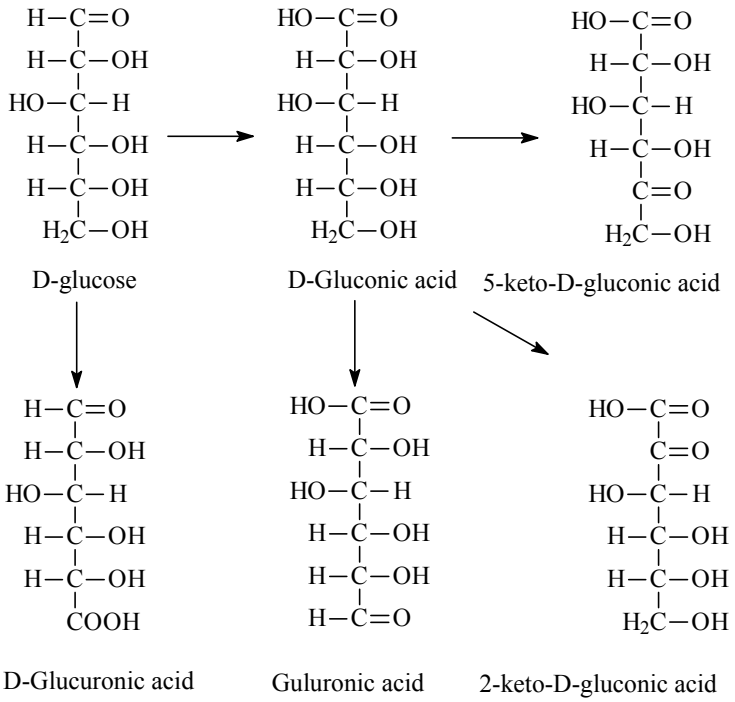

Figure 7 Reaction scheme for the oxidation of D-glucose.

L-sorbose direct oxidation to 2-KGA (see Figure 6), which is the main intermediate in vitamin C production, was performed with Pt catalysts. Pt/C (5% Pt) provides only 28-37% 2-KGA yield at 100% L-sorbose conversion. Samples of Pt colloids prepared in PEO-b-P2VP and HPS-Pt2 were studied. The best catalytic system for oxidation was found to be 3% Pt/HPS catalyst. The recycling of 3% Pt/HPS also showed promising results.

D-glucose oxidation (see Figure 7) serves as an intermediate step in calcium gluconate synthesis. Samples of Ru, Pt, Pd colloids prepared in HPS, PEO-P2VP, PS-P4VP matrix were studied, as well as zeolite based and PHEGMA-PDMAEMA based catalysts. Several methods based on chemical, electrochemical, biotechnological, and catalytic synthesis are currently available for the oxidation of D-glucose. The catalytic route promises to be the most viable. Mostly carbohydrate functional groups are initially protected from oxidation and after the initial functional groups must be recovered after oxidation resulting in loss of end product. Direct catalytic oxidation of D-glucose to D-gluconic acid avoids carbohydrate groups protection step. This reaction has been performed in the presence of O_2 over a noble metal catalyst deposited on activated carbon, aluminum oxide etc. The selectivity unfortunately decreases from 95% at 30% conversion to 40% at 100% conversion and therefore synthesis of novel catalysts is of special interest in this area.

Optimal conditions providing the selectivity of 99% at 99% conversion were found. Moreover, the novel colloidal catalyst is very active and comparatively selective in D-glucose oxidation even after the repeated use (Table 4). There is no significant loss of activity and selectivity even after 15 recycles.

Table 4 The catalytic activity of 1% Ru/HPS after recycling

Number of catalytic cycles	TOF$\times 10^{-4}$ (mol/mol Pt-s)	Selectivity (%)
1	8	99
10	7.5	99
15	7.8	99

The kinetics of the oxidation of D-glucose was studied by varying the catalyst and D-glucose loading at 60 °C. The highest TOF of D-glucose conversion and selectivity were observed for HPS-Ru 0.74%. The HPS-Ru 2.71% and HPS-Ru-0.05% have lower TOF and selectivity. Moreover, the effect of pH and temperature was studied. The maximum selectivity was discerned when the reaction was executed at pH 6.5-7.2. At values lower then pH 6 and higher than 8 the oxidation selectivity diminished.

Figure 8 shows the effect of temperature within the range from 30 to 60 °C, higher temperature results in both higher TOF and higher substrate conversion. The selectivity of the D-glucose oxidation remained 99-97%. Further rise in temperature, however, led to a drop in selectivity.

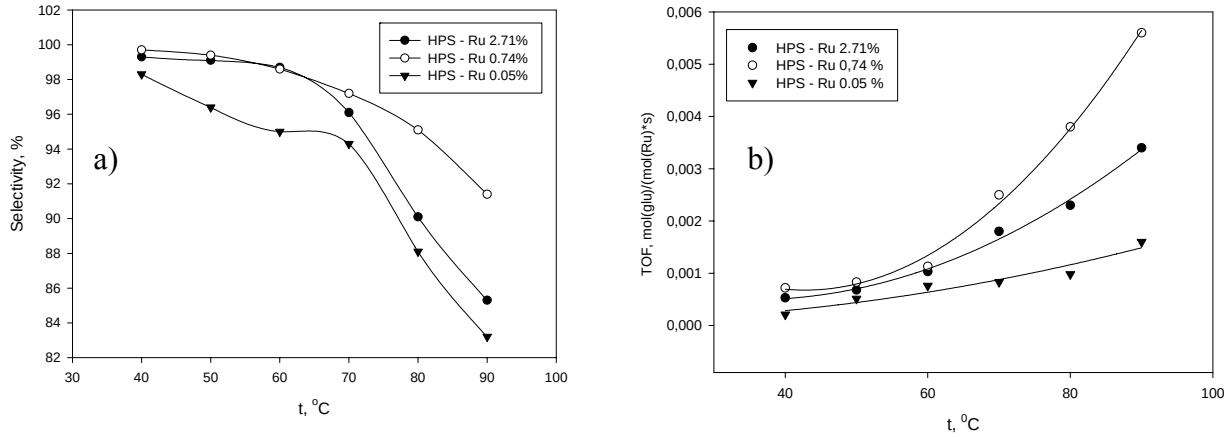

Figure 8 a) Dependence of D-glucose oxidation reaction selectivity on temperature b) Dependence of HPS based catalyst activity on temperature

1.6.2.4 Hydrogenation of crotonaldehyde and cinnamaldehyde

Partner 6 tested catalysts in crotonaldehyde and cinnamaldehyde hydrogenation. Unless otherwise stated, test reactions were performed as follows: crotonaldehyde or cinnamaldehyde were hydrogenated at 313 K and in 1200 mbar H_2. The catalyst (sieve fraction 25-90 μm) was suspended in isopropanol combined with deionised water. Deionised water was not added for the crotonaldehyde hydrogenations.

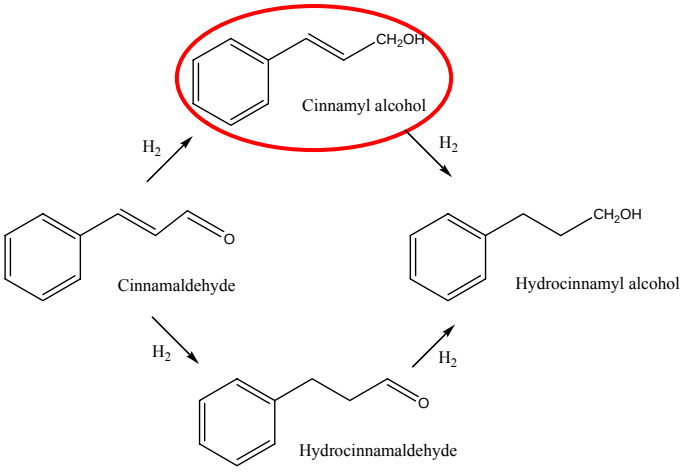

Figure 9 The hydrogenation pathway of cinnamaldehyde; the desired product is encircled.

To investigate the influence of support structure, crotonaldehyde hydrogenations were performed. The initial activity and selectivity of Pt/CNF (HDP), Pt/CNF-973 (HDP), Pt/CNT MW, Pt/CNT MW-973, Pt/CNF-PL and Pt/CNF-PL-973 were studied. Some of

the results are summarized in Table 5. Though initial activities were quite high and in the same range for all catalysts, the total activity of the CNT-MW supported catalysts decreased rapidly in time. The activity of the CNF-PL supported catalyst was hardly affected by the heat-treatment. The selectivity to crotyl alcohol was completely zero for the majority of the catalysts.

Table 5 Initial activities and selectivity's for the different catalysts during the crotonaldehyde hydrogenation

	Pt/CNF (HDP)	Pt/CNF -973 (HDP)	Pt/CNT MW	Pt/CNT MW-973	Pt/CNF-PL	Pt/CNF-PL-973
Selectivity (%) towards crotyl alcohol	0	13.7	0	0	0	0
TOF $_{intial}$ (min^{-1})	5.90	7.40	4.76	17.45	4.68	3.29

The effect of solvent in the selective hydrogenation cinnamaldehyde (see Figure 9) was studied using Pt/CNF-973 catalyst. To this purpose, different solvents were used for the reaction: THF, n-hexane, ethanol, isopropanol, isopropanol/water, DMF and DMSO. The result of this study is depicted in Figure 10. Using DMSO as solvent, no hydrogenation activity was observed and therefore, this run is not depicted in Figure 10. It was concluded that alcohols and alcohol/water mixtures show the highest activity. No deactivation was observed, since also the reaction showed a first order relation with the concentration of cinnamaldehyde during the reaction. Therefore, these solvents are the most appropriate ones to perform the catalytic tests.

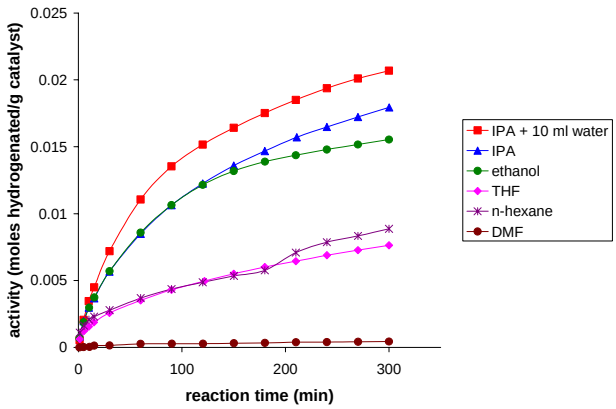

Figure 10 The catalytic activity of Pt/CNF-973 for the cinnamaldehyde hydrogenation in different solvents. IPA means iso-propanol.

The activity and selectivity of the prepared platinum-tin catalysts are plotted in Figure 11 and compared to mono-metallic *Pt/CNF-973*. *Pt-Sn RDP-ethyl* and *Pt-Sn RDP* are much more active compared to mono-metallic *Pt/CNF-973,* even more than a factor 2. *Pt-Sn RDP* shows 8-9% higher selectivity towards cinnamyl alcohol compared to *Pt-SnCl2 (l.a.)* and combines therefore the highest selectivity (72%) and activity of all prepared catalysts. The selectivity of *Pt-Sn RDP-ethyl* is of the same order as mono-metallic *Pt/CNF-973*. The Pt/CNF catalysts which were promoted using iron, gallium and germanium via RDP were also tested for the liquid-phase hydrogenation of cinnamaldehyde. The resulting initial activities and selectivity's for the promoted catalysts to cinnamyl alcohol are summarized in Figure 12. The selectivity towards cinnamyl alcohol for all mentioned catalysts was enhanced, even up to 92% for Pt-Fe(II) CNF RDP. The observed enhancement in selectivity is ascribed to a well-defined interaction of the different promoter metals with platinum. For all investigated promoter metals it is clear that either the selectivity or activity is enhanced compared to the mono-metallic catalyst. It is clear that for the tin-promoted catalysts, the RDP synthesis method is required to gain a substantial increase in activity or selectivity, though impregnation of $SnCl_2$ also results in a better-performing catalyst.

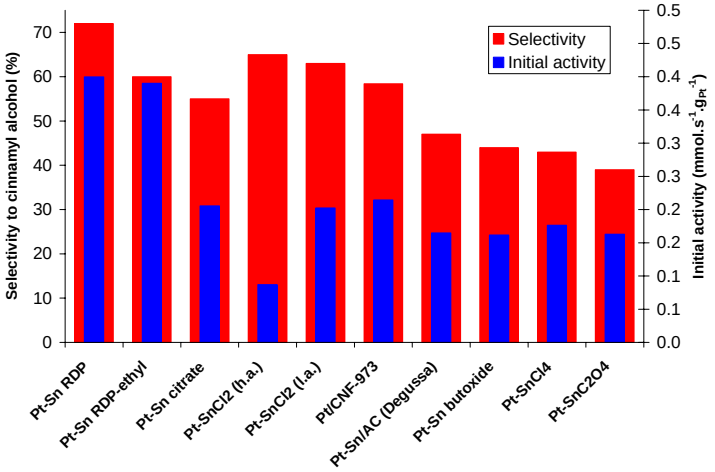

Figure 11 Selectivity and initial activity of the different platinum-tin catalysts for the selective hydrogenation of cinnamaldehyde, compared to mono-metallic platinum on CNF.

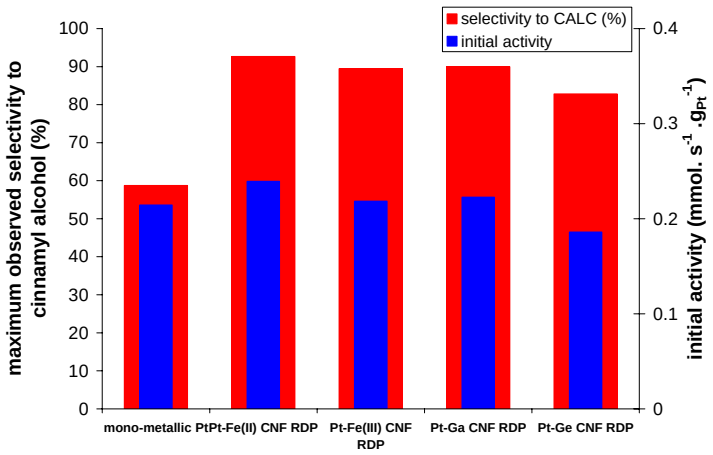

Figure 12 Initial activities (blue; right axis) and maximum observed selectivity's (red; left axis) for platinum catalysts combined with different promoter metals. The catalysts were tested for the cinnamaldehyde hydrogenation.

Particle size effects for platinum and ruthenium catalysts prepared via HDP and ALD were studied using the cinnamaldehyde hydrogenation as test reaction. Pt/CNF (HDP) and Pt/CNF (ALD) reached only about 40 % conversion of cinnamaldehyde after 300 min forming hydrocinnamaldehyde as the major product. Via a heat-treatment the oxygen surface groups were removed, which enhances the activity of all samples. Pt/CNF-973 (ALD) converted the majority of cinnamaldehyde into hydrocinnamaldehyde. Pt/CNF-973 (HDP) resulted in high amounts of cinnamyl alcohol (max 59 %). In Figure 13 the conversion of cinnamaldehyde is plotted versus the selectivity to cinnamyl alcohol. The selectivity of the non heat-treated catalysts is in the same range, Pt/CNF (ALD) is slightly more selective compared to Pt/CNF (HDP). Upon heat-treatment, the selectivity is enhanced and Pt/CNF-973 (HDP) shows the highest selectivity and activity. The latter catalyst has smaller metal particles compared to Pt/CNF-973 (ALD).

Ru/CNF-973 (HDP) catalyst converted all cinnamaldehyde within 90 min, while Ru/CNF-973 (ALD) converted 65% of cinnamaldehyde in 300 min. For both catalysts hydrocinnamaldehyde is the major primary product. In Figure 14 the conversion of cinnamaldehyde for the ruthenium catalysts is plotted versus the selectivity to cinnamyl alcohol. The selectivity to cinnamyl alcohol is higher for Ru/CNF-973 (HDP) compared to Ru/CNF-973 (ALD). Also Ru/CNF-973 (HDP) has smaller metal particles compared to the latter.

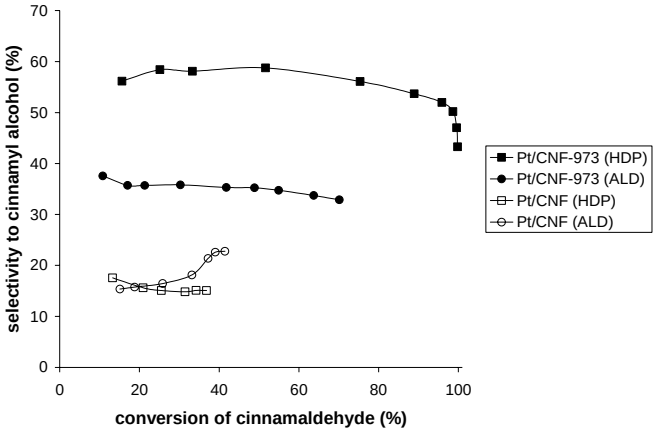

Figure 13 Conversion vs. selectivity of the four platinum catalysts. The selectivity enhances after heat-treatment; the catalysts were tested for the cinnamaldehyde hydrogenation.

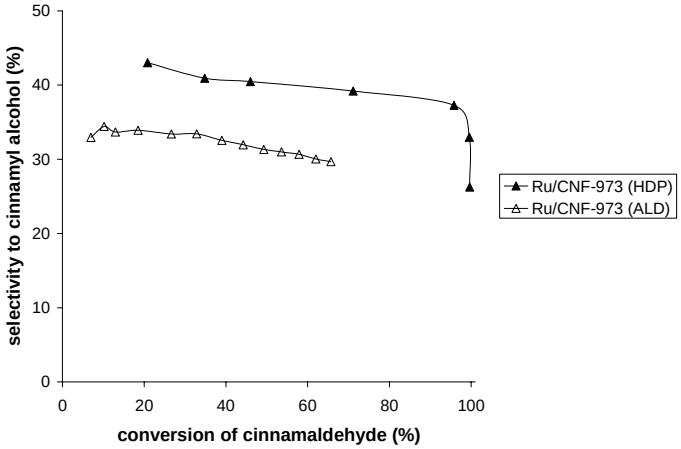

Figure 14 Conversion vs. selectivity of the two ruthenium catalysts. The catalysts were tested for the cinnamaldehyde hydrogenation.

1.6.2.5 Oxidation of piperonyl alcohol

Partner 8 conducted piperonyl alcohol oxidation to piperonal (see Figure 15) using supported metal catalysts, where the support materials were SiO_2, the polymer HPS, the zeolites Beta, Y, Mordenite, MCM-22, and ZSM-5 and the mesoporous material MCM-41, and the metals were Pd, Ru, Pt, and Au.

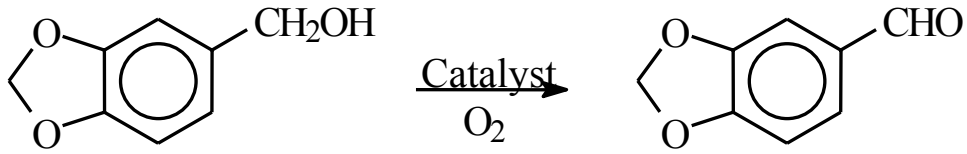

Figure 15 Reaction scheme for the oxidation of piperonyl alcohol to piperonal.

The comparison of catalytic activity of samples supported on the polymer support have shown that Pt-containing catalysts exhibit a much higher activity in benzylic alcohol oxidation than the Pd- and Ru-containing catalysts under the same conditions. The order of the catalytic activity is as follows: HPS-Pt >> HPS-Pd > HPS-Ru. The Ru- and Pd-samples anchored in zeolite matrixes possess higher catalytic activity.

The Pd/BETA zeolite catalysts with a lower silica-to-alumina ratio possess a higher catalytic activity in benzylic alcohol oxidation reaction. The order of the catalytic activity is as follows: 4.1%Pd/HBETA-11 > 4.7%Pd/HBETA-25 > 3.9%Pd/HBETA-150 > 2.0%Pd/HBETA-300.

The catalytic activity of Ru-catalysts is not so much different for the samples on different supports. The order of activity is as follows: 5%Ru/MCM-41 > 5%Ru/Y > 5%Ru/SiO_2 > 5%Ru/BETA.

The comparison of catalytic activity for both calcined and reduced Pd samples supported on different zeolites have shown that the order of activity is follows: Pd-H-Beta-25-IE-red > Pd-H-MORD-IE-red > Pd-H-MORD-IE-cal > Pd-H-Beta-25-IE-cal ≈ Pd-H-BETA-75-IE-red > Pd-H-BETA-75-IE-cal > Pd-H-MORD-20-red > Pd-H-MORD-20-cal. Moveover it was found that the order of catalytic activity in benzylic alcohol oxidation reaction for Pd calcined samples correlates with the Lewis acid sites strength.

The catalytic activity for calcined and reduced Au containing catalysts exhibit different activity in benzylic alcohol oxidation. The highest catalytic activity was found for bimetallic 2 wt% Au-0.1 wt%Ce-MCM-41-20 calcined sample. The order of catalytic activity for both calcined and reduced Au samples is follows: Au-Ce/MCM-41-20-cal > Au/BETA-150-red > Au-Ce/MCM-41-20-red > Au/BETA-150-cal ≈ Au/ZSM-5-30-red > Au/ZSM-5-30-cal > Au/MCM-41-20-red ≈ Au/MCM-41-20-cal > Au/MORD-20-cal ≈ Au/MORD-20-red > Au/MCM-22-30-cal = Au/MCM-22-30-red. The order of catalytic activity in benzylic alcohol oxidation reaction for Au samples does not correlate with the Lewis acid sites strength found on the surface.

1.6.2.6 Catalytic profiling analysis

Partner 7 (Deg) developed a method (so called “profiling analysis”) with which catalytic characteristics of precious metal powder catalysts for fine chemical application can be efficiently and comprehensively elucidated. Moreover, those physical properties can be

identified which do influence the catalytic performance profiles significantly. Thus, the profiling method takes into account the complex relationship of physico-chemical parameters of solids and catalytic performance parameters. Catalytic profiling analysis includes a set of test reactions which are very sensitive with respect to catalyst properties.

The developed high-throughput methodology and method of data analysis which allows comparing the new materials developed in the project on a very comprehensive basis with industrial catalysts (milestone 2). Advantages of new materials for industrial application can be analysed by this method with a superior view. The method was applied to diverse industrial Pd catalysts and to nano-structured catalysts developed by the partners (Partner 2: N 138 Pd 3% Ru 1% HPS, N 139 Pd 3% Au 1% HPS, N 120 H MN270/3860 5% Pt, Cat 120 H MN-200 111/100 5% Pt, N 120 H MN-202 1/02 5% Pt, PHEGMA-PDMAEMA Pd 1,68% Al2O3, PHEGMA-PDMAEMA Pt Al2O3, Partner 3: Pt catalysts on mesoporous nanostructured aluminosilicates).

In order to analyse relationships between catalytic profiles and solids' characteristics of solids, a similar procedure as for the catalytic profiling is applied to physico-chemical characteristics (milestone 3). Hereby, measurable solid properties such as metal particle size, metal dispersion, binding energies of elements such as noble metals and oxygen, pore size distribution of supports etc. are summarized in solid characteristics profiles followed by statistical similarity analysis. The methodology was validated for four Pd (5 wt-%)/C powder catalysts prepared by different methods and showing different metal particle size, metal dispersion and oxidation state of Pd.

1.6.3 WP 3 – Catalyst characterisation

The objective of WP 3 was the characterisation of the micro-mesoporous matrices, carbon nanofibres and polymer matrices as well as the nanosized metal supported catalysts synthesized in WP 1. Moreover, to characterize the solution properties and swelling behaviour of the linear and cross-linked polymers respectively, before the formation of the metal nanoparticles and to investigate the changes in the micelle and gel characteristics after the metal incorporation and the metal nanoparticle formation. Partners involved were 1 (AAU), 2 (TverTU), 3 (UPMC), 4 (FORTH), 6, (UU), 7 (Deg), and 8 (IOC). The materials were characterized using N_2-physisorption (surface area), CO- and H_2-chemisorption (dispersion, metal surface area), direct current plasma atomic emission spectrometry (DCP, metal content), inductively coupled plasma emission mass-

spectrometry (ICP-MS, metal content), Transmission electron microscopy (TEM), Scanning electron microscopy (SEM), Fourier transform infrared spectroscopy (FTIR, pyridine adsorption for determination of concentration of acid sites), titrations using NaOH for determination of acid sites, X-ray powder diffraction (XRPD), X-ray fluorescence analysis (XFA), Atomic force microscopy (AFM), ASAXS, UV-Visible spectroscopy (UV/Vis), dynamic light scattering (DLS), proton nuclear magnetic resonance spectroscopy (^{1}H NMR), and Electron paramagnetic resonance (EPR). Moreover, Diffuse-Reflectance Fourier-Transform spectroscopy (DRIFT), X-ray photoelectron spectroscopy (XPS) and bulk sensitive method: X-ray absorption spectroscopy (XAS = XANES + EXAFS) with the goals to reveal the electronic state and morphology of the supported metals, as well as to unravel the mutual effects of the acid and basic sites on the state of the metal nanoparticles and vice versa, were performed. The two milestones, M 4 with delivery of the micro-mesoporous materials and carbon nanofibres without and with metal incorporation provided with structural data and M 5 with delivery of the polymer matrices without and with metal incorporation provided with structural data, together with the two deliverables, D7 and D8 database from structural characterisation of micro-mesoporous matrices and carbon nanofibres without and with metal incorporation and database from structural characterisation of polymer matrices without and with metal incorporation. Input into WP 4, WP 5 and WP 6.

1.6.3.1 Characterization of polymers

Partner 4 characterized (i) the aqueous solution behaviour and micelle characteristics of the diblock copolymers as a function of the solution pH and the degree of protonation of the polymer, (ii) the swelling behaviour of the microgel particles as a function of solution pH, (iii) the degrees of swelling (DSs) of all random networks in acidic and neutral water and in THF, as well as (iv) the sol fraction, the effective pKs, and the degrees of swelling at low and high pH water and in THF of the model networks.

(i) The diblock copolymer prepared exhibited interesting solution properties in water upon addition of acid or base. The aqueous solution behaviour and micelle characteristics of a PHEGMA$_{50}$-*b*-PDEAEMA$_{50}$ diblock copolymer as a function of solution pH and the degree of protonation (α) of the ionizable PDEAEMA block were investigated by dynamic light scattering (DLS) and proton nuclear magnetic resonance spectroscopy (^{1}H NMR). The results suggested clearly that the micellization process is not a gradual transformation

that takes place over the whole deprotonation range but a rather sharp transition that occurs for lower than 20% protonated monomer units. The equilibrium micellar size was found around 15 nm with the PDEAEMA blocks forming the micelle cores and the PHEGMA ones comprising the micelle coronas.

Platinum nanoparticles were grown next within the cores of these micelles by incorporation of metal compounds (H_2PtCl_6, K_2PtCl_6) followed by metal reduction. The polymer behaviour, polymer-metal interactions and metal nanoparticle characteristics upon metal precursor incorporation and after metal reduction, were studied by dynamic light scattering (DLS), UV/Vis and ^{1}H NMR spectroscopy, transmission electron microscopy and X-ray diffraction.

Different synthetic procedures for the preparation of Pt nanoparticles inside the micellar cores were investigated (see Figure 16).

Method A

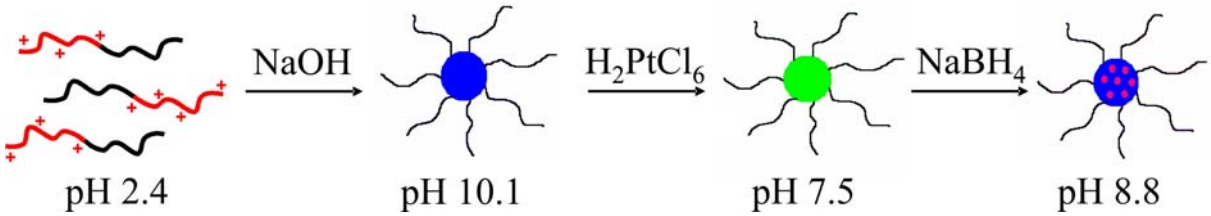

Method B

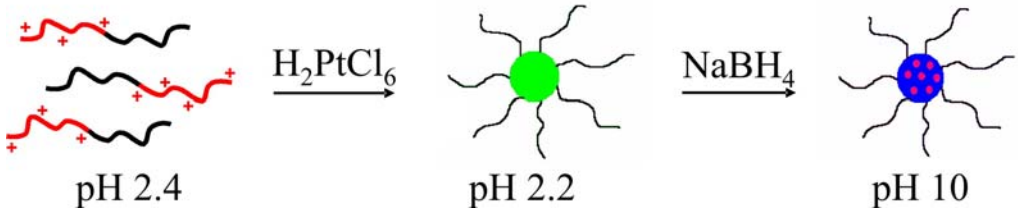

Figure 16 Schematic representation of the synthetic procedures followed for the metal nanoparticle formation using methods A and B.

Addition of the metal precursor in a molecular copolymer solution at low pH, resulted in polymer-metal complexation and a metal-induced micellization process leading to the formation of stable equilibrium structures, as revealed by DLS. ^{1}H NMR studies also confirmed the metal-induced micellization process and further verified the formation of compact non-hydrated cores resulting from the charge neutralization process. Metal reduction at low pH, carried out next, lead to the formation of metal nanoparticles and the partial decomposition of the metal-induced micelles, while the formation of only a few loose structures arising from possible weak interactions between the reduced metal and the

polymer as observed. NMR studies also revealed the hydration of both polymer blocks indicating the decomposition of the micelles. Finally, DLS showed that upon increasing the solution pH, micelles containing the metal nanoparticles, are formed again due to the hydrophobicity of the DEAEMA units. On the other hand, increase of the pH with NaOH before metal reduction showed large fluctuations in the scattered intensity suggesting that metal-PHEGMA interactions take place in the solution outside the micelles and thus lead to the formation of nanoparticles in the exterior of the micellar core after metal reduction.

In the second method, addition of H_2PtCl_6 in a micellar copolymer solution at high pH led to the partial decomposition of the micellar structures due to the protonation of the PDEAEMA block. However, the presence of the metal precursor in solution did not lead to a metal-induced micellization process similar to that described above at low pH, despite the protonation of the amine groups. Moreover, ^1H NMR studies showed that the PDEAEMA blocks remained non-hydrated upon addition of H_2PtCl_6 at high pH. It was shown that the presence of NaCl salt in the initial micellar solution did not prohibit the polymer metal interaction and it was rather the hydrolysis of the metal salt at high pH which caused this unexpected effect.

The crystalline structure of the metal nanoparticles was also confirmed by XRD studies which also allowed to estimate the size of the nanoparticles around 3.5 nm for two different loading ratios N/Pt = 3/1 and N/Pt =1/1.

(ii) Dynamic light scattering was used to characterize the microgel swelling that occurred on complexation with H_2PtCl_6 and also during the in situ metal reduction. This loading process revealed two effects that strongly influenced the swelling behavior of the microgels during metal loading. Addition of the platinic acid, H_2PtCl_6, to the latex particles caused protonation of the tertiary amine groups, leading to microgel formation. On the other hand, the divalent $PtCl_6^{2-}$ anions acted as an ionic cross-linker for the protonated amine groups, which caused microgel deswelling. The equilibrium between these two opposing effects determined the final size of the microgels after H_2PtCl_6 complexation. Both the metal salt-loaded microgel and the metal nanoparticle-containing latex particles possessed well-defined equilibrium structures with characteristics that were independent of the synthesis method, as confirmed by dynamic light scattering. Moreover, UV-visible absorption spectroscopy indicated that the in situ reduction of Pt(II) to Pt(0) was complete. Finally, the dimensions of the Pt nanoparticle-loaded microgels were

similar to those of the microgel precursor prior to H_2PtCl_6 complexation, suggesting that even at high metal loadings the Pt nanoparticles had no significant effect on the dimensions of the de-swollen latex. X-ray diffraction studies confirmed the formation of Pt nanocrystals of around 4 nm diameter, which was in reasonably good agreement with the Pt diameter estimated by TEM.

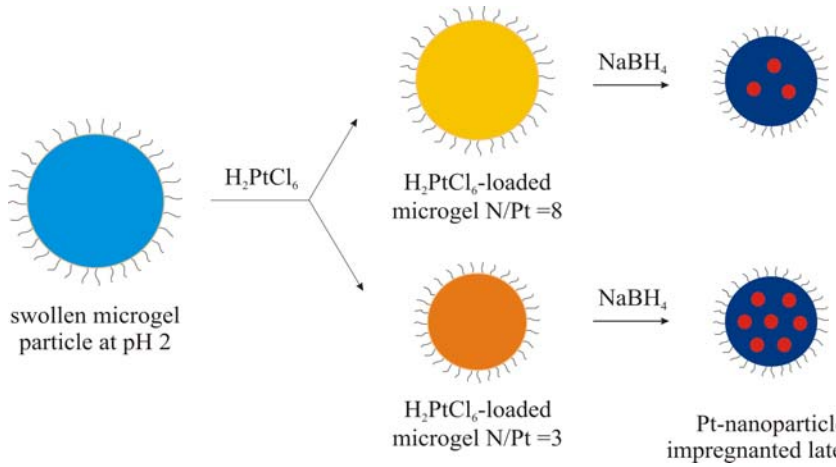

Figure 17 Schematic representation of the metal loading of the swollen microgel particles at different N/Pt molar ratios.

(iii) The ability of the networks to adsorb small metal ions from the aqueous medium was influenced by both the degree of swelling of the network in the solvent and the existence of strong polymer-metal interactions which bound the metal ions onto the network structure. Thus the hydrophobic (PMMA and PBzMA) and slightly hydrophilic (PHEGMA) networks did not bind the metal ions, while the highly hydrophilic networks (ionized PMAA, PDMAEMA and PDEAEMA) adsorbed metal ions of the same charge via the diffusion of the latter within the network phase by means of the solvent medium. The adsorption of the metal ions by the network had a significant effect on its degree of swelling which was dictated by the swelling of the network due to the protonated monomer units followed by the network shrinkage when the divalent metal ions interacted with the ionized polymer groups and increased the effective cross-link density of the network thus causing the network to shrink.

(iv) Gel permeation chromatography was used to characterize the linear and star polymer precursors to the networks, and confirmed the control achieved by synthesis regarding the molecular weight of the arms of the star polymer precursors, but not the functionality of the cross-links of the network. The model networks were characterized in terms of their sol fraction, their effective pKs, and their degrees of swelling at low and high pH water and in THF. Both the composition and the network architecture were found to affect the

swelling properties. The influence of metal incorporation and metal nanoparticle formation on the swelling properties of the networks was examined. The metal content was assessed by TGA while the metal nanoparticles were observed by TEM. The results obtained upon the addition of metal ions in the model copolymer networks were similar to those discussed above for the random networks. The effect of the conetwork characteristics on its metal capacity was found to be independent of the conetwork architecture and is primarily dictated by the composition of the conetwork.

Partner 2 characterized catalysts supported by polymers by TEM, AFM, XPS, XFA, and nitrogen physisorption. A TEM micrograph of 3% Pt/HPS is presented in Figure 18. Electron micrographs reveal a broad distribution of Pt nanoparticles, 71% of which are less or equal than 2.0 nm in diameter.

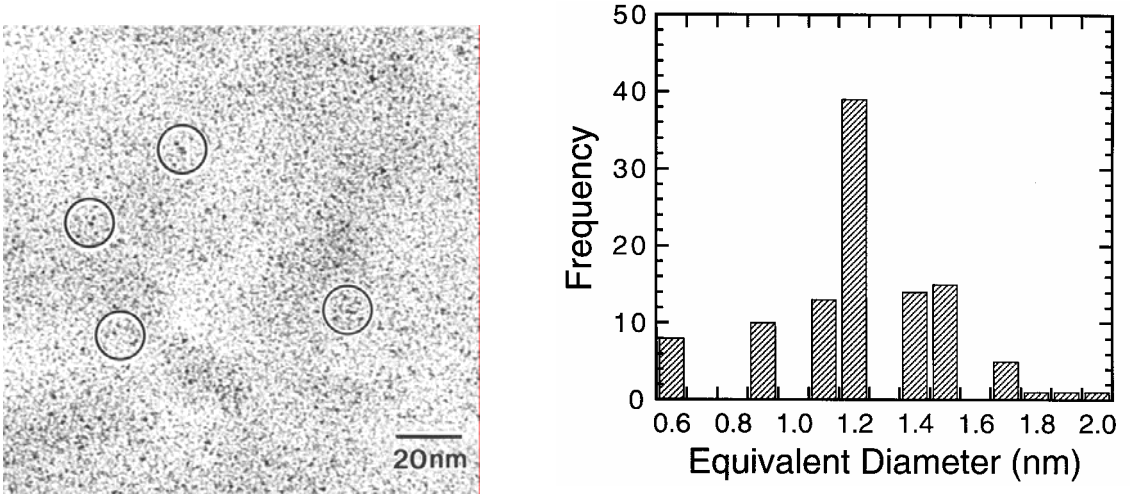

Figure 18 TEM images of 3%Pt/HPS

AFM (Figure 19) showed monomodal distribution of Pt nanoparticles formed in PEO-b-P2VP.

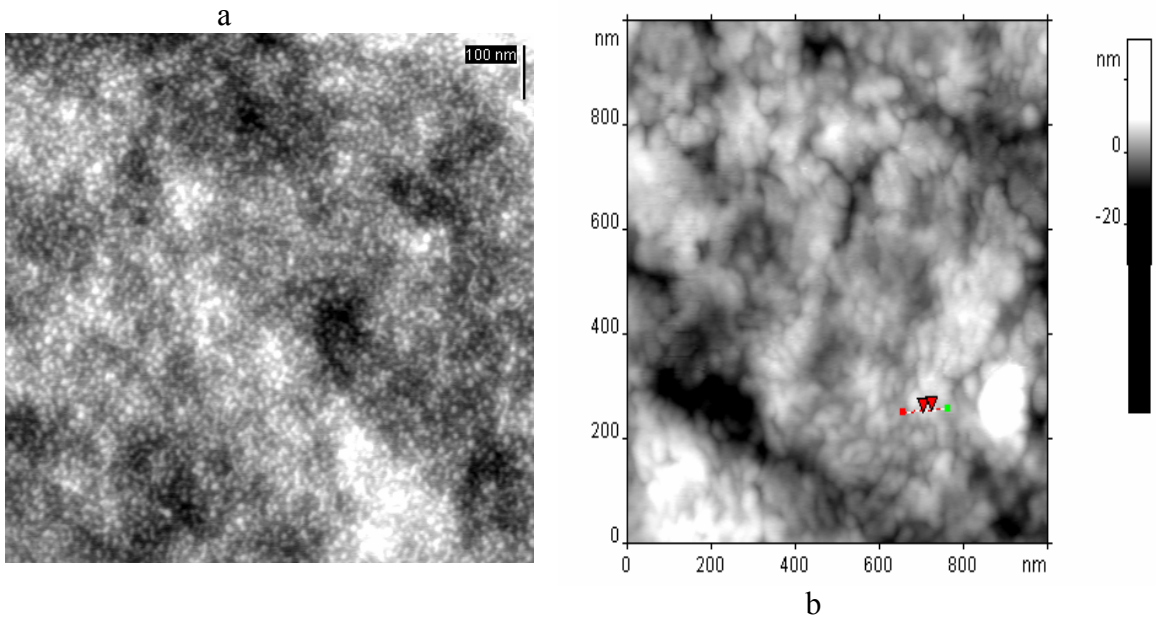

Figure 19 AFM images of diblock PEO-b-P2VP containing H_2PtCl_6 (b) or Pt nanoparticles (a).

1.6.3.2 Catalysts characterization by DRIFT-CO and CD_3CN, XPS and XAS techniques

HPS-Pt samples

Four Pt containing samples: HPS-Pt-0.1%, HPS-Pt-1%, HPS-Pt-2.6% and HPS-Pt-5% catalysts were studied.

It was revealed that platinum in as received HPS-Pt samples exists as $Pt^{\delta+}$ (where $2 < \delta < 0$). Treatment of samples at room temperature in CO (DRIFT and XAS) results in partially platinum reduction. The formation of large Pt metal particles during this treatment can be excluded. The average diameter of Pt metal particles is 3.5-3.9 Å with the assumption that the shape of particles is spherical.

HPS-Pd samples

Seven Pd containing samples: HPS-Pd-1%, HPS-Pd-1%-recycled, HPS-Pd-3%, HPS-Pd-3%-recycled, HPS-Pd-5%, HPS-Pd-5%-recycled and HPS-Pd-0.1% were studied. It was shown by DRIFT-CO and XAS that palladium in as received HPS-Pd samples exists as a mixture of Pd^{2+}, Pd^{1+} and Pd^0. The palladium species in the HPS-Pd-1%-recycled sample are more reduced. The palladium species in the HPS-Pd-5%-recycled sample are more oxidized.

HPS-Ru samples

Two Ru containing samples: HPS-Ru-0.71%, HPS-Ru-2.74% were studied. The study (DRIFT-CO and XAS) has shown that ruthenium in as received HPS-Ru samples exists as a mixture consisting of Ru^{4+} species together with a small amount of Ru metal nanoclusters.

Pd/HBETA samples

Four Pd-containing samples: 2%Pd/HBETA-300 (SiO_2/Al_2O_3 = 300), 3.9%Pd/HBETA-150 (SiO_2/Al_2O_3 = 150), 4.7%Pd/HBETA-25 (SiO_2/Al_2O_3 = 25), and 4.1%Pd/HBETA-11 (SiO_2/Al_2O_3 = 22) prepared by impregnation were studied. The DRIFT and XAS study showed that palladium in received Pd/HBETA samples exists as palladium oxide that can be easily reduced to Pd metal particles at 100°C in an H_2 flow. The average diameter of Pd particles is 9-19 Å with the assumption that the shape of particles is circular. The higher the silica-to-alumina ratio in the BETA zeolite, the bigger Pd particles is formed: 2%Pd/HBETA-300 > 3.9%Pd/HBETA-150 > 4.7%Pd/HBETA-25. The size of Pd particles formed on HBETA (commercial and home-made) with close SiO_2/Al_2O_3 ratio (25 and 22, respectively) is comparable. Pd metal clusters formed during reduction at 200°C are twice bigger in size.

Ru samples on BETA, Y, MCM-41 and SiO_2

Four Ru-containing samples: 5%Ru/BETA, 5%Ru/MCM-41, 5%Ru/SiO_2, and 5%Ru/Y (prepared by impregnation) were studied. The study (DRIFT-CO, XPS and XAS) showed that ruthenium in calcined samples exists as Ru^{4+} isolated ions in 5%Ru/MCM-41, 5%Ru/SiO_2 and 5%Ru/Y catalysts. In 5%Ru/BETA calcined samples the presence of a RuO_2 phase is possible. The ex-situ reduction of Ru samples at 250°C in an H_2 flow leads to the formation of metal Ru particles, the dispersion of nanoparticles depends upon the support nature. The bigger particles (diameter of 34-62 Å) were found on BETA zeolite. More than two-three times smaller particles were found on mesoporous SiO_2 (MCM-41) (16-22 Å) and faujasite Y (12-16 Å), respectively. The smallest clusters (9-13 Å) were formed on SiO_2 oxide.

DRIFT-CD_3CN showed that the Lewis acid sites at the surface of all Ru samples are moderate in strength. There are no Lewis acid sites but there are weak Brønsted acid sites at the surface of SiO_2. The weak Brønsted acid sites were detected at the surface of both

5%Ru/MCM-41 and 5%Ru/Y catalysts as well. Moreover, the strong Broensted and/or weak Lewis acid sites were found at the surface of 5%Ru/BETA.

Pd samples on BETA, MCM-41 and Mordenite

Four Pd-containing samples: 4.6 wt% Pd-H-MORD-20-C (prepared by impregnation), 3.0 wt% Pd-MORD-IE-C, 2.8 wt% Pd-H-BETA-25-IE-C, and 2.6 wt% Pd-H-BETA-75-IE-C (prepared by ion exchange) were studied.

The study (DRIFT-CO) showed that Pd supported on different zeolites after calcinations step contain on the surface of Pd-H-MORD-IE-C and Pd-H-BETA-25-IE-C samples three palladium cationic species, on the surface of Pd-H-BETA-75-IE-C - two species whereas on the surface of Pd-H-MORD-20-C one type of cationic species. All cationic species reduce to metallic Pd during reduction step.

Au samples on MCM-41, BETA, MORD and ZSM

Six Au containing samples (five monometallic and one bimetallic): 2 wt% Au-MCM-22-30-IMP-C, 2 wt%Au-MCM-41-20-IMP-C, 2 wt%Au-BETA-150-IMP-C, 2 wt%Au-MORD-20-IMP-C, 2 wt%Au-ZSM-5-30-IMP-C and 2 wt% Au-0.1 wt%Ce-MCM-41-20-C prepared by impregnation were studied.

The study (DRIFT-CO, XPS and XAS) showed that gold on the samples under study exists as Au^{3+} cations in all calcined samples. In bimetallic Au-Ce/MCM-41 calcined sample gold metal particles were found as well. The reduction at 300°C in H_2 flow results in the formation of Au^0 species in Au/MORD-20 and Au/ZSM-5 samples. CO does not adsorb on reduced Au/BETA-150.

The study (DRIFT-CD_3CN) showed that the order of Lewis acid sites strength for calcined samples: Au/MCM-41 > Au/MCM-22 = Au/MORD-20 > Au/BETA-150 > Au/ZSM-5 > Au-Ce/MCM-41; for reduced samples: Au/MCM-41 > Au/MCM-22 ≈ Au/MORD-20 ≈ Au/BETA-150 > Au/ZSM-5 > Au-Ce/MCM-41.

1.6.3.3 Characterization of mesoporous alumina-supported catalysts

Partner 3 characterized the mesoporous materials synthesized in WP 1 by TEM. Synthesis route B,[11] which uses a mixture of cationic and anionic surfactants in order to control the micelle charge, leads independent on pH to materials with high surface area, though

[11] L. Sicard, B. Lebeau, J. Patarin and F. Kolenda, *Oil Gas Sci. Technol.*, 2003, **58**, 557.

always significantly lower than the values reported in the literature. Alumina particles appear to be acicular (TEM); their irregular stacking explains the broader pore size distributions. The oxide prepared at pH 11 appears as heterogeneous when examined by TEM, with bulky angular grains of lamellar morphology assigned to η-Al_2O_3 (Figure 20). They originate from the decomposition below 250°C of bayerite, initially formed because of the basic pH, and have also been observed for the alumina prepared following procedure D at pH 10.4 (Figure 21). Moreover, depending on the pH of synthesis B, the calcined materials suffer from a lack of stability upon subsequent contact with water: the higher the initial pH of the synthesis, the more bayerite is formed back upon hydration.

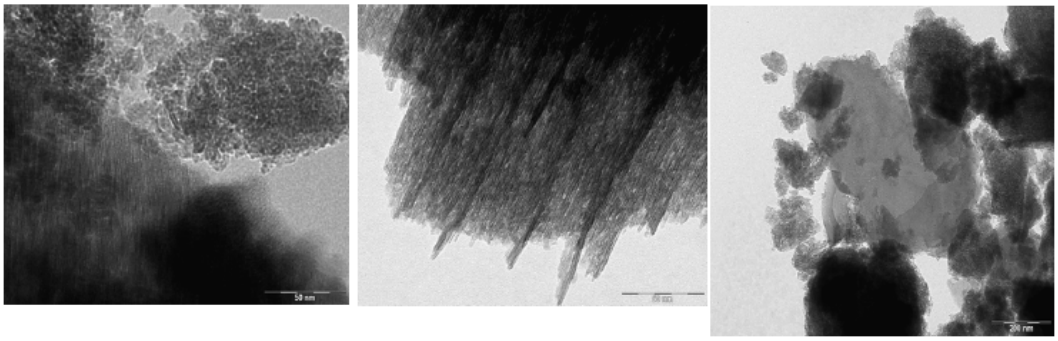

Figure 20 Transmission electron micrographs of calcined mesoporous aluminas synthesized at pH 11 following procedure B before and after (right) washing with water.

Stability is increased if neutral organic agents such as block copolymer P123 are employed, *i.e.* if strong interactions between the Al source and the surfactant are limited. The two resulting materials (C and D, Figure 21) have very close physicochemical properties but differ in terms of pore size distribution, narrower if the synthesis follows C,[12] probably because the condensation of the Al species is more controlled (careful NH_3 addition on a preformed sol, instead of mixing acidic and basic solutions). Moreover, synthesis D[13] is less reproducible in terms of specific surface area. The drawback of synthesis C, which involves ammonia addition, is the crystallization during drying of NH_4NO_3, which may explode during calcination.

[12] Z. Zhang and T. J. Pinnavaia, *J. Am. Chem. Soc.*, 2002, **124**, 12294.
[13] P. Bai, W. Xing, Z. Zhang and Z. Yan, *Mater. Lett.*, 2005, **59**, 3128.

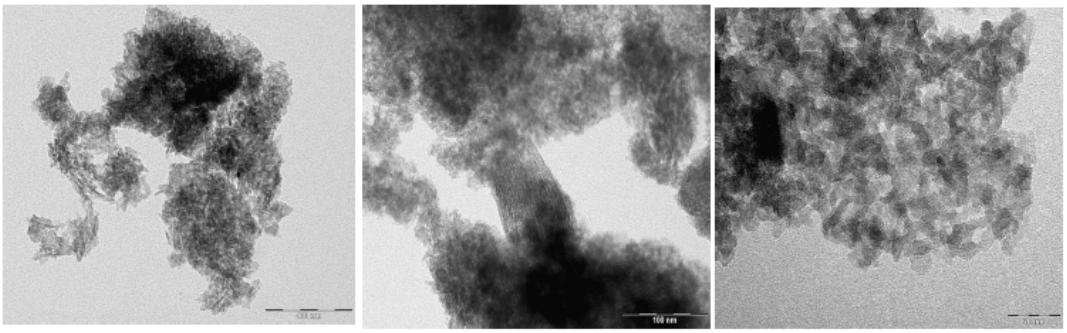

Figure 21 Transmission electron micrographs of aluminas synthesized following procedure C (left), procedure D (middle) and procedure E (right).

Interestingly, the route using glucose,[14] which cannot act as a supramolecular template of the mesoporosity, leads to a similar material, whose narrow pore size distribution is centered on 5.6 nm (close to that of SBA-15 materials) and whose morphology, according to TEM, consists of agglomerates of 4-6 nm spherical γ-Al_2O_3 nanoparticles (Figure 21). The results obtained suggest that the formation of the precipitated phase occurs not through the formation of micelles, as is the case for mesoporous silicas, but through the sticking of oxide particles stabilized by the organic agent. Glucose may act as a stabilizer of the boehmite particles formed during the first step of the synthesis, which aggregate subsequently, delimiting intergranular porosity.

1.6.3.4 Characterization of Beta zeolites incorporated with palladium

The Beta zeolites incorporated with palladium (synthesized in WP 1) were characterized by nitrogen physisorption (surface area), DCP (metal content) and CO pulse chemisorption (dispersion and metal particle size) by Partner 1. The results are shown in Table 6.

Table 6 Properties of Beta supported palladium catalysts.

catalyst	Dubinin surface area (m^2/g)	Metal content (wt-%)	Dispersion (%)	Metal particle size (nm)*
Pd-H-Beta-300	862	2.0	9	13
Pd-H-Beta-150	724	3.9	9	13
Pd-H-Beta-25	691	4.7	13	8
Pd-H-Beta-11	575	4.1	8	14

Moreover, the concentration of acid sites was determined by FTIR and pyridine adsorpition. Table 7 shows the distribution of acid sites depending on the temperature of

[14] B. Xu, T. Xiao, Z. Yan, X. Sun, J. Sloan, S. L. Gonzáles-Cortés, F. Alshahrani and M. L. H. Green, *Micropor. Mesopor. Mater.*, 2006, **91**, 293.

which pyridine retains on the surface. The metal content has been determined by DCP. The acidity at 350 and 450ºC for all the characterized catalysts was negligible, which means that palladium impregnated beta-zeolites contain no strong acid sites. The concentration of weak acid sites (250ºC) follows the Si/Al ratio.

Table 7 Concentration of acid sites determined by FTIR and pyridine adsorption on zeolites.

Catalyst	Brønsted acid sites (µmol/g)			Lewis acid sites (µmol/g)		
	250ºC	350ºC	450ºC	250ºC	350ºC	450ºC
2.0% Pd-H-Beta-300	57	0	0	16	0	0
3.9% Pd-H-Beta-150	109	0	0	29	0	0
4.7% Pd-H-Beta-25	161	26	0	75	0	0
4.1% Pd-H-Beta-11	176	20	0	111	8	0

1.6.3.5 Characterization of carbon nanofiber catalysts

Partner 6 made the characterization of the carbon nanofiber catalysts synthesized in WP 1. Using H_2-chemisorption, titrations and transmission electron microscopy (TEM), dispersion of Pt on CNF, CNT-MW and CNF-PL and the presence of oxygen surface groups were investigated (see Table 8 and Figure 22). In Figure 22A the platinum particles dispersed on carbon nanofibres can be observed as dark spots. Particles sizes are small and in the range from 1-3 nm. The fishbone-like orientation of the graphene layers and a homogeneous dispersion of platinum on the sample could be confirmed. Results for Pt/CNT-MW (see Figure 22B) showed hardly any deposited platinum particles. In the dark-field mode (not shown) some light spots, which probably originate from platinum could be observed. The parallel orientation of the graphitic layers, which is typical for carbon nanotubes was confirmed. Small platinum particles were also observed on CNF-PL (see Figure 22C). The synthesis resulted in a homogeneous distribution of particles, which size range from 2 to 3 nm. The perpendicular orientation of the graphitic layers towards the central axis was observed at high resolution. H_2-chemisorption results are summarized in Table 8. As can be observed, these results show a decrease of the amount of chemisorbed hydrogen after heat-treatment. This indicates that sintering of the metal takes place during heat-treatment, especially for Pt/CNF-PL and Pt/CNT-MW; these catalysts lost more than 50% of their original platinum surface area. According to this technique, Pt/CNT-MW contains platinum. It might well be that during sample preparation via ultrasonic treatment for TEM, a lot of metal was lost and therefore nothing was observed. The titration results show that after oxidation and metal deposition, a substantial amount of acidic oxygen surface groups is present on the surface area. After heat-treatment, the

oxygen surface groups were removed for all catalysts and the catalyst surface became slightly basic.

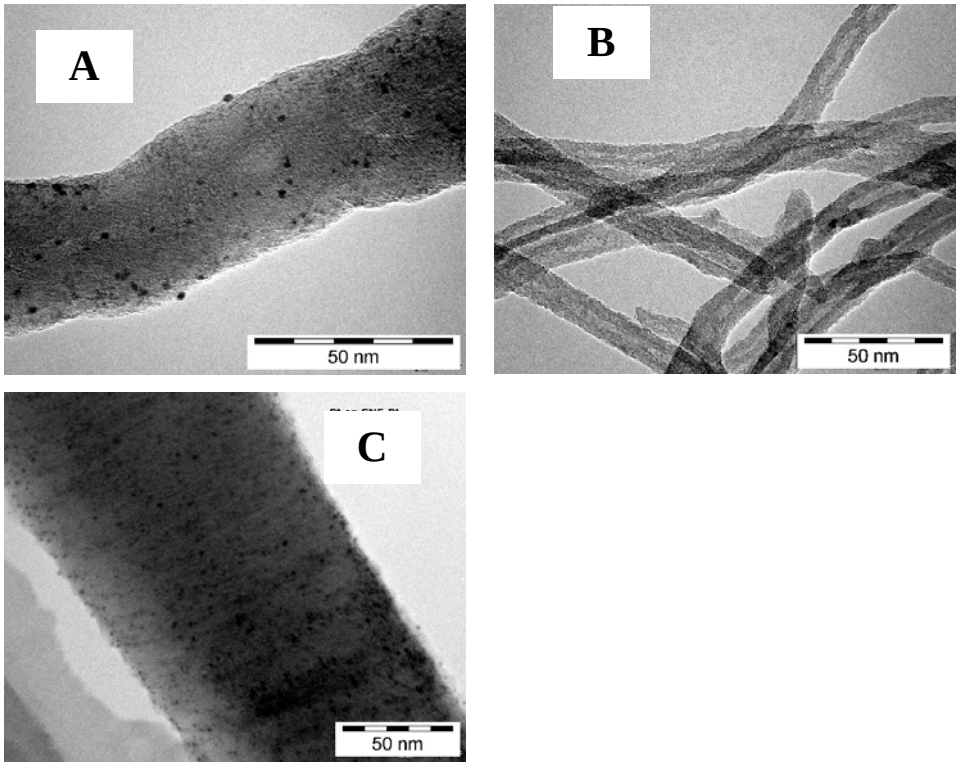

Figure 22 TEM-pictures of [A] Pt/CNF (HDP), [B] Pt/CNT-MW with no visible platinum deposition and [C] Pt/CNF-PL.

Table 8 H_2-chemisorption and titration results; b means slightly basic

	Pt/CNF	Pt/CNF-973	Pt/CNT MW	Pt/CNT MW-973	Pt/CNF-PL	Pt/CNF-PL-973
H_2-chemisorption (x 10^{-5} mol H_2/g cat)	4.9	3.6	2.5	1.1	7.4	3.0
Acidic oxygen surface groups (groups/nm^2)	0.76	b	2.04	b	1.74	b

Some TEM HAADF results for the bi-metallic platinum-tin catalysts prepared using incipient wetness impregnation, are depicted in Figure 24. The platinum particles are small: 1-3 nm in size. EDX analysis was performed in the marked areas of the pictures. These results are depicted in Figure 24. Using tin (II) chloride as precursor, both platinum and tin are observed. But using tin (IV) chloride as precursor, the tin signal is hard to detect. Using the other precursors, the result was the same as for tin (IV) chloride: tin seemed to be not combined with platinum.

The platinum catalysts combined with iron(II), iron(III), gallium and germanium were also analyzed using TEM-EDX. As a representative example, the result for Pt-Fe(III) CNF

RDP is depicted in Figure 25. The EDX signals for platinum and the promoter metal are related to each other, which means that the two metals are well combined. The successful combination of the two metals into an alloy formation is probably the explanation for the observed high selectivity towards cinnamyl alcohol in cinnamaldehyde hydrogenation.

The TEM results for the platinum catalysts (Figure 26), which were prepared to study particle size effects, show that platinum particle sizes for the HDP prepared catalysts were 2-3 nm independent of the heat-treatment. ALD resulted in Pt particles which were larger, i.e. 3-5 nm, irrespective whether the samples were subjected to a temperature treatment or not. Also for the Ru samples (see) the HDP synthesis resulted in smaller particles (2-3 nm) while ALD resulted in larger particles (3-5 nm).

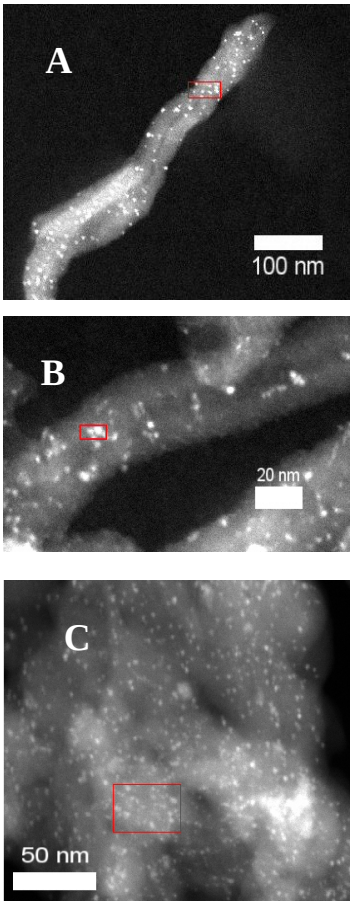

Figure 24 TEM HAADF images from different Pt-Sn catalysts.
A) Pt-SnCl2 (l.a.)
B) Pt-SnCl2 (h.a.)
C) Pt-SnCl4
The marked areas were analysed using EDX

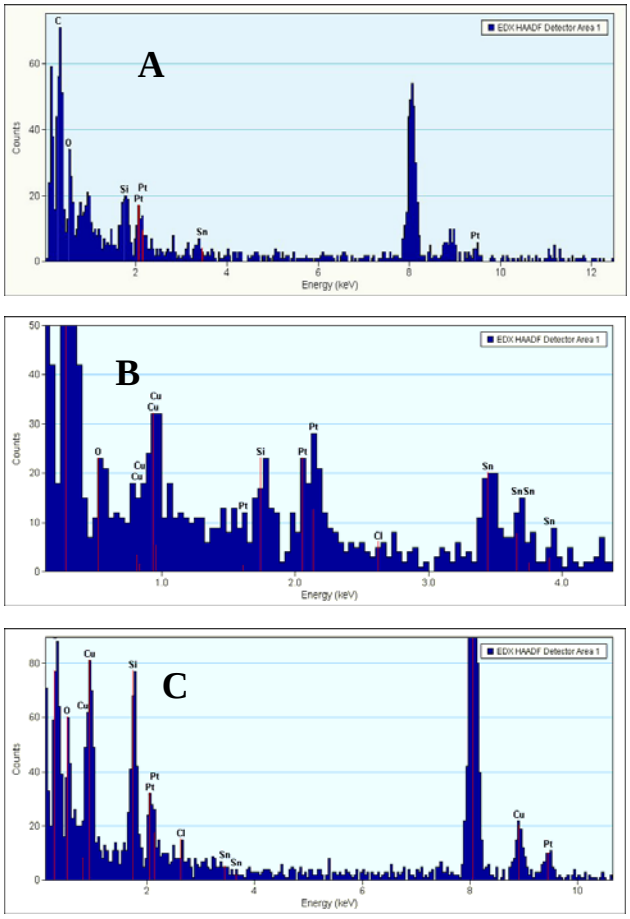

Figure 24 TEM EDX results for the different analysed areas. **A**) Pt-SnCl2 (l.a.)
B) Pt-SnCl2 (h.a.)
C) Pt-SnCl4

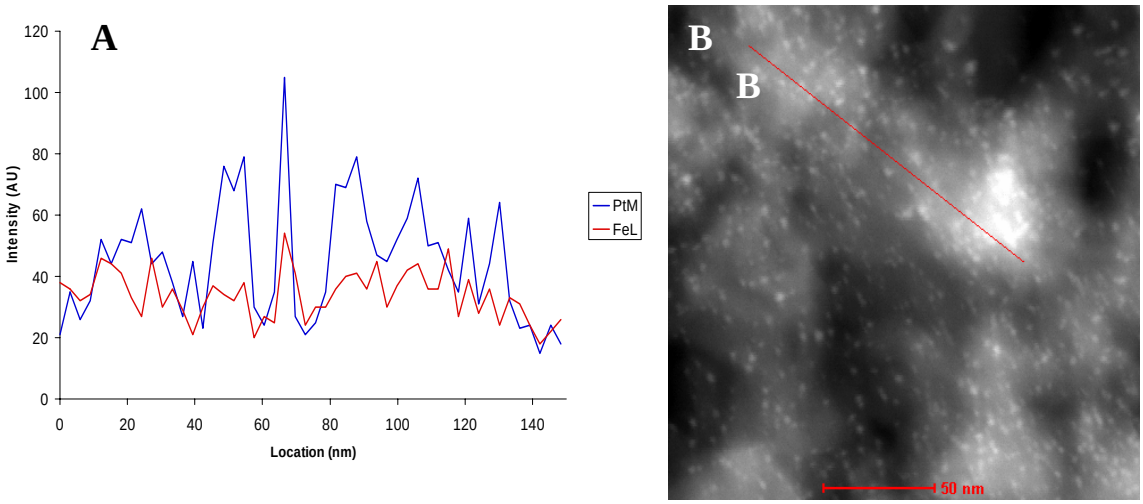

Figure 25 TEM-EDX results for Pt-Fe(III) CNF RDP - A: EDX and B: HAADF image. The red line in B represent the measured scan on the material.

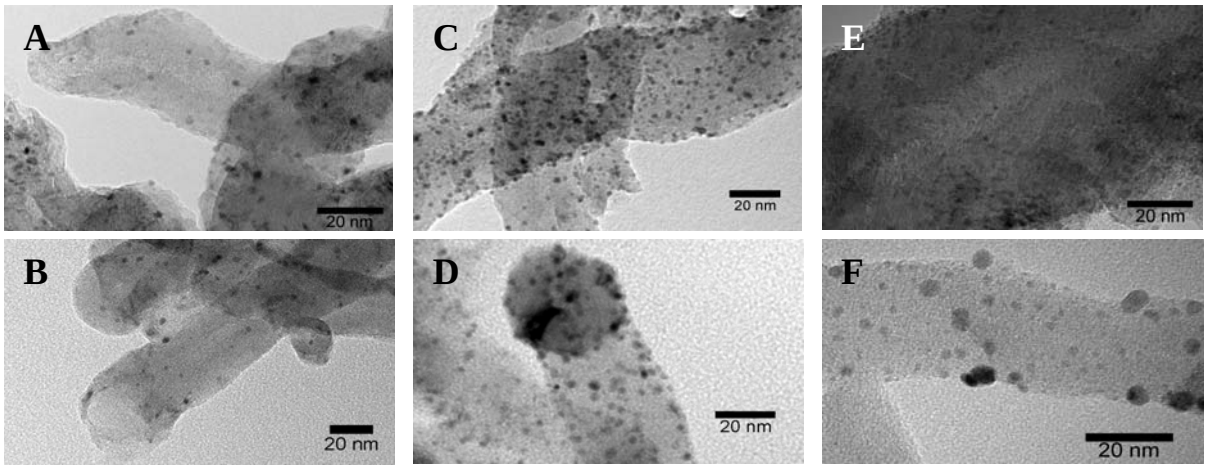

Figure 26 TEM pictures of [A] Pt/CNF (HDP) [B] Pt/CNF-973 (HDP) [C] Pt/CNF (ALD) [D] Pt/CNF-973 (ALD) [E] Ru/CNF-973 (HDP) [F] Ru/CNF-973 (ALD)

1.6.4 WP 4 – Modelling

The objective of WP 4 was to perform Monte Carlo simulations and quantum chemistry calculations based on catalyst characterisation from WP 3 as well as kinetic modelling based on the kinetic data from WP 2. Kinetic modelling was performed by partners 1 (AAU) and 2 (TverTU), quantum chemical calculations by partners 1 and 5 (DIAC-UNIPA) and Monte Carlo simulations by partner 5. Partner 1 did parameter estimation for the oxidation of lactose and quantum chemical calculations for the hydrogenolysis and dehydrogenation of hydroxymatairesinol (HMR). Partner 2 did kinetic modelling of L-sorbose and D-glucose oxidations. The milestone M6 was to derive kinetic equations,

perform numerical data fitting and statistical analysis of some reactions in WP 2. Moreover, the description of the reaction mechanism for these reactions using Monte Carlo simulations and quantum chemistry calculations in combination with the input data from catalyst characterisation from WP 3 as well as on kinetic modelling with the input data from the reaction tests from WP 2 was performed. The modelling provided interrelation with WP 5, creation of fundamental knowledge from the local metal environment of the metal particle size. The deliverables D9 and D10, description of the reaction mechanisms based on the catalyst characterisation results from WP 3 and D the kinetic data from WP 4 were delivered. Hereby, WP 4 has successfully been completed.

1.6.4.1 Quantum chemical calculations and Monte Carlo simulations

Partner 5 focused the attention on three possible classes of supports, their interaction with Group 10 metal clusters and fragments, and the resulting reactivity:
i) zeolites, with ZSM-5 and Y models of different sizes, ii) carbonaceous materials, with graphite and single-walled carbon nano-tube structures and iii) polymeric matrices, with HPS and PEO-block-P2VP systems.

Partner 5 performed quantum chemical (QC) calculations and Monte Carlo (MC) simulations for several supported catalytic systems, which were aimed at investigate i) the structural and energetic characteristics of the support, ii) the relationships occurring among the metal particle size and shape and the 3-D surrounding environment and iii) the influence of the relationships above on the kinetic properties of the considered materials, with respect to hydrogenation, isomerisation and dehydration processes. In addition to this, Partner 1 also contributed to some calculations regarding hydrogenolysis and dehydrogenation of HMR.

Event occurrence probabilities and chemical parameters, currently employed in the time-dependent Monte Carlo (tdMC) algorithms, are determined by QC methods. Thereafter, the number of “arbitrary” parameters used in the quantum stochastic – qc-tdMC – simulations is dramatically decreased, stimulating the deep analysis of concurrent, and usually non-considered, aspects involved in the heterogeneous processes. In this context, the molecular steric hindrance in confined space gained emphasis while the available surface energy (ASE) concept was hypothesized and parameterized in the tdMC models. ASE allowed to get a new molecular-level information on bi- and tri-phase reactions, by the analysis of microscopic elementary events, taking place at the interfaces, when energy

distributions could be hypothesized on the catalyst surface. Figure 27 schematically shows the main approach employed in studying heterogeneous catalytic systems.

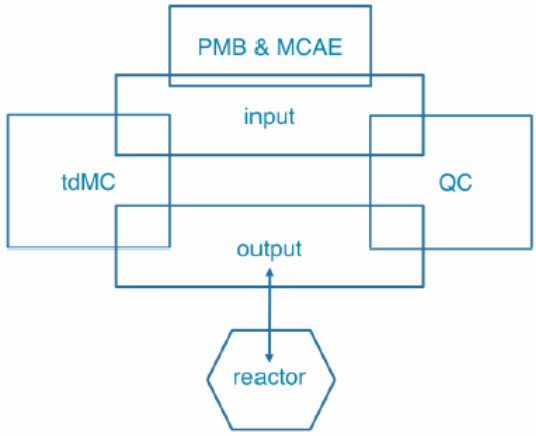

Figure 27 Schematic representation of the quantum stochastic approach used.

The QC box furnishes to the input box of the tdMC code local information on simple events – mostly used to calculate simple event occurrence probabilities. Experimental parameters – as pressure, temperature, relative density, surface properties and species concentrations – are also furnished into the input box.

After the input data, the tdMC box treats the local microscopical QC information and the physical parameters introduced by molecular potentials – algorithmically defined in the code and characterizing the chemical system – that cooperatively reconstruct the mass information. The latter can be compared with macroscopic experimental findings – output, reactor boxes – allowing stating the reliability of the inferred chemical model hence the molecular-level origin of the experimental evidences. Along the project, the QC approaches were used for themselves – in the QC structure and kinetic studies – or as basis information for the qc-tdMC applications.

1.6.4.1.1 Structural properties

Metal systems

Detailed information about the calculations for metal systems can be found in[15]. Quantum chemical calculations on the helicopter and cartwheel rotations of a CO molecule adsorbed by di-hapto coordination on metal-surface fragments, having two (M8) or three

[15] S. Giuffrida, G. Barone, D. Duca, ChemPhysChem 2008, submitted

(M14) metalatom layers (M=Ni, Pd, Pt) were performed at DFT level to rationalise the adsorption energetics, the characteristics of the steric hindrance of the adsorbed CO molecules and to determine IR spectroscopical surface properties. The reliability of the studied systems, characterized by different i) metallic fragment sizes and/or ii) relative distance of the carbon-monoxide molecules from the metallic surface and/or iii) computing approximation, was analyzed. Potential Energy Surface (PES) plots were obtained, either taking the C−O bond length fixed or allowing it to change. Multi CO surface adsorptions were also considered. The results were discussed with the aim to identify the most useful approach in studying the considered systems. The availability of large sets of Energy ÷ Bond Length computed data, following the present calculations, allowed us to obtain IR vibration parameters for the adsorbed CO stretching, including the inhomogeneous line broadening.

From a methodological point of view, it was possible to conclude that the smaller crystallite fragment is large enough to model the main characteristics of the energetic profile, pertaining to the combined effects of the helicopter and cartwheel rotations and the steric hindrance, occurring along the CO adsorption on Pd and Pt. The relevant differences among the considered models were localized in the high energy regions of the corresponding PESs that, however, had a negligible influence on the populated states of the systems. On the other hand, the CO adsorption over Ni clusters was considerably different, and to obtain reliable results it was mandatory to use the larger metal cluster model. The behaviour of the three metals, obtained from the study of the CO adsorption on our crystallite fragments, could be rationalized on the basis of the different interaction energies involved in the CO/M processes. Noticeably, and not unexpectedly, in all the systems it is observed that highly bent molecules have major stability at higher distances from the metal fragment surfaces.

Carbon systems

DFT calculations have been performed on a palladium cluster adsorbed on two different carbonaceous supports, namely two stacked polycircumcoronene units mimicking a double layer of graphite and a portion of an armchair(6,6) carbon nanotube. All the systems have been subjected to geometry optimization and to electronic structure investigation. This work was devoted to identify electronic and geometrical changes in which metal clusters and supports were involved upon interaction.

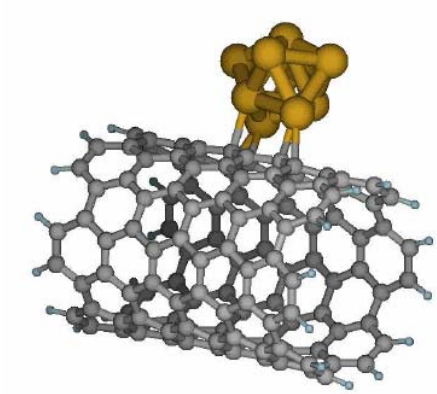

Figure 28 Optimized geometry of the Pd9/nano-tube system. Atoms of palladium in brownish, of carbon in grey, of hydrogen in bluish.

Calculations reveal a major geometrical distortion occurring in the palladium cluster supported on both graphite and nanotube, which is caused by strong Pd- C interactions. The natural curvature of an armchair (6,6) carbon nanotube seems to be more suitable in order to support small palladium clusters (see Figure 28) obtained from fcc lattice truncation than the flat surface of graphite. This evidence is also pointed out by the atomic orbital overlap occurring between the cluster and the nanotube, as revealed by the density of states (DOS) analysis. In order to give rise to stronger interactions, the cluster bends the graphite surface so that the process of supporting palladium particles on graphite could result in a local surface-atoms extraction process. The distorted D_{3h} structure of the palladium cluster adsorbed on the graphite and on the carbon nanotube models shows the relevant influence of the supports on the fragment geometry and the importance of the macromolecular treatment for the investigation of the supported clusters and of eventual small molecules interacting with them. More information about the calculations for carbon systems can be found in[16].

Zeolite systems

A ZSM-5 fragment, containing 52 tetrahedral moieties, each of them formed by one silicon or one aluminium atom surrounded by four oxygen atoms, was employed to model (52T systems) by quantum chemical calculations i) the influence of the positions of the acidic sites on the energetics of twenty-two aluminium mono-substituted and bi-substituted 52T acidic zeolite (H-ZSM-5) systems and ii) the local adsorption properties (see Figure 29) and acidic strength of the corresponding −OH sites. The energetics and the structural properties of simpler acid H-ZSM-5 systems containing only 5 tetrahedral

[16] D. Duca, F. Ferrante, G. La Manna, J. Phys. Chem. C 2007, 111, 5402

moieties (5T systems) were also modelled for comparison. The results showed that the orientation and the position of the acidic hydrogen atoms within the zeolite channel strongly affect the stability of the model systems, irrespective of the starting local topology characterizing the Al↔Si substitution site.

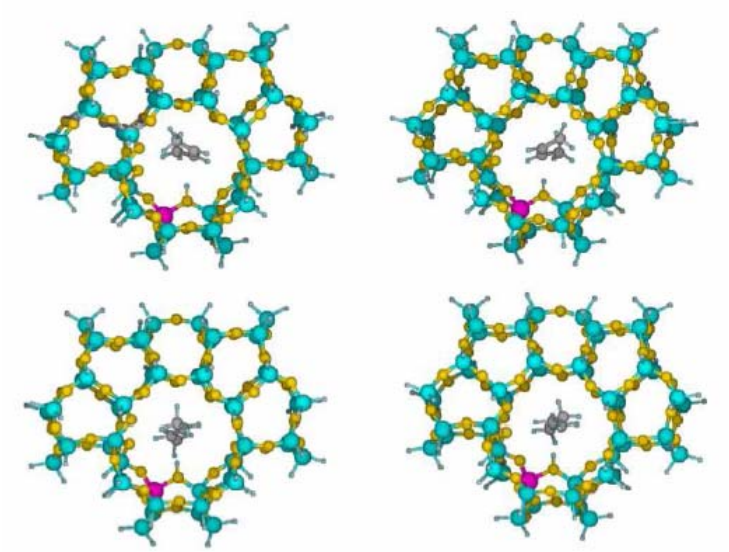

Figure 29 Partially optimized geometries of cis-but-2-ene (top) and trans-but-2-ene (bottom) molecules adsorbed – in specular displacements – on 52T H-ZSM-5 mono acidic fragments. Atoms of silicon in cyan, of aluminium in purple, of oxygen in gold-yellow.

Brønsted gas-phase acidity strength and adsorption-ability were evaluated through the analysis of the energy involved in i) the proton dissociation from the acidic sites and ii) the cis-but-2-ene and trans-but-2-ene adsorption on the same acidic sites. Both were affected, although to a very different extent, by the location and number of the considered −OH acidic groups. In particular, two among the twelve modelled acidic sites resulted in highly stabilized in the zeolite structure, pointing that the Al↔Si substitutions in the synthesis of aluminated ZSM-5 zeolites hence the corresponding catalytic activity could preferentially occur on special sites. The choice of the computational method along with the size and the cut-off of the mimicked structures influenced the reliability of the calculations. Finally, the suggested alternative approach (that is, the ONIOM followed by the DFT single-point calculation) provided reasonable findings at very low computational cost. The topics of this section are extensively treated in[17].

[17] G. Barone, G. Casella, S. Giuffrida, D. Duca, J. Phys. Chem. C 2007, 111, 13033

Polymer systems

Two polymeric matrices have been studied as nanoscopic micro-environments for reactive events: a micro-porous hyper-cross-linked polystyrene (HPS) matrix and a poly-ethyleneoxide- block-poly-2-vinyl-pyridine (PEO-b-P2VP) copolymer. The comparison between the two systems, from the point of view of the electronic properties of both the matrix, of the embedded metal nanoclusters and of their mutual interaction, allowed a rationalization of the properties of such polymeric systems. Three models were taken into account for the HPS matrices. They were built by connecting together $(PS)_{11}$ fragments, previously optimized at PM3 level, with the joining styrene units added, taking care that the resulting systems were compactly shaped. Then, the cross-link (*cl*) units were added, trying to reproduce the polymeric experimental structure. The resulting system showed a main pore able to accommodate the Pd_9 cluster utilized for the carbon-based systems.

The first, smaller model, constituted by 196 C atoms with a formal *cl* degree of 106%, was optimized by the PM3 semi-empirical method, and then by the mPWB95/6-31G(d,p) DFT method. The 196 C matrix model was used to study the metal supported systems. Besides the palladium cluster atoms, just the PS units of the first coordination sphere of the metal crystallite was included in the ONIOM model system. A second, larger model, including 445 C atoms, with a formal (*cl*) degree of 117% has been optimized by PM3 method, then, after re-optimization by UFF, has been directly employed for ONIOM full optimizations with the Pd_9 cluster embedded in the main micropore of the structure. A likewise randomly built PEO-b-P2VP block copolymer was also studied.

The computational difficulty of the metal supported study is, in this case, represented by the choice of the size of the nanocluster/micelle system. For this reason, several approximations need to correctly model the PEO-b-P2VP structures. Therefore, a qualitative analysis on the interactions between the Pd9 cluster and the pyridine unit of P2VP and between the same cluster and the oxygen atoms of PEO sub-units was performed, with the aim to identify the most favourable interaction sites. The models of the metal/polymer systems were consequently built assuming that a metal cluster is allowed to bind a micellar substrate essentially on two sites: i) at the PEO-b-P2VP interface and ii) in the micellar core where essentially P2VP subunits are present.

1.6.4.1.2 Kinetic properties

In vacuo but-2-ene isomerisation

The trans- to cis-but-2-ene, in vacuum, isomerisation should proceed by, at least, a three step process, involving i) double-bond breaking, ii) rotation of 180◦ around the C2−C3 bond and iii) double-bond formation. The first step is highly energetic, requiring an electronic transition from the ground to the excited states.

The results obtained allowed us to conclude that such isomerisation reaction in the gas phase cannot easily occur, for at least two reasons: i) the product is thermodynamically less stable than the reagent and ii) very high energies are required for the inter-conversion.

But-2-ene hydro-isomerisation on palladium cluster

The processes of adsorption of molecular hydrogen on bare and supported palladium cluster, with subsequent fragmentation and diffusion have been studied by means of DFT approches in order to obtain information on hydrogen availability for reduction reactions.

The mechanisms of hydro-isomerisation of cis-but-2-ene on the bare cluster has been investigated as well. A Pd_9 cluster with D_{3h} symmetry has been chosen to model the metal particle, and an armchair(6,6) carbon nanotube of finite length has been used as support, getting closer this way to potential experimental conditions.

The calculations, performed by starting from all different positions in the palladium cluster, revealed that the H_2 molecule interacts with both H atoms atop a Pd centre, with an interaction energy of ca. 30 kJ/mol, irrespective of the coordination number of the palladium atom in the cluster. The lowest energy barrier to hydrogen fragmentation occurs when H_2 is atop a Pd atom with maximum coordination, to give a product 11 kJ/mol lower in energy than the reactant, where the two H atoms are located at the centre of a Pd_3 site arrangement.

Although the but-2-ene molecule could interact with two adjacent Pd cluster atoms, the sp^2 interacting carbons, in the optimized structures, resulted bound to vertex palladium atoms, showing very small energy changes with modifying the orientation of the methyl groups. The first step of the hydro-isomerisation of the cis-but-2-ene molecule on the metal surfaces involved the migration of one H atom in the direction of a co-adsorbed but-2-ene molecule. This process required the overcoming of an energy barrier of 87 kJ/mol.

The fragmentation of H_2 and the most representative diffusion paths have been investigated also on the supported Pd_9 cluster. Although the presence of the support inhibits adsorption on certain surface sites and causes distortions of the cluster, no sensible changes were observed for the adsorption positions preferred by the hydrogen molecule (and by but-2-ene as well). Further calculations also revealed that very small variations occur in the energetics of the diffusion pathways of H on the supported Pd_9, even if some new minima have in this case been found. These evidences finally prove that palladium clusters supported on carbon nanotubes should not be affected by reduced availability of atomic hydrogen atoms.

But-2-ene isomerisation inside zeolite cavity

The isomerisation of trans- to cis-but-2-ene within a 22T H-ZSM-5 zeolite model cavity, also in the presence of adsorbed Pd atoms, has been studied by DFT calculations. The reaction involves two intermediates and three transition states, whose energy content, at least for the not metal supported systems, is never higher than 30 kJ/mol, with respect to that of the reactants (see Figure 30).

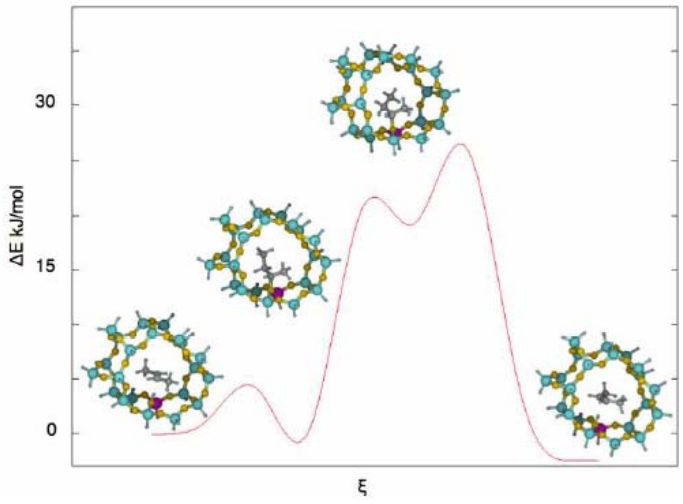

Figure 30 Catalytic pathway for the but-2-ene isomerisation inside the 22T H-ZSM-5 fragment. The structures of the initial, final and intermediate states are shown.

The reaction is in principle allowed also in the presence of two Pd atoms adsorbed inside the zeolite cavity. However, steric hindrance constraints and the strong H−Pd interaction increase the energy of intermediates and transition states formed along the reaction path. The preferential binding sites of the Pd atoms within a zeolite cavity are the −OH acidic groups surrounding the Al atoms. Such result shows that the acidic sites represent nucleation centres for metal deposition on aluminated zeolite. An interesting related

phenomenon evidenced by the calculations is the inverse hydrogen spill-over, i.e. the system stabilization following the acidic hydrogen species dissociation, from the zeolite fragment, and the corresponding hydrogen binding to the adsorbed Pd atoms. This finding could explain the role of the adsorbed Pd clusters on the apparent decrease of the acidic strength of the aluminated zeolites.

Propan-2-ol dehydration inside zeolite cavity

In order to mimic the propan-2-ol dehydration, the interaction of the starting reagents, intermediates and products (the latter being the propene molecule plus water), with the acidic site of 22T H-ZSM-5 and 48T H-Y zeolite fragments have been considered (see Figure 31).

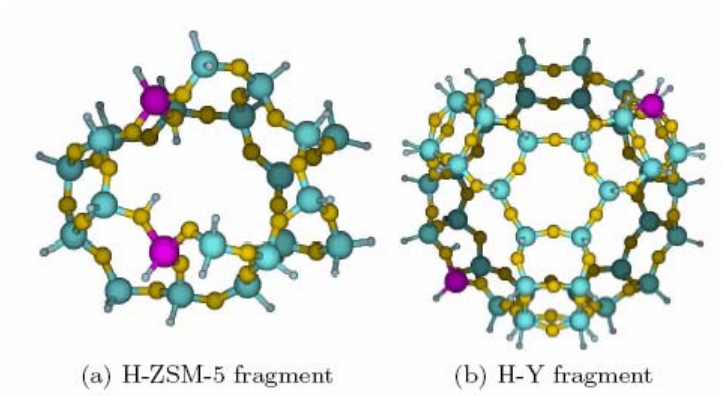

Figure 31 Optimized zeolite models.

H-ZSM-5 consisted of 81 atoms of which 27 hydrogens bound to silicon atoms substituted the original oxygens to truncate the polymeric zeolite structure. Similarly the larger H-Y zeolite model system consisted of 182 atoms of which 48 hydrogen bound to silicon atoms. To mimic the aluminated zeolite systems, one aluminium substituted one silicon atom and one hydrogen atom was added, bound to an oxygen vicinal to the aluminium atom and pointing within the zeolite cavity. In this study a possible route was hypothesized, where propan-2-ol simultaneously interacts with two Al−OH moieties, within the 22T H-ZSM-5 and 48T H-Y zeolite fragments, and where the formation of propene and water takes place by a concerted mechanism, requiring that both the propanol dehydration and the protonation/deprotonation of zeolite acidic sites occur simultaneously.

The results obtained point out that the energy required for propan-2-ol dehydration inside the H-ZSM-5 cavity is equal to 57.5 kJ/mol, with a calculated activation energy of ca. 131 kJ/mol. An explanation of the high energy content of the product, compared to the reagent, can be provided by considering the effect of the steric hindrance, here called steric

pressure (SP). SP arises from the fact that, within the H-ZSM-5 cavity, propene and water molecules are close to each other hence they exert a strong reciprocal repulsion. Similar conclusions were found for the propan-2-ol dehydration inside the larger H-Y cavity. Additional information can be found in[18].

Catalytic hydrogenolysis of hydroxymatairesinol

Matairesinol (MAT) shows antioxidant and anticancer properties. MAT can be easily obtained by hydrogenolysis of the natural product hydroxymatairesinol (HMR) over supported Pd catalyst. There are two diastereoisomers of HMR, namely (7R,8R,8'R)-(-)-7-allo-hydroxymatairesinol (RRR-HMR) and (7S,8R,8'R)-(-)-7-hydroxymatairesinol (SRR-HMR) (see Figure 32). Experimental studies pointed out that the SRR isomer reacts 2-3 times faster than the RRR isomer during hydrogenolysis. Partner 1 and partner 5 performed calculations for this system, having different approaches.

Partner 1 assumed the mechanism to have the following steps: i) the protonation of the hydroxyl group (OH7) followed by water abstraction and formation of a carbenium ionic intermediate, ii) the formed carbenium ionic intermediate is attacked by a hydride resulting in formation of MAT. The protonation of the hydroxyl group was studied, and the protonation energy for the RRR isomer was lower than for the SRR isomer. However, when attaching the proton, the optimization did not result in protonated HMR molecules, instead a water abstraction and consequently a complex of water molecule and carbenium ion was observed. In other words, protonation of the hydroxyl group leads to formation of a carbenium ion without any activation barrier. This is in line with the experiments as the corresponding hydroxyl group is the reactive one. After protonation and formation of water along with the carbenium ion complex, the formed complex of SRR becomes 11.0 kJ mol^{-1} more stable than that of RRR. If these complexes are studied further and water is removed, i.e. only carbenium ions are considered, the carbenium ion formed from SRR is 20.3 kJ mol^{-1} more stable than that formed from RRR. As water is removed carbon C7 becomes achiral, which means that the formed carbenium ions are only different conformations not different molecules as RRR and SRR isomers are. The reason for different reaction rates is either the reaction intermediates formed or the interactions between the HMR isomers and catalyst surface. The protonation of the hydroxyl group at position C7 in HMR results in spontaneous abstraction of water and formation of

[18] A. Prestianni, G. Barone, N. Armata, T. Rubino, D. Duca, J. Catal. 2008, to be submitted

carbenium ion. As the protonation of SRR leads to a more stable complex and carbenium ion than protonation of RRR, formation of such carbenium ion (intermediate in the formation of MAT) is thermodynamically favoured. According to the Polayni relationship[19], a decrease in the energy for a reactant also decreases the activation energy, i.e. for a more stable intermediate the activation energy is lower and subsequently the reaction rate higher. This could explain why the SRR isomer reacts to MAT with higher rate than the RRR isomer. More details about the calculations performed by Partner 1 can be found in[20].

Somewhat alternative reaction mechanism was considered by Partner 5 and was assumed to involve: i) the protonation of the alcoholic group (OH7) with the consequent water elimination, followed by the H in C8 (H8) removing, through an E1 β-elimination mechanism, with the formation of an olefin intermediate; ii) the hydrogenation of the introduced double bond by palladium catalysts. Following such mechanism, the elimination of water in the first step would induce the loss of chirality that discriminates between the SRR and RRR HMR isomers. As a consequence, the different reaction rate observed for the two isomers of HMR should be essentially ascribed to the protonation and water elimination steps, in the hypothesis that the double bond reduction catalyzed by palladium is a faster and non-selective reaction step.

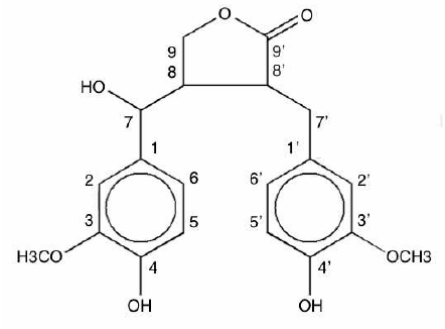

Figure 32 Hydroxymatairesinol.

To suggest a heuristic reaction mechanism, an extensive conformational search has been performed on the potential energy surfaces of the two diastereoisomers (reactants) and of the reaction product, by allowing discrete rotations of the most significant dihedral bond angles.

[19] R.I. Masel, Principles of adsorption and reaction on solid surfaces, John Wiley & Sons, inc., New York, 1996, p. 621.
[20] Markus, H., Plomp, A.J., Sandberg, T., Nieminen, V., Bitter, J.H., Murzin, D.Yu., *J. Mol. Catal. A* **274** (2007) 42-49.

The found lowest energy minimum conformations of RRR and SRR HMR species were essentially iso-energetic in solution (with a calculated energy difference of just 0.5 kJ/mol), suggesting that the different reactivity, experimentally found between the two diastereoisomers, should be justified taking into account reaction intermediates, not the starting reagents. Moreover, considering that both the HMR isomers, RRR and SRR, following the first step of the E1 β -elimination mechanism, converge to the same carbocation intermediate with RR chirality, it can be concluded that the different reactivity of the RRR and SRR isomers could also be attributed to their different interaction with the acidic sites within the zeolite cavity during the protonation step. In this case, an E2 elimination mechanism could also be considered, leading to the formation of the alkene intermediate, by invoking a concerted protonation elimination process aided by vicinal acidic and nucleophilic centers present on the catalyst support. In fact, in such a case the two isomers SRR and RRR would give, respectively, E and Z geometric isomers as products of the first reaction step. Following this hypothesis, it has been found that in ethanol solution the Z isomer, coming from the RRR isomer, is 5 kJ/mol more stable than the E isomer, coming from the SRR isomer.

This result is in disagreement with the greater experimental reactivity of the SRR compared with the RRR isomer, and does not support the hypothesis of the occurrence of an E2 elimination mechanism in the first reaction step, i.e. the formation of the olefin intermediate. A possible solution to this dilemma can be suggested by analyzing the structures of the lowest energy minima of the RRR and of the SRR HMR species, looking in particular at the H8 and OH7 groups that are eliminated in the dehydration step. In fact, while in the RRR diastereoisomer the H8 and OH7 groups are in anti, i.e. the dihedral angle H8−C−C−OH7 is about 180◦, the same groups are in syn in the SRR diastereoisomer, i.e. the dihedral angle H8−C−C−OH7 is about 60◦. This feature could be related to the interaction of HMR with the catalyst sites. It is in fact highly probable that acidic and nucleofilic centres are contiguous, although not very close to one another, on the support surface and, while one acidic centre interacts with the OH7 group, another nucleophilic centre can concomitantly interact with the H8 atom of the HMR molecule. In this way an E2 mechanism could be favoured by the concerted protonation + β -elimination of water in the anti SSR HMR species, giving the E isomer of the olefinic intermediate as the only possible product.

Of course this mechanism could not be invoked for the syn RRR diastereomer that can be converted to MAT only following an E1 elimination mechanism, in any case also imputable to the SRR isomer. Finally, this hypothesis could indeed explain why the HMR SRR isomer is both more reactive and selective than the HMR RRR isomer.

1.6.4.1.3 Monte Carlo applications

T-tdMC

IDEA, Interface Dynamics and Energetics Algorithm, was designed and implemented, in FORTRAN, under different operating systems, to mimic dynamics and energetics of elementary events involved in interfacial processes. IDEA can be regarded as the first thermal time dependent Monte Carlo (T-tdMC) code employed in surface studies.

The main surface elementary events, including the molecular diffusion, were taken into account. IDEA reproduced the foremost characteristics of the simulated surface and bulk phenomena, giving also an interpretation of the involved microscopic aspects. With respect to this, the deduction of the microscopic properties and characteristics of the investigated system – in particular the determination of the role and of the origin of the steric hindrance and of the available surface energy (ASE) in regulating the carbon monoxide adsorption-desorption processes and the connected hot-atom (HA) and adsorption assisted desorption (AAD) phenomena deserves a special interest.

With slight modifications, the code could extend its applicability to the investigation of other substrate/ metal/support systems, taking into account thermal gradients. In particular, Partner 5 has also analyzed bi-phase systems, including light unsaturated hydrocarbons inside zeolite supported materials, which used qc preliminary information. The topic is treated extensively in[21].

qc-tdMC

Monte Carlo algorithms, developed by Partner 5 have been applied to study kinetics and reaction mechanisms of various catalyzed processes, by also using structural and energetic data obtained by qc calculations.

In the tdMC approaches, the catalytic reaction is arranged into a set of elementary steps. To each of these steps an occurrence probability (P) is assigned for given reference time

[21] D. Duca, G. Barone, S. Giuffrida, Zs. Varga, J. Comput. Chem. 2007, 28, 2483

and number of active surface sites. These probabilities, whose sum during simulations is constrained to never exceed 1, are related to the activation energy (Ea), characterizing the events, by the transition state theory.

In the test reaction, i.e. the but-2-ene isomerisation, reactive events, adsorption (sticking), desorption and diffusion phenomena were taken into account, considering very large systems.

Promising results have been obtained on the dynamics of the but-2-ene isomerisation, by the qc-td-3DMC simulations carried out for more than 10 seconds of real time. The calculated values of TOF and Ea are in good agreement with the corresponding experimental values obtained, by the Wei and Prater approach[22], employing a continuous flow reactor and using the 5% Pd supported Pd-H-ZSM-5 – ÅAEU-NANO1 – and the H-ZSM-5 – ÅAEU-NANO17 – catalysts. These catalytic systems were working at 1-2 bar and different starting reagent (but-1-ene, cis-but-2-ene, trans-but-2-ene and butane) partial pressure in the temperature range 303-363 K.

1.6.4.2 Kinetic modelling and parameter estimation

Partner 1 performed kinetic modelling for the oxidation of lactose, and partner 2 for L-sorbose and D-glucose oxidations.

1.6.4.2.1 Oxidation of lactose

Partner 1 studied the lactose oxidation over Au/Al_2O_3 catalyst prepared. Catalytic experiments were performed at 60-90 °C and pH from 6 to 10 at different oxygen flow rates, e.g. partial pressures. The overall mass of the reaction mixture was 100 g and lactose concentration was 99.6 mmol/l.

Langmuir type of kinetics based on the following mechanism was tested

1. $O_2+2^* \equiv 2\ O^*$
2. $A+^* \equiv A^*$ (1)
3. $A^*+O^* \Rightarrow C+ 2^*$
4. $OH^-+^* \equiv OH^-{}^*$

$A+O_2 \Rightarrow C$

Leading to the following equations

[22] D. Duca, G. La Manna, G. Deganello, Catal. Lett. 1998, 52, 73.

$$r_{LA} = \frac{k_3 K_L C_L \sqrt{K_o P_{O_2}}}{(1 + \sqrt{K_o P_{O_2}} + K_L C_L + K_{OH} C_{OH^-})^2} \quad (2)$$

It was proposed that initially adsorption of oxygen occurs on edges, corners and perimeter of nanoparticles, migrating further to faces, where it is transferred into inactive in catalysis oxide

5. $O^*+^*{}' \Rightarrow O^*{}'+ ^*$ (3)

In alkali media hydroxyls could be adsorbed on the catalyst

6. $OH^- + ^* \rightarrow O^* + H^+ + 2e^-$ (4)

The denotation used is θ_V for fraction of vacant sites, θ_o and θ_o' for coverage of oxygen of active and inactive sites respectively.

From quasi-equilibrium of oxygen adsorption

$$\theta_o = \sqrt{K_O P_{O_2}}\,\theta_V \quad (5)$$

and

$$\frac{d\theta_o'}{dt} = k_5 \theta_o \theta_V' - k_8 \theta_V \quad (6)$$

Taking into account that

$$\theta_V = \frac{1}{1 + \sqrt{K_o P_{O_2}} + K_L C_L + K_{OH} C_{OH^-}} \quad (7)$$

One arrives at

$$\theta_o' = 1 - \frac{k_8}{k_5 \sqrt{K_o P_{O_2}}} \frac{1}{(1 + \sqrt{K_o P_{O_2}} + K_L C_L + K_{OH} C_{OH^-})} - e^{-k_5 \sqrt{K_o P_{O_2}} t} \quad (8)$$

and

$$E = \frac{RT}{2F} \ln \left(\frac{k_7 \sqrt{K_O P_{O_2}} + k_8 \left(1 - \frac{k_8}{k_5 \sqrt{K_o P_{O_2}}} \frac{1}{(1 + \sqrt{K_o P_{O_2}} + K_L C_L + K_{OH} C_{OH^-})} - e^{-k_5 \sqrt{K_o P_{O_2}} t}\right)}{k_6 C_{OH^-}} \right) \quad (9)$$

For kinetic modelling eq. (2) and (9) were used. Oxygen concentration was calculated from its solubility. Analogously to lactose oxidation of lactobionic acid takes a form

$$r_{LBA} = \frac{k'' C_L C_{OH^-} \sqrt{K_o P_{O_2}}}{(1 + \sqrt{K_o P_{O_2}} + K_A C_L + K_{OH^-} C_{OH^-})^2} \quad (10)$$

The rate for formation of unidentified products was described by

$$r_{unkn} = \frac{k_{unkn} c_L K_L K_O p_O K_{OH^-} C_{OH^-}}{(1 + \sqrt{K_o P_{O_2}} + K_A C_L + K_{OH^-} C_{OH^-})^2} \quad (11)$$

Formation of lactulose is non catalytic and depends on basicity of the media

$$r_{Le} = k_{LE} c_{OH} \frac{c_L - c_{LE}}{K_{eq}} \quad (12)$$

The system of differential equations was solved with the aid of regression software MODEST applying simplex- Levenberg-Marquardt method for the following objective function

$$Q = \left\| x_{\exp} - x_{est} \right\|^2 = \sum_t \sum_i (x_{\exp,it} - x_{est,it})^2 \quad (13)$$

The degree of explanation defined in the following way R^2

$$R^2 = 100 \cdot \left(1 - \frac{\left\| x_{\exp} - x_{est} \right\|^2}{\left\| x_{\exp} - \bar{x}_{\exp} \right\|^2} \right) \quad (14)$$

was equal to 99.42%. Modelling results showed very good agreement between experimental and calculated values. The values of the parameters are given in Table 9.

Table 9 Values of kinetic constants for lactose oxidation (pH=8)

KLBA	**KLE**	**kEQ**	**k2keto**	**kunkn**	**KOH**	**kelepr**
$0.486*10^{-5}$	1.659	0.65	4.8	$0.115*10^{3}$	8.20	$0.335*10^{-7}$
E_{a1}	**KL**	**E_{a3}**	**E_{a4}**	**KO**	**E_{a2}**	**pot**
$0.270*10^{5}$	$0.124*10^{2}$	$0.373*10^{5}$	0.107E4	$0.10*10^{-2}$	$0.982*10^{5}$	$0.152*10^{-6}$

1.6.4.2.2 Oxidation of L-sorbose and D-glucose

Partner 2 developed modelling of the reactions of L-sorbose oxidation from the data obtained in WP 2. The kinetic equations was derived, perform numerical data fitting and statistical analysis. For the computation the integral method using cubic spline and combined gradient method of Levenberg-Marquardt was used. The kinetic models were chosen which describe well the oxidation kinetics.

1.6.5 WP 5 – Creation of fundamental knowledge

The objective of WP 5 was to create fundamental knowledge from the relation between the metal particle size and its local environment and the catalytic performance in the test reactions carried out in WP 2. The knowledge developed in WP 2 (testing), WP 3 (characterisation) and WP 4 (modelling) was used as input data. The milestone M7

establishing of correlation between the metal particle size and the local environment of metals with the catalytic performance and the establishing of the surface reaction mechanisms together with the deliverables, D11 and D12 (patent and scientific manuscripts) were all fulfilled. WP 5 interrelates with WP 6, prototype catalyst synthesis, characterisation and testing, and WP 7, dissemination of the knowledge. All partners participated in the work within WP 5.

The local environment can affect the metal particle size and the shape/morphology. This environment is changed for example varying the pretreatment of the catalyst. Moreover, the acidity or basicity of the support affects the stabilisation of the metal particle. The size and shape of the metal particle can have a great influence on some reactions, whereas for others no correlation between the metal particle size and activity/selectivity is noticed. In addition to the, effect of metal particle size, the support material as such can also have an influence on the reaction as it provides acidic and/or basic sites that can participate in the reaction. Within WP 1, several catalysts have been synthesized, having different pore size distribution, structure, concentration of acid sites, different metals and metal particle size. The catalysts were characterized in WP 3, to determine the physical properties in order to be able to relate these properties with the results obtained in WP 2, as the catalysts were then tested in different important reactions and to be able to tailor make catalysts for each and every reaction in WP 2. Below are some interesting results presented, and more results and information are found from the publications listed in section 2.1.

1.6.5.1 Influence of support acidity

In order to assess the nature, number and strength of the acid sites on the surface of the catalysts, Partner 3 used three characterization methods: ^{27}Al NMR, infrared (IR) spectroscopy applied to CO adsorbed at liquid nitrogen temperature and model catalytic tests (cumene cracking and isopropanol dehydration). The type of information provided by these last two techniques is detailed below.

CO adsorption at 100 K followed by IR spectroscopy in the transmission mode allows discriminating the acid sites not only according to their nature (Brønsted vs. Lewis) but also according to their strength. It is a semi-quantitative method, in that the number of sites determined in a series of similar materials can be compared (though not quantified by lack of knowledge of the extinction coefficients for each adsorbed species). The

adsorption of CO on an acidic site leads to a high-frequency shift of the CO stretching mode. The larger the shift is (compared to free CO, 2139 cm^{-1}), the stronger the acid site.

Results of the fits in the ν(CO) vibration region took into account:

1- A band at 2231±4 cm^{-1} due to CO adsorbed on a tetrahedrally coordinated Al^{3+} site (strong Lewis acid sites, like in silica-aluminas): band StL
2- A band at 2205±5 cm^{-1} due to medium strength Lewis acid sites: band MiL
3- A band at 2189±5 cm^{-1} due to CO adsorbed on Al^{3+} in octahedral coordination, as is the case on alumina surfaces (weak Lewis acid sites): band WL
4- A band at 2176±1 cm^{-1} corresponding to CO adsorbed on strong Brønsted acid sites: StB
5- A band at 2170±2 cm^{-1} corresponding to CO adsorbed on mild Brønsted acid sites: MiB
6- A band at 2158±1 cm^{-1} assigned to CO adsorbed on weakly acid Si-OH groups:WB
7- A band at 2139±3 cm^{-1} assigned to physisorbed CO
8- A band around 2100 cm^{-1} assigned to CO adsorbed on Pt particles (not discussed here).

Cumene decomposition in benzene and propene is a simple tool for the characterization of Brønsted acidity, but it is sensitive to strong acidic properties only. For this reason, a second test was set up, based on isopropanol dehydration into propene and water.

It was checked that no activity for these reactions was measured on silicic micro- or mesoporous systems, or on aluminic systems. As a consequence, the next paragraphs deal only with silicoaluminic systems.

In order to understand if differences in acidity between supports and catalysts arise from the presence of Pt nanoparticles or from other parameters, “blank” samples were prepared from meso- and microporous silicoaluminic supports, by contacting them with solution whose pH was identical to that of the solution used to introduce platinum, but without platinum compounds inside.

The blank sample for mesoporous $SiAl_6$ was prepared by contact with a tetrapropylammonium hydroxide solution at pH = 10. After calcination at 400°C, the

organic base was completely removed. NMR spectra are compared for the three following samples: $SiAl_6$, $Pt/SiAl_6$ (reduced at 400°C) and the blank sample (calcined at 400°C).

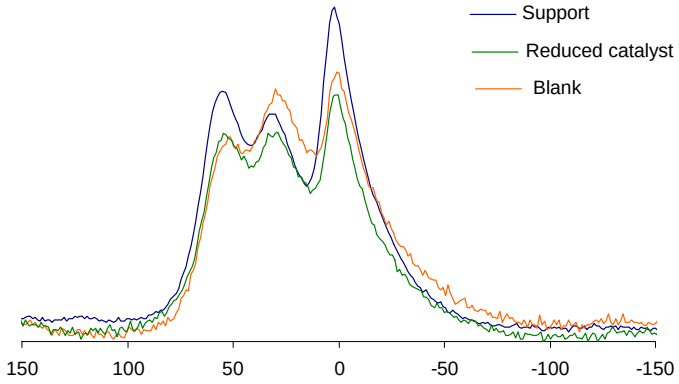

Figure 33 ^{27}Al NMR spectra of support $SiAl_6$ compared with $Pt/ SiAl_6$ and the blank sample.

As it can be seen from Figure 33, the NMR spectra of the catalyst and the blank sample have almost the same distribution of Al species and they differ from the pristine support. This suggests a redistribution of Al during contact with the aqueous solution, whether it contains Pt complexes or not. Modifications in terms of surface properties were checked by IR spectroscopy. An important quantity of strong Lewis acid sites has appeared both on the blank sample and on the catalyst (Table 10). Moreover the band attributed to mild Lewis acid sites (MiL) usually present at 2206 cm^{-1} is shifted to higher energies (2214 cm^{-1}) compared with the support. Some zones of the support may be transformed into silica-alumina-like patches upon contact with water.

Table 10 Position (in italics) and surface area (in bold characters) of CO absorption bands after saturation of strong and mild Brønsted acid sites ($SiAl_6$ systems).

Sample	StL	MiL	WL	StB	MiB	WB	Phys
$SiAl_6$	*2229* **0.49**	*2206* **0.17**	*2190* **0.47**	*2175* **0.44**	*2169* **1.07**	*2157* **1.89**	*2140* **1.46**
Blank	*2230* **0.82**	*2214* **0.19**	*2192* **0.56**	*2175* **0.36**	*2169* **0.54**	*2158* **1.6**	*2139* **0.83**
$Pt/SiAl_6$	*2230* **0.88**	*2214* **0.27**	*2192* **0.58**	*2175* **0.32**	*2169* **0.75**	*2159* **1.84**	*2140* **0.77**

A blank sample was also prepared from microporous H-MCM-22 in the same conditions as for catalyst preparation, this time at low pH (2.5, in contrast with $SiAl_6$). An important increase of the quantity of strong and mild Brønsted acid sites is observed between H-

MCM-22 and the blank sample, as it was on the catalyst (see Table 11). This is in line with the ^{27}Al NMR spectra which show a more intense peak at 55 ppm related to strong Brønsted acid sites.

In conclusion, when the initial Al speciation on the supports is complex, differences in acidity between support and catalyst are due to changes in Al speciation during the contacting with water linked to Pt introduction, and not to the presence of Pt nanoparticles. Consequently, it may not be straightforward to deduce the acidic properties of a catalyst from those of its bare support, because the surface species are not identical.

It can be reminded here that other types of measurements used to assess acidity on such catalysts may be perturbed by the presence of Pt: the catalytic activity of Pt nanoparticles toward hydrocarbons conversion, due to accelerated deactivation processes (see the remark above about cumene cracking on Pt catalysts); the use of Lewis bases, by the presence of non-reduced metal ions which may coordinate them.

In order to link results from IR and catalytic measurements from model test reactions, microporous and mesoporous samples were characterized by both techniques.

Table 11 Position (in italics) and surface area (in bold characters) of CO absorption bands after saturation of strong and mild Brønsted acid sites (microporous and H-MCM-41 systems).

	StL	MiL	WL	StB	MiB	WB	Phys
H-ZSM-5 (Si/Al = 15)	*2231* **0.08**	**0**	*2190* **0.12**	*2176* **0.97**	*2170* **1.29**	*2158* **0.33**	*2138* **0.34**
Pt/H-ZSM-5 (Si/Al = 15)	*2235* **0.04**	**0**	*2190* **0.14**	*2176* **1.16**	*2172* **1.75**	*2159* **0.60**	*2138* **0.93**
H-MCM-22	*2230* **0.19**	*2200* **0.21**	*2184* **0.13**	*2176* **0.54**	*2170* **0.41**	*2157* **1.05**	*2137* **1.37**
Pt/H-MCM-22	*2228* **0.15**	*2205* **0.15**	*2184* **0.35**	*2176* **1.20**	*2168* **0.69**	*2157* **1.23**	*2138* **1.27**
H-MCM-41	*2231* **0.13**	*2210* **0.03**	*2192* **0.09**	*2177* **0.18**	*2171* **0.31**	*2157* **0.49**	*2142* **0.22**
Pt/H-MCM-41	*2230* **0.30**	*2210* **0.08**	*2192* **0.07**	*2177* **0.18**	*2171* **0.34**	*2158* **0.28**	*2140* **0.33**

According to IR, H-ZSM5 and H-MCM-22 systems (supports and catalysts) possess the highest content in strong Brønsted sites and H-MCM-41 the lowest total number of Brønsted sites (strong and mild) (Table 11). On the other hand, H-MCM-22 and H-MCM-41 systems exhibit the highest number of strong Lewis sites, while H-ZSM-5 contains only a small quantity of them. On H-MCM-41, the number of strong Lewis sites increases upon Pt introduction, in line with the results presented in the former section.

H-MCM-41 systems appear as almost inactive in cumene cracking and isopropanol dehydration. Both H-ZSM-5 and H-MCM-22 systems are very active in cumene cracking (between 35 and 44% of conversion for 10 mg of solid), in agreement with their population of strong Brønsted sites. However, while H-MCM-22 systems reach a conversion higher than 70% in isopropanol dehydration, H-ZSM-5 systems (support and catalyst) are only poorly active for this less demanding reaction (less than 20%).

One hypothesis being the possible poisoning of the strong Brønsted sites, cumene cracking and isopropanol dehydration tests were performed on H-ZSM-5 following the sequence: cumene cracking, isopropanol dehydration (same conversion as when measured directly) and cumene cracking for the second time. H-ZSM-5 still exhibited a high activity in cumene cracking after isopropanol dehydration, which allows discarding the poisoning of the acid sites; cumene conversion is even higher without intermediate thermal pretreatment of the sample between the second and the third steps. It is assumed that upon isopropanol dehydration, strong acid sites in H-ZSM-5 systems may be temporarily blocked by molecules which do not desorb easily (water, diisopropylalcohol ether) and which may influence the catalytic activity of the system if they are not eliminated.

In conclusion, isopropanol dehydration should be used to compare acidity only on similar materials, provided that they do not exhibit a too high acidity.

1.6.5.2 The influence of catalyst properties on different reactions

The catalysts were tested in several reactions and some of the reactions were very much affected by the catalyst properties. Partner 1 performed the hydrogenolysis of hydroxymatairesinol (HMR) to matairesinol (MAT) using supported palladium catalysts. This reaction has shown to be very sensitive to both the acidity of the catalyst and to the reaction conditions. Figure 34 shows the initial rate versus concentration of acid sites for Pd/CNF catalysts (first four points) and Pd/H-Beta catalysts (last four points). It is visible that there is a maximum in the initial rate at 0.025 mmol/g_{cat} concentration of acid sites. Brønsted acid sites, palladium and hydrogen are all necessary for the hydrogenolysis of HMR to take place. The initial rate has an optimum for both concentration of acid sites and hydrogen pressure. The reaction mechanism proposed by Partner 1 (see WP 4), where the initial step is protonation of the hydroxyl group followed by abstraction of water and addition of a hydride, was used in the quantum chemical calculations performed by Partner 1. This reaction mechanism is also confirmed by the dependence of concentration

of acid sites (Figure 34) and the dependence of hydrogen pressure that has been observed in the kinetic study. At low concentration of acid sites, the rate limiting step could be the protonation of the hydroxyl group. Also the adsorption strength could be depending on the acidity of the support, the molecule should bond strongly enough but not too strongly in order to obtain an optimum reaction rate. At lower hydrogen pressure, the addition of a hydride to the HMR carbenium ion intermediate could be the rate limiting step, in case of a catalyst that is not deficient in acid sites. At higher pressure, the hydrogen could hinder the hydrogenolysis if the amount of hydrogen present on the catalyst surface is much higher than the amount of HMR carbenium ionic intermediate.

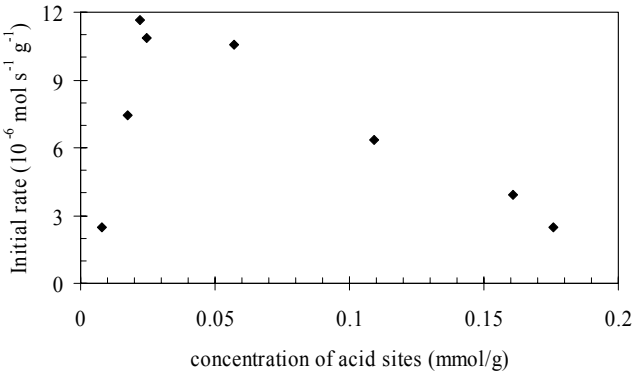

Figure 34 Initial rate for the conversion of HMR as a function of concentration of acid sites. The first four points stand for Pd/CNF catalysts, having lower acidity, the last four points stand for Pd/H-Beta catalysts, having higher acidity.

The same Pd/CNF and Pd/H-Beta catalysts were tested in the oxidation of lactose as in the hydrogenolysis of HMR. The same relationship was observed; the reaction rate increases as the acidity increases for Pd/CNF catalysts and the rate decreases with acidity increase for Pd/H-Beta catalysts (see Figure 35).

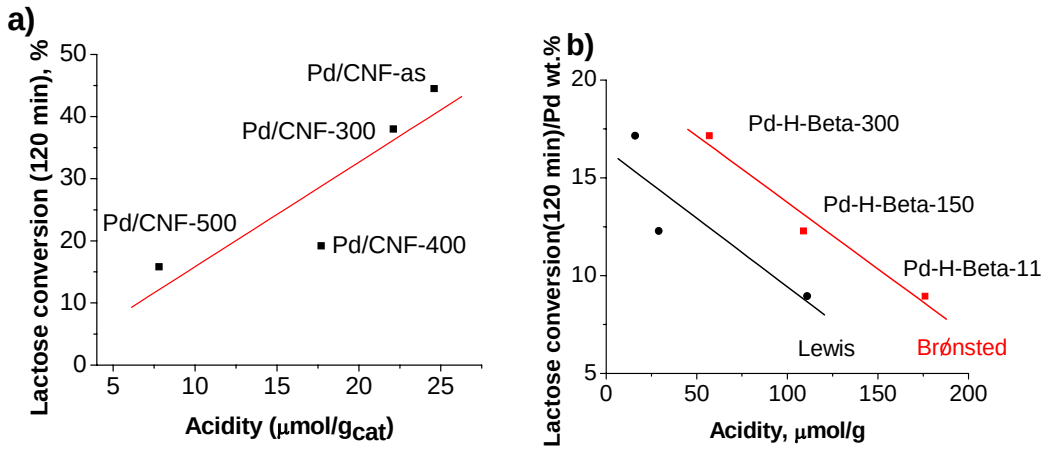

Figure 35 Influence of acidity on catalytic activity in lactose oxidation a) Pd/CNF catalysts, b) Beta zeolites.

Partner 6 observed a reversed particle size effect for CNF supported platinum and ruthenium catalysts for the cinnamaldehyde hydrogenation. The platinum catalysts with oxygen on the CNF surface showed the highest selectivity for the largest metal particles, which is in line with results described in literature. After removal of the oxygen surface groups via a heat-treatment, the smallest metal particles resulted in the highest selectivity towards cinnamyl alcohol, resulting in a reversed particle size effect compared to the catalytic results obtained with oxygen-rich supports. The observed particle size effects are explained by a change in the adsorption mode of the reactant as a function of the polarity of the support.

1.6.5.3 Catalytic profiling analysis

Partner 7 (Deg) developed a method (so called "profiling analysis") with which catalytic characteristics of precious metal powder catalysts for fine chemical application can be efficiently and comprehensively elucidated. Moreover, those physical properties can be identified which do influence the catalytic performance profiles significantly. Thus, the profiling method takes into account the complex relationship of physico-chemical parameters of solids and catalytic performance parameters. Catalytic profiling analysis includes a set of test reactions which are very sensitive with respect to catalyst properties.

Several catalysts were tested in different reactions within WP 2. From activity and selectivity values measured for a set of test reactions (Figure 36a) corresponding performance profiles (Figure 36b) can be derived which can be understood as catalytic fingerprints for individual catalysts. Thus, performance profiles allow a statistical analysis of correlations and, hence, similarities (Figure 36b).

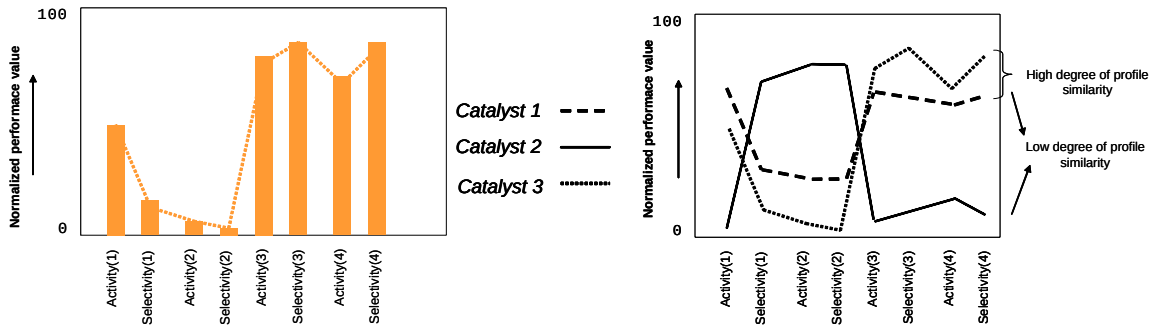

a) b)

Figure 36 Illustration of the concept for catalyst profiling based on a set of sensitive test reactions: a) Determination of particular performance data for an individual catalyst (activity and selectivity values in different test reactions), b) Visualization of performance profiles from the particular performance values as fingerprints for individual catalysts as a basis of similarity analysis.

The test set-up by which the catalysts can be differentiated was validated with respect to reproducibility of catalyst behaviour and exclusion of mass transfer phenomena. Moreover, it was analyzed whether the different test reactions are sensitive with respect to structural properties of catalysts using diverse industrial Pd catalysts covering a wide range of particle size and metal oxidation states.

With the heuristic method ("profiling analysis") a methodology is available which allows the comparison of new materials developed in the project on a very comprehensive basis with industrial catalysts. Advantages of new materials with respect to industrial application can be analysed by this method with a superior view. Furthermore, the physical properties which are the key for high catalytic performance can be analysed based on the profiling method. The latter aspect allows a rational approach for the nano-catalyst development.

By application of both profiling methods (catalytic performance and solids' characteristics) Partner 7 has analyzed correlations between catalytic and solid properties (Milestone 7).

1.6.6 WP 6 – Prototype catalyst

The objective of WP 6 was prototype catalyst preparation, characterisation and testing. The fundamental knowledge served as basis for the preparation, characterisation and testing of prototype catalysts in the test reaction in WP 2. Scale-up of preparation recipes

was studied by partner 7. For deliverable D13, the goal was to have five prototype catalysts and this was fulfilled since six prototype catalysts have been delivered.

The development of preparation routes for heterogeneous (powder) catalysts aims at reliable recipes capable of producing catalysts with reproducible performance. Conventional techniques (e.g. [incipient wetness] impregnation, deposition precipitation) are marked by a strong interaction between catalyst precursors (mostly dissolved in water) and suspended support materials. An important parameter in this regard is f. ex. the charge of the support surface, determined by its point of zero charge (the pH corresponding to charge neutrality). Above this point, the support's surface is negatively charged and therefore suited for adsorption of positively charged precious metal precursors. However, the precursors' charges in most cases as well depend on the pH, and the situation becomes even more complex taking into account all possible equilibria between the precursors and their reaction products. As a consequence, interface phenomena and liquid-solid equilibria influence active site formation (f. ex. via the extent of metal loading), and the support's surface actively determines metal nanoparticles' size (-distribution) and / or morphology. Taking into account the complex interplay between different physico-chemical mechanisms in such multiphase systems, it is desirable for prototype catalysts to separate the preparation steps as far as possible but to keep at the same time the handling simple.
The immobilization of preformed (precious) metal ([hydr-] oxide) sols in contrast offers the opportunity to control nanoparticle characteristics in a much simpler system (without influence of the support), according to the well-known recipes of colloid chemistry. Opportunities of this concept are scrutinized in the Nanocat project for the formation and immobilization of palladium ([hydr-] oxide) colloids for powder catalyst production. The preparation process begins with adjusting the pH of a suitable Pd-precursor solution, in presence of a (polymeric) stabilizing agent. The resulting colloid is immobilized on a powder support and optionally gas-phase treated at elevated temperatures.

Partner 7 prepared catalysts based on (hydr-) oxidic colloids of palladium and platinum which were mostly stabilized with the cationic polymer poly-(diallyldimethyl)-ammonium chloride (PDAMDAC). However, by variation of parameters such as, f. ex., immobilization pH, -time and –temperature, PDADMAC turned out to be unsuitable for catalyst preparation. Hence, poly-(vinylpyrrolidone) (PVP) was introduced as a new protecting agent which much better stabilizes the investigated (hydr-) oxidic colloids and

affords a much easier immobilization. It was the first time that PVP could be successfully used for the preparation of supported palladium (hydr-) oxide catalysts, and first attempts were made to investigate preparation parameters' influence on catalyst activity.

In this context, the catalytic behaviour has been analyzed for more complex reaction, namely the selective hydrogenation of 2-hexyne (Figure 37) with high demand concerning chemo- and stereo-selectivity.

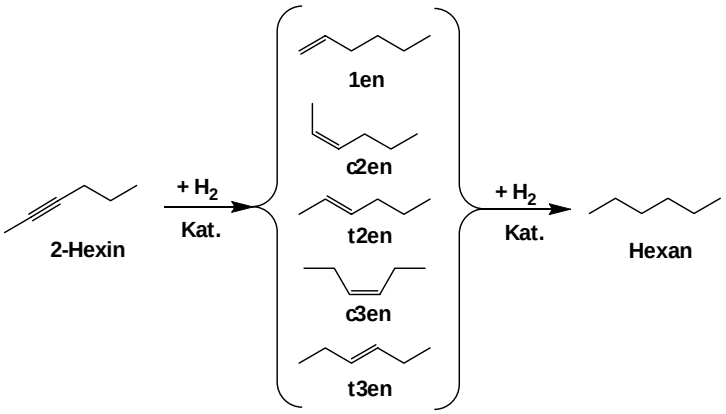

Figure 37 2-hexyne hydrogenation network

Usually, stereochemical discrimination requires the application of organic modifiers and / or selective poisons. Most prominent example for the latter is the Lindlar catalyst, a $CaCO_3$-supported, partially lead-poisoned Pd catalyst which upon addition of certain nitrogen-containing bases (preferentially quinoline) affords cis-2-hexenes in high yields. Recently, Pd-colloid derived catalysts gained interest for this reaction, as systems both with and without Pb exhibited high cis-selectivities; hence, the PVP-PdO_x/C system was expected to be a promising system, not at least because of a potential promoting effect of the nitrogen-containing PVP.

Applying each a conventional reduced and non-reduced Pd/C catalyst in this reaction, both types turned out to produce cis-configured 2-hexene as the main product, even without any additive or promoter. At the same time, formation of the trans-isomer and hexane occurs only to a minor extent. In comparison to the reduced type, the non-reduced Pd/C catalyst generates much less unidentified byproducts, however, high cis-2-hexene selectivity (87 % vs. 59 %) is accompanied by significantly lower 2-hexyne conversion (33 % vs. 50 %).

In the selective liquid-phase hydrogenation of 2-hexyne, the PVP-PdO_x/C catalysts afforded higher yields of cis-2-hexene in comparison to conventional Pd/C catalysts. Inasmuch, PVP-PdO_x/C represents promising alternatives to Lindlar systems which reach

high cis-selectivity with the help of noxious promoters (Pb) and additives (quinoline). By variation of the preparation parameters, one can distinguish between sets of variables with strong and weak influence on catalytic performance. During catalyst characterization by XRD / DFA, an amorphous state of the PdO_x particles couldn't be proved. The PVP stabilizer strongly interacts with the PdO_x/C system, as deduced from TPD-MS experiments, and after reduction of PdO_x by the stabilizer upon heating; the resulting Pd catalyzes further thermal degradation of PVP. Measurements of adsorption enthalpy in the PVP/C system revealed two mechanisms of interaction between stabilizer and support and justify the heating step during colloid immobilization ($\Delta H_{ads} > 0$).

Different prototype catalysts for selective alkyne hydrogenation based on different types of polymers have been prepared. During testing their advantage in catalytic selectivity against conventional precious metal powder catalysts was demonstrated (Milestone 8).

1.6.7 WP 7 – Dissemination of knowledge

The objective of WP 7 was to disseminate the fundamental knowledge from the metal particle size and environment as well as its relation to the catalyst activity/selectivity in forms of summer schools and workshops.

The summer school was not arranged, since Partner 1 organized the VIII EuropaCat conference, attracting 1500 participants from European Union and from the rest of the world. This event also collected many graduate students that took part in the presentations given by the partners in the Nanocat project.

Due to the formerly experienced low attendance in customer workshops related special scientific projects it was decided to have an alternative approach for dissemination of the Nanocat results. Instead of the workshop, selected output of the Nanocat project (which will be summarized in an issue of "Topics in Catalysis") in addition to several papers in peer-reviewing journals will be disseminated on the occasion of commercially oriented trade shows / conferences such as "Organic Process Research & Development Conference" (OPRD) and "New Horizons in Catalysis" were the industrial partner is represented regularly.

By replacing the formerly planned summer school and workshop by a European conference on Catalysis and several publications in international journals and conferences, it can be concluded that Milestone M9 has been achieved.

1.6.8 WP 8 – Project management

The objective of WP 8 was to arrange project management and mid-term assessment as well as final project assessment. Two meetings per year were arranged within the NANOCAT project. The deliverables within WP 8 were D16 Mid-term assessment (fulfilled in September 2006) and D17 Final assessment (March 2008). The milestone M10, the mid-term assessment of the NANOCAT project, was accomplished.

Below is a list of the meetings held within the Nanocat project.

Date	**Place**	**Meeting**	**Organizing partner**
1.4.2005	Åbo Akademi University, Turku, Finland	Kick-off meeting	1
16.9.2005	Utrecht University, Utrecht, The Netherlands	Project meeting	6
20.5.2006	FORTH, Heraklion, Crete, Greece	Project meeting	4
15.9.2006	Universite Pierre et Marie Curie, Paris, France	Mid-term assessment, project meeting	3
9.3.2007	University of Palermo, Palermo, Italy	Project meeting	5
21.9.2007	Evonik-Degussa, Hanau, Germany	Project meeting	7
25.1.2008	Tver State Technical University, Tver, Russia	Final assessment, project meeting	2

1.6.9 WP 9 – Economic evaluation of catalysts

The objective of WP 9 was the economical evaluation. Based on results of prototype and scale-up study economic potential of catalysts and processes using respective catalysts was evaluated. Partner 7 performed analysis of market potential and cost estimation of materials production. Deliverable D18/19, benchmark study has been accomplished and so has milestones M 11, M 12, recommendation on catalyst application.

In order to evaluate the feasibility of producing prototype catalysts production costs and safety aspects of production were analyzed and compared with commercial catalysts based on respective indices. For this purpose, three different indexes have been defined:

1. Index $\underline{I_V}$ related to variable costs (mainly material costs which were derived from catalogs of chemical distributors (see Table 12)). Since precious metal (PM)

strongly fluctuate and, on the other hand, correspond to the main cost proportion, two different cost indices were considered, one including the precious metal costs and one excluding them. Reference costs refers to a commercial catalyst recipe.

$$I_{V,withPM} = \frac{prototype\ material\ costs\ including\ PM\ costs}{cost\ reference\ including\ PM\ costs} - 1$$

$$I_{V,without\ PM} = \frac{prototype\ material\ costs\ excluding\ PM\ costs}{cost\ reference\ excluding\ PM\ costs} - 1$$

2. Index I_f related to fixed costs (see Table 13) depending on space time yield (kg of catalyst / m^3 / min). Fixed costs are determined by both the absolute batch time and the required concentrations of metal and salt solutions.

$$I_f = \frac{prototype\ space\ time\ yield}{reference\ space\ time\ yield}$$

3. Index I_s related to safety aspects for estimation of potential hazards during catalyst production. This index is calculated based on pre-defined safety levels indicated in Table 14. I. e. potential hazards are evaluated for all catalyst components and precursors and added up.

$$I_f = \frac{\sum safety\ indicators\ related\ to\ reference\ recipe}{\sum safety\ indicators\ related\ to\ prototype\ recipe}$$

Table 12 Variable cost related Indices: Estimation of material costs (based on catalogues of chemical distributors).

Catalyst	Type of support	Precoius metal	reduced / nonreduced	total material costs w/o PM	total material costs (EUR) per kg (with PM)	costs (EUR) of support related to 1 kg Catalyst	costs (EUR) of precious metal component related to 1 kg Catalyst	costs (EUR) of addtivies and solvents related to 1 kg Catalyst	Costs (EUR) of base/acid related to 1 kg catalyst	Costs (EUR) of reducing agent related to 1 kg catalyst
DEG	carbon	Pt	R	20,44	4675,44	20,00	4655,00	0,00	0,00	0,44
P6 Utrecht	Nanofibre	Pt	R	16,32	17836,32	10,00	17820,00	6,32	0,00	0,00
DEG	carbon	Pd	N	20,00	2210,00	20,00	2190,00	0,00	0,00	0,00
P7 (Florian)	carbon	Pd	N	24,85	2215,36	20,13	2190,51	3,40	1,32	0,00
P2 (Tver)	polystyrol	Ru	R	937,52	2158,09	937,50	1220,57	24,57	0,00	0,02
DEG	carbon	Ru	R	21,51	1252,51	20,00	1231,00	0,00	1,02	1,50
P3 (Paris)	Alumina	Pt	R	20,00	1392,14	20,00	1372,14	0,00	0,00	0,00
DEG	Alumina	Pt	R	19,95	2093,95	19,00	2074,00	0,00	0,00	0,95

Table 13 Fixed costs related Indices:

- Batch time
- Space time yield (kg of catalyst / m3 / min)

Catalyst	Type of support	Precoius metal	reduced / nonreduced	time absolute (min) per batch	space time yield / kg / min / m3	Kennzahl Gesundheits-gefährdend
DEG	carbon	Pt	R	60,00	2,46	7,00
P6 Utrecht	Nanofibre	Pt	R	1200,00	0,02	8,00
DEG	carbon	Pd	N	60,00	2,56	3,00
P7 (Florian)	carbon	Pd	N	240,00	0,12	4,00
P2 (Tver)	polystyrol	Ru	R	170,00	0,55	14,00
DEG	carbon	Ru	R	100,00	1,31	9,00
P3 (Paris)	Alumina	Pt	R	240,00	0,02	9,00
DEG	Alumina	Pt	R	80,00	1,80	3,00

Table 14 Safety related Index: Estimation of potential hazards during catalyst production

	Symbols	Index
explosive	E	4
oxidizing	O	1
highly inflamable	F+	3
inflamable	F	2
highly toxic	T+	4
toxic	T	3
harmful to health	Xn	2
corrosive	C	1
irritant	Xi	1
carcinogenic	R40, 45	4
mutagenic	R47	4
reprotoxic	R40, 46	4
chronic impairment	R48	3
sensitising compound	R42, 43	2

In principle, high index values are critical since they indicate disadvantageous situations against commercial catalysts. If a prototype catalyst shall have indeed commercial potential disadvantages from the cost perspective, it must be compensated by a respective higher catalytic performance. To take this into account in the benchmark analysis, a catalyst performance index was defined which indicates how much its productivity must exceed that of the commercial reference in order to become competitive. Of course it must be emphasized that this can be only a rough indicator since for real applications all aspects of process operation (separation issues, deactivation behaviour, leaching, …) must be considered.

$I_p = \textit{required factor of catalyst prototype productivity}$

Exemplarily the benchmark analysis was applied to two prototype catalysts developed in the Nanocat project:

a) Pt catalyst support an carbon Nanofibres developed by Partner 6

b) Polymer stabilized Pd supported on activated carbon

For the first example, the comparison between a nanofibre based catalyst and a commercial Pt catalyst with activated carbon as support is shown in Figure 38. High values of the indices for the prototype catalyst and large difference between prototype and commercial catalyst indicate critical situations. Thus, for the nanofibre catalyst, the usage of expensive metal precursors results in high overall material costs, i.e., an alternative metal source would help to improve this situation. An additional disadvantage of the prototype recipe results from the low space time yield which is mainly driven by the long reduction / calcination procedure. Here, further optimization effort is required. For the present situation, the disadvantageous in material costs and space-time yield result in a productivity compensation factor of about 150 which is still significant.

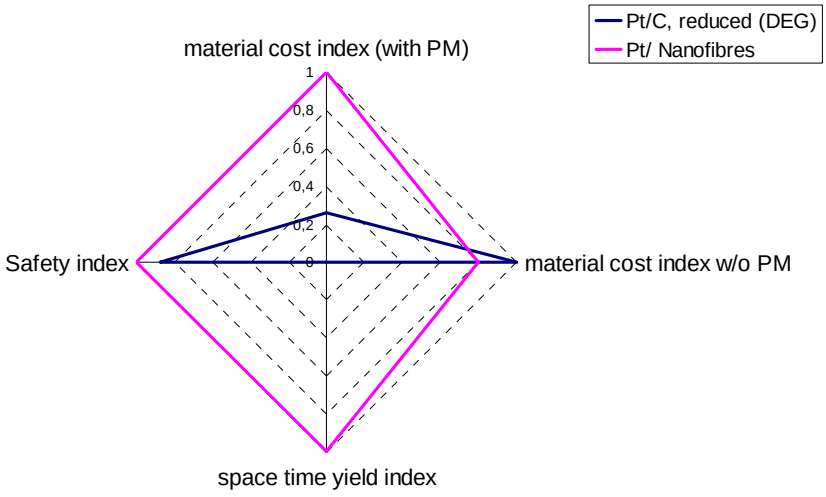

Figure 38 Comparison of benchmark indices for Pt on carbon catalysts

A similar analysis was performed for a polymer-stabilized Pd catalyst (Figure 39). Here, the main potential for improvement lies in the space time yield. To compensate this disadvantage the productivity of this catalyst should be 17 times higher than its commercially available alternative. The benchmark analysis indicates that the usage of much higher concentrations of metal precursors would improve the commercial attractiveness of such type of catalysts.

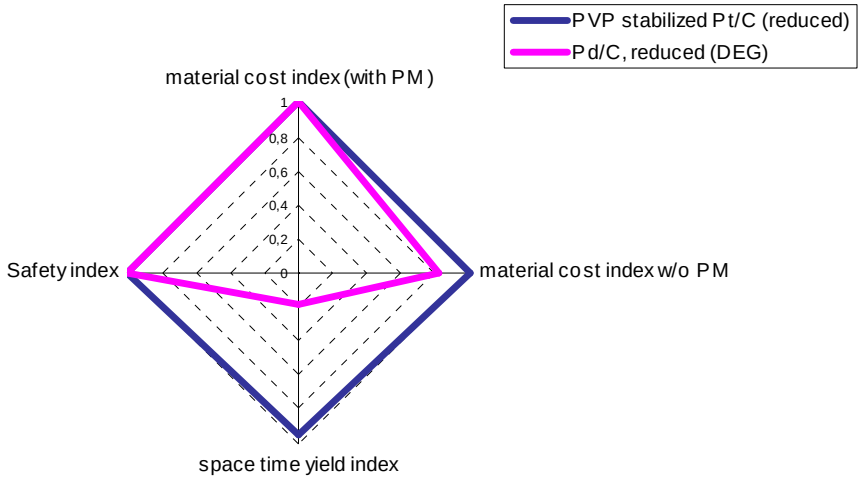

Figure 39 Comparison of benchmark indices for Pd on carbon catalysts

Recommendations for a methodology to evaluate the preparation of nano-structured commercial point of view as well as recommendations on how to optimize the preparation procedure were given. Polymer-stabilized precious metal catalysts were identified to have a commercial potential in highly complex reactions with high demand concerning chemo- and stereo-selectivity such as stereo-selective hydrogenation of alkynes (milestones 11 and 12).

The chosen approaches by the different partners were made based on scientific considerations. We are well aware that for commercialization other catalyst preparation routes are needed. There is ample room for improvement with that respect. For example homogeneous deposition precipitation method for incorporation of metal can be replaced by pore volume impregnation which results in a much shorter catalyst hold-up during preparation. These attempts were not made within the project and leave room for further study.

1.7 Conclusions and impact of the project

Specific metal-polymer nanoscale systems that can be applied in modern research and industry have been designed and prepared:

(i) pH-responsive diblock copolymers.

(ii) pH-responsive microgels for the in situ synthesis of Pt nanoparticles at high metal loadings. The metal loading process revealed two effects that strongly influence the swelling behaviour of the microgels during metal loading; the protonation of the polymer amine groups and the effective cross-linking caused by the metal precursor. The

equilibrium between these two opposing effects determines the final size of the microgels after metal complexation.
(iii) Random polymer gels with different functionalities. The metal loading of the networks was found to increase with the degree of swelling of the network and primarily with the presence of strong polymer-metal interactions, signifying the role of the molecular polymer structure on its binding capacity.
(iv) pH-responsive model co-networks based on cross-linked stars. Both the co-network composition and architecture was found to influence the metal incorporation and the metal nanoparticle formation.

The efficient method of different structure and morphology platinum metals nanoparticles formation in matrix of hypercrosslinked polystyrene was developed. The formation of metals nanoparticles take place in polymer pores and determined by hypercrosslinked polystyrene, precursors and solvent sorption interactions. The method provides control over nanoparticles mean diameter via using solvents and precursors of different hydrophobicity.

When aqueous media are used, the formation of mesoporous aluminic systems occurs not around micelles, but through the sticking of boehmite nanoparticles stabilized by organic agents in a molecular form or as aggregates; in these conditions of synthesis, specific surface area is limited by the size of the oxidic nanoparticles between which the intergranular mesoporosity develops.

When the initial Al speciation of a meso- or microporous silicoaluminic support is complex, differences in acidity between support and catalyst may arise from changes in Al speciation during the contacting with water linked to metal introduction, and not to the presence of metal nanoparticles. Consequently, it may not be straightforward to deduce the acidic properties of a catalyst from those of its bare support, because the surface species are not identical.

The interesting lignan matairesinol was syntesized starting from hydroxymatairesinol using palladium catalysts on carbon, zeolites and carbon nanofibre support materials and it was concluded that the acidity of the support material had a great influence on the activity and selectivity; an optimum in activity as a function of acidity was found.

A large influence of support structure is observed when carbon nanofibers (CNF), carbon nanotubes (CNT) and carbon nanoplatelets (CNP) were used as catalyst support. Platinum on CNF and platinum on CNP turned out to be catalytic active for the cinnamaldehyde hydrogenation and the CNT supported platinum catalyst was not active, which is ascribed to an extremely fine dispersion and strong interaction with surface oxygen for the latter catalyst.

Platinum-tin, platinum-iron, platinum-gallium and platinum-germanium catalysts prepared via reductive deposition precipitation (i.e. hydrogen-induced interaction of promoter metal ions with the platinum surface) result in a close contact of platinum and promoter, which leads to an enhanced catalytic activity and selectivity for the cinnamaldehyde hydrogenation.

Platinum and ruthenium were deposited on carbon nanofibers via atomic layer deposition and homogeneous deposition precipitation and heat-treated afterwards. After heat-treatment, a reversed particle size effect was observed for these catalysts in the cinnamaldehyde hydrogenation: larger metal particles resulted in a higher selectivity. The observed particle size effects are explained by a change in the adsorption mode of the reactant as a function of the polarity of the support.

Hydrogenation of cinnamaldehyde on Pt catalysts supported on mesoporous oxides is accelerated when the support exhibits strong Brønsted and Lewis acid sites, due to a likely influence of the support acidity on the particles electronic properties (facilitated desorption of the reactants); on the other hand, selectivity toward cinnamyl alcohol dramatically increases when alumina is the support, because of a participation of the Lewis sites surrounding the metal particles, which may contribute to the adsorption of the reactants on the catalyst via their C=O bond.

The developed nanocatalytic systems based on hypercrosslinked polystyrene showed high activity in investigated reactions of fine organic synthesis (partial oxidation of D-glucose and L-sorbose) compared to traditional methods. Increasing of nanoparticles mean diameter from 1-2 nm up to 10-15 nm decreases D-glucose and L-sorbose oxidation rates.

The Pd/H-Beta zeolites with lower silica-to-alumina ratio possess higher catalytic activity in the oxidation of the benzylic alcohol piperonyl alcohol. Pt supported on HPS polymer shows high activity in the benzylic alcohol oxidation.

The higher the silica-to-alumina ratio (25, 150, 300) in the Beta zeolite, the larger Pd particles are formed during reduction.

Analysis of supported metal catalysts showed a variety of metal species in different oxidation states.

Energetic and kinetic of metal supported catalysts have been analyzed by quantum chemistry and Monte Carlo methods. Modelling of the catalyst structures has taken into account the active sites and their surrounding environments. A thermal time dependent Monte Carlo approach has been developed and the influence of the thermal gradients and spots on the surface processes has been investigated. A 3-D representation of the materials helped to get more realistic insights in the systems studied by Monte Carlo methods. The suggested quantum-stochastic algorithmic technique allowed to reproduce macroscopic findings, having confidence on the microscopic details used to model the same findings.

Modelling of lactose oxidation on Au/Al_2O_3, which included O_2 concentration dependence as well as differences in activity of different Au faces, was performed.

The industrial partner (P7) developed a high-throughput methodology and method of data analysis which allows comparing the new materials developed in the project on a very comprehensive basis with industrial catalysts. Advantages of new materials for industrial application can be analysed by this method with a superior view. Two patents were also filed.

Benchmark studies were performed. Recommendations for a methodology to evaluate the preparation of nano-structured commercial point of view as well as recommendations on how to optimize the preparation procedure were given. Polymer-stabilized precious metal catalysts were identified to have a commercial potential in highly complex reactions with high demand concerning chemo- and stereo-selectivity such as stereo-selective hydrogenation of alkynes.

2 DISSEMINATION AND USE

The knowledge generated within the NANOCAT project has been disseminated in international peer-review journals, in two patents and at several conferences all around the world. Lists of patents, publications and conferences are presented in section 2.1 and a list of public deliverables in section 2.2. In the future, a special issue in “Topics in Catalysis”

will appear and the results will be also be presented at conferences and in different peer-review journals.

All public information and results of the NANOCAT project can be accessed through the public project website: http://web.abo.fi/fak/ktf/tek/p_nanocat.html

2.1 Presentations and publications

Patents
Partner 7 has applied for two patents within the Nanocat project:
"Evaluation of the performance profile of catalysts"
European patent application: Appl.-No 06110693.6, Publication-No. 1837651
US: Appl.-No. 11/651,582

List of publications
The following publications have been made in refereed or other journals:

H. Markus, P. Mäki-Arvela, N. Kumar, T. Heikkilä, V-P. Lehto, R. Sjöholm, B. Holmbom, T. Salmi, D.Yu. Murzin, Reactions of hydroxymatairesinol over supported palladium catalysts. Journal of Catalysis 238 (2006) 301-308.

H. Markus, P. Mäki-Arvela, N. Kumar, N.V. Kul'kova, P. Eklund, R. Sjöholm, B. Holmbom, T. Salmi, D.Yu. Murzin, Hydrogenolysis of hydroxymatairesinol over carbon supported palladium catalysts. Catalysis Letters 103 (2005), 125-131.

D. Kubicka, N. Kumar, T. Venäläinen, H. Karhu, I. Kubickova, H. Österholm, D.Yu. Murzin,"The metal-support interactions in zeolite-supported noble metals: the influence of metal crystallites on the support acidity", Journal of Physical Chemistry B, 2006, 110, 4937-4946.

J. Hajek, D.Yu. Murzin, Short introduction to sol-gel chemistry in heterogeneous catalysis, in "Nanocatalysis" (ed. D.Yu. Murzin), Research Signpost, Kerala, India, 2006, 9-32.

A.V. Tokarev, L.M. Kustov, A. Ivaska, D.Yu. Murzin, "Cyclic voltammetry as a tool for characterization of supported VIII group metal catalysts", Applied Catalysis. A. General, 2006, 309, 52-61.

A.V. Tokarev, E.V. Murzina, J. Kuusisto, J-P. Mikkola, K. Eränen, D.Yu. Murzin, "Kinetic behaviour of electrochemical potential in three-phase heterogeneous catalytic oxidation reactions", Journal of Molecular Catalysis. A. Chemical, 2006, 255, 199-208.

D.Yu. Murzin, P. Mäki-Arvela, " Nanocatalysis", in "Nanocatalysis" (ed. D.Yu. Murzin), Research Signpost, Kerala, India, 2006, 1-7.

N. Kumar, D. Kubicka, T. Heikkilä, H. Karhu, M. Tiitta, T. Salmi, D.Yu. Murzin, "Ir-modified MCM-41 mesoporous molecular sieve catalysts synthesized using in-situ, impregnation and ion-exchange methods for ring opening of decalin", in "Nanocatalysis" (ed. D.Yu. Murzin), Research Signpost, Kerala, India, 2006, 33-50.

N. Kumar, O.V. Masloboischikova, L.M. Kustov, T. Heikkilä, T. Salmi, D.Yu. Murzin, Synthesis of Pt modified ZSM-5 and beta Zeolite catalysts: Influence of ultrasonic irradiation and preparation methods on physico-chemical and catalytic properties in pentane isomerization. Ultrasonics Sonochemistry 14, **2007**, 122-130.

J. Kuusisto, A.V. Tokarev, E.V. Murzina, M. Roslund, J-P. Mikkola, D.Yu. Murzin, T. Salmi, From renewable raw materials to high value-added fine chemicals catalytic hydrogenation and oxidation of D-lactose. Catalysis Today, 121, **2007**, 92-99.

H. Markus, P. Mäki-Arvela, N. Kumar, T. Salmi, D.Yu. Murzin, Hydrogenolysis of a wood extractive to an anticarcinogenic and antioxidative compound. Catalysis Today 121, **2007,** 100-105.

H. Markus, A.J. Plomp, P. Mäki-Arvela, J.H. Bitter, D.Yu. Murzin, The influence of acidity of carbon nanofibre-supported palladium catalysts in the hydrogenolysis of hydroxymatairesinol. Catalysis Letters 113, **2007,** 141-146.

H. Markus, A.J. Plomp, T. Sandberg, V. Nieminen, J.H. Bitter, D.Yu. Murzin, Dehydrogenation of hydroxymatairesinol to oxomatairesinol over carbon nanofibre-supported palladium catalysts. Journal of Molecular Catalysis A 274, **2007,** 42-49.

D.Yu. Murzin, E. Toukoniitty, Nanocatalysis in asymmetric hydrogenation. Reaction Kinetics and Catalysis Letters, 90, **2007**, 19-25.

D.Yu. Murzin, On validity of Langmuir adsorption on supported nanoparticles. Reaction Kinetics and Catalysis Letters, 91, **2007**, 37-43.

D.Yu. Murzin, P. Mäki-Arvela, T. Salmi, B. Holmbom, Catalytic transformations for production of fine chemicals and pharmaceuticals from wood derived raw materials. Chemical Engineering and Technology, 30, **2007**, 569.

A.V. Tokarev, E.V. Murzina, J-P. Mikkola, J. Kuusisto, L.M. Kustov, D.Yu. Murzin, Application of in-situ catalyst potential measurements for estimation of reaction performance: D-lactose oxidation over Au and Pd catalysts. Chemical Engineering Journal, 134, **2007**, 153.

E. Sulman, L. Bronstein, V. Matveeva, M. Sulman, V. Lakina, V. Doluda, P. Valetsky, "Polymer stabilized Pd and Pt nanoparticles: Structure and catalytic properties " in "Nanocatalysis" (ed. D.Yu. Murzin), Research Signpost, Kerala, India, 2006, 51-98.

V.Yu. Doluda, E.M. Sulman, V.G. Matveeva, M.G. Sulman, N.V. Lakina A.I. Sidorov, P.M. Valetsky, L.M. Bronstein Kinetics of phenol oxidation over hypercrosslinked polystyrene impregnated with Pt nanoparticles Chemical Engineering Journal 134 (2007) 256–261

E.M. Sulman, V.V. Alferov, Yu.Yu. Kosivtsov, A.I. Sidorov, O.S. Misnikov, A.E. Afanasiev, N. Kumar, D. Kubicka, J. Agullo, T. Salmi, D.Yu. Murzin The development of the method of low-temperature peat pyrolysis on the basis of alumosilicate catalytic system Chemical Engineering Journal 134 (2007) 162–167

E. Sulman, V. Doluda, S. Dzwigaj, E. Marceau, L. Kustov, O. Tkachenko, A. Bykov, V. Matveeva, M. Sulman, N. Lakina Catalytic properties of Ru nanoparticles introduced in a matrix of hypercrosslinked polystyrene toward the low-temperature oxidation of d-glucose Journal of Molecular Catalysis A: Chemical 278 (2007) 112–119

I.B. Tsvetkova, L.M. Bronstein, S.N. Sidorov, O.L. Lependina, M.G. Sulman, P.M. Valetsky, B. Stein, L.Z. Nikoshvili, V.G. Matveeva, A.I. Sidorov, B.B. Tikhonov, G.N. Demidenko, L. Kiwi-Minsker, E.M. Sulman Structure and behavior of nanoparticulate catalysts based on ultrathin chitosan layers Journal of Molecular Catalysis A: Chemical 276 (2007) 116–129

L.M. Bronstein, V.G. Matveeva, E.M. Sulman Nanoparticulate Catalysts Based on Nanostructured Polymers Pp 93-127 Nanoparticles and Catalysis Ed. Didier Astruc Wiley-VCH , Weinheim, 640 pp

E. Marceau, "Characterizing a supported catalyst: A methodological approach" in "Nanocatalysis" (ed. D.Yu. Murzin), Research Signpost, Kerala, India, 2006, 127-176.

S. Handjani, J. Blanchard, E. Marceau, P. Beaunier, M. Che - "Mesoporous aluminas prepared in aqueous media: a comparative study of their synthesis, stability and physicochemical properties", Mesopor. Micropor. Mater., (10.1016/j.micromeso.2008.03.006).

M. Vamvakaki, L. Papoutsakis, V. Katsamanis, T. Afchoudia, S.H. Anastasiadis, P.G. Fragouli, H. Iatrou, N. Hadjichristidis, S.P. Armes, S. Sidorov, D. Zhirov, V. Zhirov, M. Kostylev and L.M. Bronstein, "Micellization in pH-sensitive amphiphilic block copolymers in aqueous media and the formation of metal nanoparticles" *Faraday Discuss.* **2005,** *128,* 129-147.

L.M. Bronstein, M. Vamvakaki, M. Kostylev, V. Katsamanis, B. Stein, S.H. Anastasiadis, "Transformations of Poly(Methoxy hexa(ethylene glycol) methacrylate)-*b*-(2-(Diethyl amino)ethyl methacrylate) Block Copolymer Micelles upon Metallation" *Langmuir* **2005,** *21,* 9747-9755.

M. Vamvakaki, D. Palioura, A. Spyros, S. P. Armes, S. H. Anastasiadis, "Dynamic Light Scattering *vs.* ^{1}H NMR Investigation of pH-Responsive Diblock Copolymers in Water" *Macromolecules* **2006**, *39,* 5106-5112.

A. Athanassiou, M. I. Lygeraki, D. Pisignano, K. Lakiotaki, M. Varda, C. Fotakis, R. Cingolani, and S. H. Anastasiadis "Photocontrolled Variations in the Wetting Capability of Photochromic-Polymers Enhanced by Surface Nanostructuring" *Langmuir* **2006,** *22,* 2329-2333.

A. Athanassiou, M. Varda, E. Mele, M. I. Lygeraki, D. Pisignano, M. Farsari, C. Fotakis, R. Cingolani, and S. H. Anastasiadis "Combination of Microstructuring and Laser-light Irradiation for the Reversible Wettability of Photosensitised Polymer Surfaces" *Appl. Phys. A* **2006,** *83,* 351-356 [Rapid Communication].

K. Chrissopoulou, S. H. Anastasiadis, E. P. Giannelis and B. Frick "Quasielastic Neutron Scattering of Poly(methyl phenyl siloxane) in the Bulk and under Severe Confinement" *J. Chem. Phys.* **2007,** *127,* 144910-1-13.

A.I. Triftaridou, D. Kafouris, M. Vamvakaki, T. K. Georgiou, T. C. Krasia, E. Themistou, N. Hadjiantoniou, C. S. Patrickios, "Three different types of quasi-model networks: synthesis by group transfer polymerization and characterization" *Polym. Bull.* **2007,** *58,* 185-190.

D. Palioura, S. P. Armes, S. H. Anastasiadis, M. Vamvakaki, "Metal Nanocrystals Incorporated within pH-Responsive Microgel Particles" *Langmuir* **2007,** *23,* 5761-5768.

A. I. Triftaridou, M. Vamvakaki, C. S. Patrickios "Cationic Amphiphilic Model Networks Based on Symmetrical ABCBA Pentablock Terpolymers: Synthesis, Characterization and Modeling" *Biomacromolecules* **2007**, *8,* 1615-1623.

M. Vamvakaki, C. S. Patrickios, Peter Lindner, Michael Gradzielski, "Amphiphilic Networks Based on Cross-Linked Star Polymers: A Small-Angle Neutron Scattering Study" *Langmuir* **2007,** *23,* 10433-10437.

M. Vamvakaki, C. S. Patrickios, "Synthesis and Characterization of the Swelling and Mechanical Properties of Amphiphilic Ionizable Model Conetworks Containing *n*-Butyl Methacrylate Hydrophobic Blocks" *Soft Matter* **2008,** *4,* 268-276.

S. H. Anastasiadis, M. I. Lygeraki, A. Athanassiou, M. Farsari, and D. Pisignano "Reversibly Photo-responsive Polymer Surfaces" *J. Adh. Sci. Techn.* **2008,** in press.

S. H. Anastasiadis and M. Vamvakaki "Synthesis of Metallic Nanoparticles within pH-sensitive Polymeric Matrices" *Int. J. Nanotechnology* **2008,** in press.

D. Duca, S. Giuffrida, A. Fontana, Zs. Varga, "Computational aspects in heterogeneous nano-catalysis" in "Nanocatalysis" (ed. D.Yu. Murzin), Research Signpost, Kerala, India, 2006, 177-229.

D. Duca, F. Ferrante, G. La Manna, J. Phys. Chem. C, 2007, 111, 5402.

D. Duca, G. Barone, S. Giuffrida, Zs. Varga, J. Comput. Chem., 2007, 28, 2483.

G. Barone, G. Casella, S. Giuffrida, D. Duca, J. Phys. Chem. C, 2007, 111, 13033.

D. Wolf, K. Möbus, S. Seebald, T. Tacke, "Rapid Identification of Suitable Pd-Catalysts for Hydrogenation of multi-functional substrates" Proc. on Fifth Tokyo Conference on Advanced Catalytic Science and Technology Tokio, July 2006

D. Wolf, S. Seebald, T. Tacke, "Accelerated identification of the preferred precious metal powder catalysts for selective hydrogenation of multi-functional substrates" Proc. 21st ORCS Conference on the Catalysis of Organic Reactions, Orlando, April 2006

F. Klasovsky, P. Claus, D. Wolf, Katalysatorpräparation mit nicht-metallischen Kolloiden: ein modulares Konzept, 41. Jahrestreffen Deutscher Katalytiker, 27-29 Februar 2008, Weimar.

Conferences

The participants of the project have also given presentations on the project results at national and international conferences and seminars listed below:

Planned / Actual Dates	Type	Type of audience	Countries addressed	Size of audience	Partner responsible /involved
22-27 May 2005	19th NAM, Philadelphia, USA	Research	EU, America	50	1
28 Aug-1 Sept 2005	7th Europacat, Sofia, Bulgaria	Research	EU	70	1, 5
23-27 Oct 2005	7th CAFC, Bingen, Germany	Research	EU	200	1
28 Oct 2005	Darmstadt	Research	EU	50	1

15-19 May 2006	XVII International Conference on Chemical Reactors, Greece	Research	EU	200	1
2006	Conference on mechanisms of catalytic reactions, St. Petersburg, Russia,	Research	EU	200	1
2006	International conference on the scientific basis for the preparation of heterogeneous catalysts, Louvain-la-Neuve, Belgium	Research	EU	400	1, 2
2006	APCAT-4, Singapore	Research	World	400	1
26-31 Aug 2007	VIII Europacat, Turku, Finland	Research	World	1500	1-3,5-8
September 16 – 20, 2007	8th Catalysis Applied to Fine Chemicals, Verbania, Italy	Research	EU	150	1, 2
April 2-6, 2006	21st Conference on Catalysis of Organic Reactions, Orlando, USA, April 2-6, 2006	Research	USA	200	2
July 16-20, 2007	ISHHC XIII International Symposium on the Relations between Homogeneous and Heterogeneous Catalysis.	Research	USA	250	2
4-8 July, 2007	III International Conference "Catalysis: Fundamentals and Application" dedicated to the 100th anniversary of Academician Georgii K. Boreskov	Research	Russia, EU	150	2
July 1-5, 2007	3th International Energy, Exergy and Environment Symposium, IEEES-3, Evora, Portugal	Research	EU	100	2
May 2007	French conference on catalysis, Gecat, La Grande Motte, France	Research	France	100	3
July 2007	European conference on chemistry, SFC07, Paris, France	Research	EU	500	3
Nov 2007	European symposium on catalysis, 39th Symposium of the J. Heyrovsky Institute, Prague, Czech Rep.	Research	EU	80	3
March 2005	General Meeting 05, American Physical Society, Los Angeles, CA, U.S.A.	Research	World	>200	4
May 2005	5th Panhellenic Chemical Engineering Conference, Thessaloniki, Greece	Research	Greece	100	4
June 2005	European Polymer Congress 2005, European Polymer Federation, Moscow, Russia	Research	EU	>200	4
August 2005	XXI Panhellenic Conference on Solid State Physics and Materials Science, Nicosia, Cyprus	Research	Greece, Cyprus	100	4
September 2005	International Symposium on Polymer Conetworks, Gels and Membranes – Science, Technology and Applications, Budapest, Hungary	Research	EU	100	4
December	Pacifichem 2005, Honolulu, Hawaii,	Research	World	>200	4

2005	U.S.A.				
March 2006	General Meeting 06, American Physical Society	Research	World	>200	4
April 2006	3rd Annual European Rheology Conference	Research	World	100	4
July 2006	3rd Workshop on Nanosciences and Nanotechnologies, Thessaloniki, Greece	Research	Greece	70	4
October 2006	IUPAC International Symposium on "Advanced Polymers for Emerging Technologies" [PSK30]	Research	World	>200	4
October 2006	Brain Korea 21 (BK21) Symposium on Macromolecular Science	Research	World	30	4
November 2006	6th Panhellenic Polymer Conference	Research	Greece	100	4
July 2005	SCI 2005- XXXIII Congresso Nazionale della Divisione di Chimica Inorganica della Società Chimica Italiana, Siena, Italy	Research	Italy	200	5
Dec 2005	SCI - Convegno Congiunto delle Sezioni Calabria e Sicilia, Catania, Italy	Research	Italy	50	5
Dec 2005	SCI - XIV Congresso Nazionale della Divisione di Didattica, Palermo, Italy	Research	Italy	50	5
Sept 2006	SCI 2006- XXII Congresso Nazionale della Società Chimica Italiana, Firenze, Italy	Research	Italy	1000	5
Aug 2006	I European Chemistry Congress, Budapest, Hungary	Research	EU	2500	5
Aug-Sept 2006	ECRICE-8, Budapest, Hungary	Research	EU	100	5
Sept 2006	EUCOCC6, Tále, Slovakia	Research	EU	150	5
Dec 2006	GICC06, Venezia, Italy	Research	Italy	50	5
March 2007	36th IRMG, York, United Kingdom	Research	EU	100	5
May-June 2007	MQM-2007, Budapest, Hungary	Research	EU	150	5
June 2007	XIV CNC-GIC2007, Tirrenia, Italy	Research	Italy	200	5
July 2007	II ICC, Novosibirsk, Russia	Research	EU	200	5
Dec 2007	Grid Open Days, Palermo, Italy	Research	Italy	50	5
March 2006	7th Netherlands' Chemistry and Catalysis Conference	Research	The Netherlands	40-100	6
June 2006	XIth Roermond Conference on Catalysis, Kerkrade, The Netherlands	Research	The Netherlands	50	6
October 2006	Invited lecture at Fritz-Haber-Institut, Berlin, Germany	Research	Germany	30	6
March 2007	8th Netherlands' Chemistry and Catalysis Conference, Noordwijkerhout, The Netherlands	Research	The Netherlands	40-100	6
June 2007	20th North American Meeting, Houston, USA	Research	USA	700	1, 6

2.2 Public deliverables

Deliverable No.	Deliverable title
D 5	Creation of database from catalyst screening
D 6	Creation of database from kinetic testing
D 7	Database from structural characterisation of catalysts: I
D 8	Database from structural characterisation of catalysts: II
D 9	Description of reaction mechanism by Monte Carlo simulations, quantum chemistry calculations and kinetic modelling: I
D 10	Description of reaction mechanism by Monte Carlo simulations, quantum chemistry calculations and kinetic modelling: II
D 11	Creation of fundamental knowledge I
D 12	Creation of fundamental knowledge II
D 16	Project management, mid-term assessment
D 17	Project management, final assessment
D 18/19	Benchmark study